SORBONNE UNIVERSITÉ

EURECOM
Sophia Antipolis

Decentralized coordination methods for beam alignment and resource allocation in 5G wireless networks

Dissertation

submitted to

Sorbonne Université

in partial fulfillment of the requirements for the degree of
Doctor of Philosophy

Author:
Flavio MASCHIETTI

Thesis advisor:
Prof. David GESBERT

Scheduled for defense on the 11th of December 2019, before a committee composed of:

Reviewers

Prof. Stefano BUZZI	*Univ. of Cassino and Southern Lazio, Italy*
Prof. Tharmalingam RATNARAJAH	*Univ. of Edinburgh, UK*

Examiners

Prof. Mari KOBAYASHI	*CentraleSupélec, France*
Prof. Dirk SLOCK	*EURECOM, France*
Prof. Gábor FODOR	*Ericsson Research & KTH, Sweden*

SORBONNE UNIVERSITÉ

EURECOM
Sophia Antipolis

Sorbonne Université
EDITE de Paris
EURECOM

Méthodes de coordination décentralisées pour alignement de faisceaux et allocation de ressources pour la 5G

Par **Flavio MASCHIETTI**

Thèse de doctorat en
Sciences de l'Information et de la Communication

Dirigé par **Prof. David GESBERT**

Soutenance de thèse prévue le 11 décembre 2019 devant un jury composé de:

Rapporteurs

Prof. Stefano BUZZI	*Univ. de Cassino et du Lazio Méridional, Italie*
Prof. Tharmalingam RATNARAJAH	*Univ. d'Edimbourg, Royaume-Uni*

Examinateurs

Prof. Mari KOBAYASHI	*CentraleSupélec, France*
Prof. Dirk SLOCK	*EURECOM, France*
Prof. Gábor FODOR	*Ericsson Research & KTH, Suède*

Abstract

More than 10 billions connected devices are predicted for 2020. While the mobile data continues to grow, future mobile networks are expected to deliver on improved spectral efficiencies, reduced latencies, better and more consistent throughput experience in the radio cell. The conventional and still prevailing approach to optimize the radio resources places the radio devices under the tight control of a central coordinator. Nevertheless, such approach makes the mobile network dependent on a considerable amount of measurement data that must be communicated in real-time to the centralized processor, which is impossible or undesirable in some practical cases. Moreover, the centralized approach ignores the computational and decision making capabilities of the modern radio devices such as smartphones, drones and connected cars, with great chance for direct device-to-device communication. Decentralized optimization methods are thus viewed with increased interest for future mobile networks.

In the context of 5G and 5G+ mobile networks, massive multi-antenna transmission is an established technique to manage multi-user interference and improve the network performance through beamforming and multiplexing gain. In the massive antenna regime, the leading forms of distributed cooperation that can be envisioned are *i)* the beam selection and alignment across multiple mobile users – in particular, at mmWave frequencies – and *ii)* the cooperation among base stations for user scheduling, whose centralized solution requires significant coordination and resource overhead.

In this thesis, we focus on *decentralized* cooperative methods for massive multi-antenna transmission optimization that are implemented at the cooperating devices themselves. We first tackle the beam alignment and selection problem from both single-user and multi-user perspectives, where the radio devices coordinate their beam strategies using long-term spatial side-information such as location information, to reduce the coordination overhead. In particular, we consider the important limitation factors which hinder perfect coordination such as the measurement noise and the limited information exchange capabilities between the cooperating nodes, so as to introduce robust approaches to side-information-aided beam selection and overcome conventional

schemes unsuitable to the distributed information configuration. In parallel, we show that multi-user beam selection in the massive antenna regime must deal with an interesting *trade-off* between *i)* harvesting large channel gain, *ii)* avoiding catastrophic multi-user interference, and *iii)* minimizing the channel acquisition overhead. To explore such trade-off, we propose a novel beam-domain coordination framework exploiting low-rate direct device-to-device side-links. Our results demonstrate the effectiveness of the proposed beam selection algorithms.

Since coordination entails some information flowing from one node to the others, we then expose the existence of an additional, but different trade-off between coordination and user *privacy*, of high practical relevance. In particular, we consider beam-domain coordination among competing mobile operators for user scheduling in mm-Wave spectrum sharing, where a clear correlation is found between the channel data and the users' locations. Our proposed *privacy-preserving* scheduling algorithm exploiting obfuscated beam-related information outperforms the uncoordinated benchmark.

Abrégé [Français]

Plus de 10 milliards d'appareils connectés sont prévus pour 2020. Tandis que les données mobiles continuent de croître, les futurs réseaux mobiles devraient permettre d'améliorer l'efficacité spectrale, de réduire la latence, de fournir une expérience de débit meilleure et plus uniforme dans la cellule radio. L'approche conventionnelle pour optimiser les ressources radio place les appareils radio sous le contrôle étroit d'un coordinateur central. Une telle approche rend le réseau mobile dépendant d'une quantité considérable de données de mesure qui doivent être communiquées en temps réel au processeur centralisé, ce qui est impossible ou indésirable dans certains cas pratiques. De plus, les approches centralisées ne profitent pas des capacités de calcul et de prise de décision des appareils radio modernes tels que les smartphones, les drones et les voitures connectées, avec de grandes chances de communication directe de dispositif à dispositif. Les méthodes d'optimisation décentralisées sont ainsi perçues avec un intérêt accru pour les futurs réseaux mobiles.

Dans le contexte des réseaux mobiles 5G et 5G+, la transmission massive multi-antennes (Massive MIMO) est une technique établie pour gérer les interférences multi-utilisateurs et améliorer la performance du réseau grâce à la formation de faisceaux et au gain de multiplexage. Dans le régime Massive MIMO, les principales formes de coopération distribuée qui peuvent être envisagées sont *i)* la sélection et l'alignement des faisceaux entre plusieurs utilisateurs mobiles – en particulier, aux fréquences millimetriques – et *ii)* la coopération entre les stations de base pour le scheduling des utilisateurs, pour lesquelles les solutions centralisées ont besoin d'un important overhead de coordination et de ressources radio.

Dans cette thèse, nous nous concentrons sur les méthodes de coopération *décentralisées* pour l'optimisation de la transmission multi-antennes massive qui sont mises en œuvre sur les nœuds coopérants eux-mêmes. Nous nous attaquons d'abord au problème d'alignement et de sélection des faisceaux, dans lequel les dispositifs radio coordonnent leurs stratégies à l'aide d'informations spatiales à long terme telles que leurs emplacements, afin de réduire l'overhead de coordination. En particulier, nous prenons

en compte les facteurs limitatifs importants qui entravent la parfaite coordination des utilisateurs, tels que le bruit de mesure et les capacités limitées d'échange d'informations entre les nœuds coopérants, afin d'introduire une approche robuste pour la sélection des faisceaux et de surmonter les schémas conventionnels, inadaptés à la configuration distribuée de l'information. En parallèle, nous montrons que la sélection de faisceaux dans le Massive MIMO doit trouver un *équilibre* entre *i)* obtenir un gain de canal important, *ii)* éviter les interférences multi-utilisateurs catastrophiques, et *iii)* minimiser l'overhead d'acquisition du canal. Pour explorer ce compromis, nous proposons un nouveau cadre de coordination dans le domaine spatial qui exploite les liaisons dispositif à dispositif. Nos résultats démontrent l'efficacité des algorithmes de sélection des faisceaux proposés.

Étant donné que la coordination implique une certaine circulation de l'information d'un nœud à l'autre, nous exposons ensuite l'existence d'un compromis supplémentaire, mais différent, entre la coordination et la *vie privée* des utilisateurs, ce qui revêt un intérêt pratique considérable. En particulier, nous considérons la coordination dans le domaine spatial entre plusieurs opérateurs mobiles concurrents afin de mieux scheduler les utilisateurs dans le partage du spectre en bande millimetrique, où l'on trouve en effet une corrélation claire entre les données du canal et l'emplacement des utilisateurs mobiles. L'algorithme de scheduling proposé exploite un mécanisme d'obscurcissement de l'information spatiale echangée et dépasse le benchmark non coordonné.

Acknowledgements

This thesis would have not been possible without the continuous support and supervision of *Prof. David Gesbert*. His impressive technical knowledge, passion in research and strive for innovation make me feel honored for having had the chance to pursue the Ph.D. under his guidance. David gave me boundless freedom in research and *continuously* pushed me to think outside the box. I am much grateful to him for that. Also, his personal qualities and gentle attitude helped in maintaining a pleasing atmosphere within the team. I owe immense gratitude to *Dr. Paul de Kerret* as well, who contributed to this thesis with great interest, insightful discussions and invaluable encouragement.

Part of this thesis has been carried out while I was at Ericsson Research, under the supervision of *Prof. Gábor Fodor*. Working with Gábor has been a real pleasure and a memorable experience. I have much appreciated his enthusiastic, open-minded and fun approach to research, and I am grateful to him and all the Radio team there for having hosted me in Stockholm. I would also like to thank *Prof. Stefano Buzzi*, *Prof. Tharm Ratnarajah* and the examiners for their time and attention in reviewing this thesis, and the European Research Council for having provided the generous funding without which this thesis and related publications would never have surfaced.

I owe a deep gratitude to friends and colleagues who were there for me throughout all the Ph.D. time and brightened the dark periods to which I have been exposed with smiles, laughs and fun. Thanks *Cult of Luna*, too, for the time spent together.

To conclude, I am much grateful to *my family* for their unconditional moral and economic support, and to K for her love, patience, and for adding some randomness to an otherwise predictable life. I dedicate this thesis to them.

Antibes, December 7, 2019



Contents

Abstract i
Abrégé [Français] iii
Acknowledgements v
Contents x
List of Figures xiv
List of Tables xv
Abbreviations xvii
Notations xix

1 Introduction and Motivation **1**
1.1 Multi-Antenna Coordination in Mobile Networks 1
1.2 Coordination in Massive MIMO Communications 2
1.2.1 Challenges in CSI Acquisition in FDD mMIMO 3
1.2.2 Challenges in CSI Acquisition in mmWave mMIMO 4
1.2.3 Massive MIMO and D2D 5
1.3 Decentralized Coordination 6
1.4 Focus of the Thesis 7
1.5 Coordination with Decentralized Information 7
1.5.1 Decentralized Beam-Domain Coordination 8
1.5.2 Distributed Information Structures 9
1.6 Thesis Outline 11

2 Models for Massive MIMO and mmWave Communications **15**
2.1 Geometric Channel Model 15
2.1.1 Channel Parameters in Sub-6 GHz Communications 17
2.1.2 Channel Parameters in mmWave Communications 17
2.2 Beam Codebook 18
2.2.1 Beam-Domain Channel Representation 18

3 Location-Aided Beam Alignment in Single-User mmWave mMIMO **21**
3.1 Introduction 21
3.2 Models and Scenario 22

3.3 Information Model . . . 23
3.3.1 Definition of the Model . . . 23
3.3.2 Distributed Information Model . . . 25
3.3.3 Shared Information . . . 25
3.4 Coordinated Beam Alignment Methods . . . 26
3.4.1 Beam Alignment under Perfect Information . . . 26
3.4.2 Optimal Bayesian Beam Alignment . . . 27
3.4.3 Naive-Coordinated Beam Alignment . . . 28
3.4.4 1-Step Robust Coordinated Beam Alignment . . . 28
3.4.5 2-Step Robust Coordinated Beam Alignment . . . 30
3.5 Simulation Results for the Single-User Scenario . . . 31
3.5.1 Beam Codebook Design . . . 31
3.5.2 Location Information Model . . . 32
3.5.3 Results and Discussion . . . 32
3.6 Conclusions . . . 38

4 Multi-User Beam Selection in mmWave mMIMO Using OOB Information 39
4.1 Introduction . . . 39
4.2 Models and Problem Formulation . . . 40
4.2.1 Uplink mmWave Signal Model . . . 40
4.2.2 Problem Formulation . . . 41
4.3 Out-of-Band-Aided Beam Selection . . . 42
4.3.1 Exploiting Sub-6 GHz Information . . . 43
4.3.2 Uncoordinated Beam Selection . . . 43
4.3.3 Hierarchical Coordinated Beam Selection . . . 45
4.4 Simulation Results . . . 47
4.4.1 Multi-Band Channels . . . 47
4.4.2 Results and Discussion . . . 47
4.5 Conclusions . . . 49

5 Multi-User Beam Selection for Training Overhead Reduction 51
5.1 Introduction . . . 51
5.2 Models and Problem Formulation . . . 52
5.2.1 Channel Estimation with Grid-of-Beams . . . 52
5.2.2 Data Signal Model . . . 55
5.2.3 Optimal Precoders and Combiners . . . 55
5.3 Data Beamformers Design . . . 57
5.4 Grid-of-Beams Beamformers Design . . . 59
5.4.1 Harvesting Large Effective Channel Gain . . . 60
5.4.2 Minimizing Multi-User Interference . . . 63

5.4.3 Minimizing Training Overhead . . . 65
5.5 Decentralized Coordinated Beam Selection Algorithms . . . 68
5.6 Simulation Results . . . 71
5.6.1 Winner II Channel Model . . . 71
5.6.2 Results and Discussion . . . 71
5.7 Conclusions . . . 74

6 Spectrum Sharing in mmWave: Coordination vs Privacy Trade-Off **77**
6.1 Introduction . . . 77
6.2 Models and Problem Formulation . . . 78
6.2.1 3D Millimeter Wave Channel Model . . . 78
6.2.2 Beam Codebook . . . 80
6.2.3 Coordinated Time Division Scheduling Problem . . . 80
6.3 Successive Scheduling . . . 81
6.3.1 SINR-Based Successive Coordinated Scheduling . . . 82
6.3.2 SLNR-Based Successive Coordinated Scheduling . . . 82
6.3.3 Average Leakage Power Through Beam Footprints . . . 83
6.3.4 Low-Overhead SLNR-Based Coordinated Scheduling . . . 85
6.4 Privacy-Preserving Coordinated Scheduling . . . 86
6.4.1 Trade-Off Between Coordination and Privacy . . . 86
6.4.2 Privacy-Preserving SLNR-Based Coordinated Scheduling . . . 88
6.5 Simulation Results . . . 88
6.5.1 Results and Discussion . . . 89
6.6 Conclusion . . . 91

7 Conclusions **93**

Appendices **95**
A.1 Proofs of Chapter 3 . . . 95
A.2 Proofs of Chapter 4 . . . 97
A.3 Proofs of Chapter 5 . . . 99
A.4 Proofs of Chapter 6 . . . 101

Résumé [Français] **103**
F.1 Introduction et Motivation . . . 103
F.1.1 Coordination Multi-Antennes dans les Réseaux Mobiles . . . 103
F.1.2 Coordination dans le Massive MIMO . . . 104
F.1.3 Coopération Décentralisée . . . 108
F.1.4 Objet de la Thèse . . . 109
F.1.5 Coordination avec l'Information Décentralisée . . . 109
F.2 Coordination dans le Domaine Spatial pour le mMIMO . . . 111

F.2.1 Alignement des Faisceaux Robuste en Bande Millimetrique . . . 111
F.2.2 Sélection des Faisceaux à l'aide d'Information Hors Bande 114
F.3 Partage du Spectre en Bande Millimetrique : Selection des Faisceaux et Conservation de la Vie Privée 118
F.3.1 Formulation du Problème de Scheduling 119
F.3.2 Compromis entre la Coordination et la Protection de la Vie Privée 119
F.3.3 Scheduling Coordonné visé à la Protection de la Vie Privée 121

References **123**

List of Figures

1.1 Beam decision with distributed information. The k-th device makes its decision on the basis of its own global network state estimate $\hat{\mathbf{H}}^{(k)}$. . . . 8
1.2 Scenario example for the considered decentralized coordination problems. 12

2.1 Geometric channel model and notations with 3 clusters of paths. 16
2.2 Beam-domain representation of a geometric channel. 19

3.1 Scenario example with one Line-of-Sight (LOS) path and two reflected Non-Line-of-Sight (NLOS) paths. 23
3.2 Example of the distributed location information setting. The estimated location information is denoted with blue (at the Base Station (BS) side) and orange (at the User Equipment (UE) side) points, along with their *uncertainty* circles. The black points represent the actual locations. In this sketch, a bounded error model is assumed. 26
3.3 SE vs SNR. Stronger LOS path, settings $\mathcal{A}$ and $D_{\text{BS}} = D_{\text{UE}} = 4$. 33
3.4 SE vs number of pre-selected beams at the BS and the UE (among $M_{\text{BS}} = M_{\text{UE}} = 64$). Stronger LOS path, settings $\mathcal{A}$, for an Signal-to-Noise Ratio (SNR) $= 10$ dB. 34
3.5 SE vs SNR. Stronger LOS path, settings $\mathcal{B}$ and $D_{\text{BS}} = D_{\text{UE}} = 4$. 35
3.6 Beam sets selected for pilot transmission with the proposed beam alignment (BA) algorithms, for a given realization. Stronger LOS path, i.e. $\sigma^2_{\text{LoS}} = 0.4$ as shown, settings $\mathcal{A}$, and $D_{\text{BS}} = D_{\text{UE}} = 7$. 36
3.7 Beam set selected for pilot transmission with the proposed beam alignment (BA) algorithms, for a given realization. LOS blockage, i.e. $\sigma^2_{\text{LoS}} = 0$ as shown, settings $\mathcal{B}$, and $D_{\text{BS}} = D_{\text{UE}} = 4$. 37

4.1 Scenario example with $K = 2$ UEs and 3 clusters per UE. The UEs are assumed to reside in a disk of radius r. In this illustration, two *closely-located* UEs share some reflectors and the signal waves reflecting on the top ones arrive quasi-aligned at the BS, leading to severe interference and degraded sum-rate. 41
4.2 Simulated example of the available $\mathbb{E}[|\underline{\mathbf{S}}_k|^2]$ at two neighboring UEs, with $r = 11$ m. Some strong reflectors are being shared, while others are uncommon. The average power of the paths – based on (4.15) – can be different across the UEs. 48
4.3 Sum-Spectral Efficiency (SE) vs (mmWave) SNR. The average inter-UE distance is 13 m. The OOB-aided coordinated algorithm outperforms the uncoordinated one. 49
4.4 Sum-SE vs average inter-UE distance. The SNR is fixed to 1 dB. The performance gain achieved through coordination decreases with the inter-UE distance. 50

5.1 Intuitive example with $K = 2$ UEs highlighting the trade-off between *i) energy* (i.e. activating strong paths), *ii) spatial separability*, and *iii) training overhead* (i.e. lighting up a smaller set of beams at the BS). The blue and orange circles represent the multi-path clusters, *possibly* shared among the UEs. Stronger paths are marked in bold. 53
5.2 CSI-RS locations in a Downlink (DL) New Radio (NR) resource block. When Grid-of-Beams (GoB) precoding is used, the effective channels are mapped to one precoded Reference Signal (RS) each (or antenna port each, according to 3GPP) sent over τD_{BS} non-overlapping resource elements (here in light blue and orange). Therefore, less resource elements are available for transmitting data to the UEs, leading to throughput degradation. 57
5.3 Average SE vs SNR for a single-user case. Beam selection is based on the relevant beams. The upper bound in (5.23) can be used to approximate the actual SE. 63
5.4 Comparison of the actual effective network throughput $\mathcal{R}$ as in (5.10) and its approximations defined in (P0)-(P4). In this plot, $K = 7$ UEs. The beam selection at each UE is based on the local SNR. The approximation used for (P4) is the closest to the actual effective network throughput. . . 68

5.5 Signaling sequence of the proposed coordinated beam selection (P3) for $K = 3$. The beam decision made at each UE leverages the Device-to-Device (D2D)-enabled long-term statistical information coming from the lower-ranked UEs in a hierarchical fashion. 70
5.6 Average effective throughput vs SNR for (a) $K = 7$ and (b) $K = 11$ *randomly-located* UEs. $D_{\text{UE}} = 3$ beams activated at each UE. $T_{\text{coh}} = 15$ ms. The coordinated algorithms (P3) and (P4) outperform the uncoordinated (P1), as opposed to (P2). 72
5.7 Average effective throughput gain over uncoordinated beam selection (P1) vs T_{coh} for $K = 7$ UEs. The SNR is 11 dB. Taking the pre-log factor into account is essential for an effective coordinated beam selection under *fast-varying* channels where $T_{\text{coh}} < 20$ ms. 73
5.8 Average D_{BS} for the proposed algorithms vs T_{coh} for (a) $K = 7$ and (b) $K = 11$ UEs. The SNR is 11 dB. The coordinated algorithm (P2) activates more beams at the BS side in order to achieve greater spatial separation among the UEs. 74
5.9 Average effective throughput gain over uncoordinated beam selection (P1) vs T_{coh} for $K = 7$ *closely-located* UEs. The SNR is 11 dB. Owing to high spatial correlation among the UEs, the algorithm (P2) achieves high gains compared to the solutions which neglect the multi-user interference. 75

6.1 Scenario example with $B = 2$ BSs. Each base station serves its UEs through forming *highly-directional* beams towards them. We consider 3D beamforming with UPAs, such that beam footprints result around the UEs and *possibly overlap*. 79
6.2 Time division scheduling with $B = 3$ BSs and a sample assignment. In each time slot, each BS selects one UE to schedule. In this example, the BS 1 chose the UEs $\{1, 23, \ldots, 4, 5\}$ overall. 80
6.3 Beamforming gain per location obtained with two beams in (6.5) and their associated footprints, considered as the spatial region where the normalized gain is higher than $1/2$. 84
6.4 Average SE per UE vs average LDP in a full-LOS scenario. The proposed *privacy-preserving* algorithm succeeds in striking a balance between privacy and average SE performance. 90

6.5 Gain over uncoordinated scheduling vs normalized NLOS variance. Here, the UE LDP $\simeq 0.1$. The performance of the proposed *privacy-preserving* low-overhead scheduling algorithm decreases as more NLOS links are used to communicate. 91

F.1 Sélection des faisceaux avec information distribuée. Le k-ème dispositif prend sa décision sur la base de sa propre estimation $\hat{\mathbf{H}}^{(k)}$ de l'état du réseau global. 110
F.2 Efficacité spectrale contre rapport signal-à-bruit (SNR). 113
F.3 Efficacité spectrale contre nombre de faisceaux présélectionnés à la BS et à l'UE parmi un total de 64 faisceaux. SNR $= 10$ dB. 113
F.4 Exemple d'interférence de faisceau avec $K = 2$ UEs. Les UEs sont supposés résider dans un disque de rayon r. Dans cette illustration, deux UEs situés à proximité partagent certains réflecteurs et les ondes de signal réfléchissant sur les réflecteurs du haut arrivent quasi-alignées à la BS – bref, captées par le même faisceau à la BS - alors qu'elles proviennent de différentes UEs. 115
F.5 Efficacité spectrale globale contre SNR. L'algorithme coordonné surpasse l'algorithme non-coordonné. Le gain de coordination augmente avec le SNR. 117
F.6 Efficacité spectrale globale contre distance moyenne entre les UEs. Le gain de performance atteint avec la coordination diminue avec la distance inter-UE. 117
F.7 Gain en termes d'efficacité spectrale par rapport au scheduling non coordonné contre probabilité de localisation des UEs (avec une précision de 10 mètres). 121

List of Tables

1.1 The coordination scenarios which are studied throughout this thesis. . . 11

5.1 The proposed optimization problems (P1)-(P4) with their considered sub-problems. 67

5.2 The proposed algorithms and their required information at the k-th User Equipment (UE). The information relative to the lower-ranked UEs $1, \ldots, k-1$ is exchanged through Device-to-Device (D2D) side-links. 69

Abbreviations

The abbreviations used throughout this thesis are specified in the following. Their plural forms are constructed as e.g. BS (base station) to BSs (base stations). The abbreviations are also expanded on their first use, in each chapter. The English abbreviations are also used for the French résumé.

AoA	Angle-of-Arrival
AoD	Angle-of-Departure
BD	Block Diagonalization
BS	Base Station
C-RAN	Cloud-Radio Access Network
CMD	Correlation Matrix Distance
CS	Compressive Sensing
CSI	Channel State Information
D2D	Device-to-Device
DFT	Discrete Fourier Transform
DL	Downlink
FD-MIMO	Full-Dimensional MIMO
FDD	Frequency Division Duplex
GCMD	Generalized Correlation Matrix Distance
GNSS	Global Navigation Satellite System
GoB	Grid-of-Beams
GPS	Global Positioning System
LI	Linearly Independent
LMMSE	Linear Minimum Mean Square Error
LOS	Line-of-Sight
MIMO	Multiple-Input Multiple-Output
mMIMO	Massive MIMO
mmWave	Millimeter Wave

MRC	Maximum Ratio Combining
NLOS	Non-Line-of-Sight
NR	New Radio
OFDM	Orthogonal Frequency-Division Multiplexing
OOB	Out-of-Band
PDF	Probability Density Function
PMI	Precoding Matrix Indicator
RRM	Radio Resource Management
RS	Reference Signal
RX	Receiver
SE	Spectral Efficiency
SINR	Signal-to-Interference-and-Noise Ratio
SLNR	Signal-to-Leakage-and-Noise Ratio
SNR	Signal-to-Noise Ratio
SVD	Singular Value Decomposition
TD	Team Decision
TDD	Time Division Duplex
TDOA	Time Difference of Arrival
TX	Transmitter
UE	User Equipment
UL	Uplink
ULA	Uniform Linear Array
UPA	Uniform Planar Array
ZF	Zero-Forcing

Notations

The next list gives an overview on the notation used throughout this manuscript. Bold lowercase letters are reserved for vectors, while bold uppercase letters for matrices.

$\lvert x \rvert$	Magnitude of the scalar x
$\mathbf{I}_N$	Identity matrix of dimension $N \times N$
$\mathrm{conj}\,(\mathbf{A})$	Conjugate of the matrix $\mathbf{A}$
$\mathbf{A}^{\mathrm{T}}$	Transpose of the matrix $\mathbf{A}$
$\mathbf{A}^{\mathrm{H}}$	Hermitian transpose of the matrix $\mathbf{A}$
$\mathrm{tr}\,(\mathbf{A})$	Trace of the matrix $\mathbf{A}$
$\det(\mathbf{A})$	Determinant of the matrix $\mathbf{A}$
$\mathrm{rank}\,(\mathbf{A})$	Rank of the matrix $\mathbf{A}$
$\mathrm{null}\,(\mathbf{A})$	Null space of the matrix $\mathbf{A}$
$\mathrm{span}\,(\mathbf{A})$	Span of the matrix $\mathbf{A}$
$\mathbb{E}_X\big[f(x)\big]$	Expectation of $f(x)$ over X
$\mathrm{diag}\,(\mathbf{x})$	Diagonal matrix with the entries of the vector $\mathbf{x}$ along its diagonal
$\mathrm{col}\,(\mathbf{A})$	Set containing the columns of the matrix $\mathbf{A}$
$\mathrm{row}\,(\mathbf{A})$	Set containing the rows of the matrix $\mathbf{A}$
$\mathrm{card}\,(\mathbf{A})$	Number of elements in the set $\mathcal{A}$
$\mathrm{vec}\,(\mathbf{A})$	Vectorization of the matrix $\mathbf{A}$ into a column vector
$\mathbf{A} \otimes \mathbf{B}$	Kronecker product of the matrices $\mathbf{A}$ and $\mathbf{B}$
$\lVert \mathbf{A} \rVert_{\mathrm{F}}$	Frobenius norm of the matrix $\mathbf{A}$
$\mathcal{CN}\,(0, \mathbf{\Sigma})$	Zero-mean complex Gaussian distribution with covariance matrix $\mathbf{\Sigma}$
$\mathbf{x}_{n:m}$	Short-hand notation for $\mathbf{x}_n, \ldots, \mathbf{x}_m$
$[\![1, N]\!]$	Short-hand notation for $\{1, \ldots, N\} \subset \mathbb{N}$

Chapter 1

Introduction and Motivation

The full or partial reuse of the radio resources (spectrum, time, power, pilots, etc.) in wireless mobile networks leads to severe interference, which in turn limits the performance offered to the connected devices – in particular those located at the cell edge [1]. Several approaches aimed at mitigating interference have emerged in the last decade. A central notion in all such approaches is *coordination*: interfering transmitters have to agree on *jointly* optimizing their transmission parameters so as to increase the global network performance. Towards this end, the optimization strategies should take into account the limited (finite-rate) feedback overhead constraint [2], which otherwise degrades the network throughput. In multi-device cooperation, the notion of feedback is large and encompasses several kinds of prior information – such as the Channel State Information (CSI) – that are exchanged among the devices.

In general, cooperative or coordinated communications with limited feedback can be divided in *i)* Radio Resource Management (RRM) methods, such as power control or user scheduling [1], and *ii)* signal processing-based methods, such as (coordinated) multi-antenna processing. Considering the focus of this thesis, an overview on the literature of multi-antenna coordination techniques is given in the following.

1.1 Multi-Antenna Coordination in Mobile Networks

The role that multiple antennas at the devices have in mitigating the interference and improving the network performance through linear Multiple-Input Multiple-Output (MIMO) precoders and combiners is well established [3]. The powerful combination of multi-antenna techniques and cooperation among interfering wireless devices has been studied in depth over the last decade. To give some examples, transmitter coordination allows for the avoidance of the interference even before it takes place as e.g.

in Network MIMO [4], or can help to shape it such that it is easier for the receivers to suppress it, through the so-called *interference alignment* [5]. Nevertheless, the benefits of multi-antenna transmitter coordination depend on the accurate knowledge of the global CSI [1, 4]. In an effort to limit the requirements for *low-latency* CSI sharing over the backhaul network, several approaches have been proposed. Among them, rank-coordination is possible, where distributed rank adaptation algorithms aim at reserving some spatial degrees of freedom for interference rejection rather than using them all for spatial multiplexing [6]. A significant step forward has been made with the introduction of the so-called Massive MIMO (mMIMO) [7]. In mMIMO, the number of antennas at the Base Station (BS) is much larger than the number of devices per signaling resource. As a consequence, the radio channel of a desired device tends to become more orthogonal to the channel of another selected interfering device, and simple distributed beamforming schemes such as Maximum Ratio Combining (MRC) can *asymptotically* – for an infinite number of antennas – eliminate the interference and offer performance comparable to much more complex centralized schemes. To design such beamformers, the *local CSI* is needed at the transmitter. In the massive antenna regime, acquiring the local CSI is *not always* trivial. Several challenges hinder the potential application of mMIMO in future 5G/5G+ networks. In the next section, we will describe such challenges and how coordination can help in addressing them.

1.2 Coordination in Massive MIMO Communications

The original mMIMO implementation is based on Time Division Duplex (TDD) operation, which allows to estimate the Downlink (DL) channels through orthogonal Uplink (UL) sounding exploiting the *channel reciprocity* [7]. The relative ease with which the large-dimensional local CSI can be acquired in TDD operation with *single-antenna* users has led research groups to focus on such mMIMO configuration, where the so-called *pilot contamination* represents the main concern [7]. To avoid conflicting pilot transmissions, coordination has a central role and extensive research efforts has been made, fostering both time-domain [8–10] and spatial-domain methods [11–15].

In this thesis, we focus on different mMIMO architectures, which are expected to emerge in the next generation of mobile networks: *i) Frequency Division Duplex (FDD)* mMIMO with a small-to-moderate number of antenna elements at the User Equipment (UE) side, and *ii)* Millimeter Wave (mmWave) *doubly* mMIMO with massive antennas at both the BS and UE sides [16]. In all the above cases, the acquisition of the local CSI at the transmitter is not trivial, as we explain in the following sections.

1.2.1 Challenges in CSI Acquisition in FDD mMIMO

In FDD mode, DL Reference Signals (RSs) and subsequent UL feedback are required to acquire the local CSI, since the *channel reciprocity* does not hold. In general, there exists a one-to-one correspondence between RSs and antenna elements, such that few radio resources are left for data transmission [17]. Several work has been done to cope with the training and feedback overhead issue in FDD mMIMO. Such existing methods can be divided in three categories: *i)* second-order statistics-based approaches, *ii)* Compressive Sensing (CS)-based approaches, and *iii)* Grid-of-Beams (GoB)-based approaches.

Among the approaches based on second-order statistics, the pioneering works [11, 12] exploit *strictly spatially-orthogonal* channel covariances to discriminate across interfering UEs with even correlated non-orthogonal RSs, thus reducing the training overhead. Since such condition is seldom experienced in practical scenarios [18], the recent work [19] has introduced a precoding method to *artificially* forge low-dimensional effective channels, *independently* from the covariance structure. In the MIMO literature, such methods have been known under the term *covariance shaping* [20–22].

CS techniques for estimating high-dimensional channels with few measurements are known for decades [23] and have been applied to FDD mMIMO as well [24–27]. The significant overhead reduction in all these works relies on the existence of an intrinsic sparse representation of the radio channels. Alternative CS-based methods such as [28–32] capitalize on the DL/UL *angular reciprocity*. In such approaches, the spatial spectrum is estimated from UL sounding and used to design the mMIMO precoder, under the reasonable assumption that the dominant Angles-of-Departure (AoD) are almost invariant over the spectrum range separating the DL and the UL channels.

The GoB approach has raised much interest within the 3GPP group, due to its practical implementation convenience [33, 34]. According to this concept, reduced channel representations are obtained through a spatial transformation based on fixed transmit-receive beams. In this case, there exists a one-to-one correspondence between RSs and beams, such that estimating the effective channels reduces the total overhead. However, the substantial reduction in overhead often entails a drastic performance degradation [35] as the mMIMO data precoder is optimized for reduced channel representations which might not capture the prominent characteristics of the actual channels. On the upside, profitable low-dimensional representations can be obtained through activating the appropriate subset of beams. In general, the decision on which beams to activate at both the BS and UE sides is not a trivial one, since several factors participate in the sum-rate optimization problem. Coordinated approaches to beam selection are thus fundamental, as we will expose throughout this thesis (Chapters 3, 4 and 5).

1.2.2 Challenges in CSI Acquisition in mmWave mMIMO

Among the enabling technologies for future wireless mobile networks, mmWave communication offers the chance to deal with the bandwidth shortage affecting wireless carriers. There are indeed large portions of unused spectrum above 30 GHz, which can be used as a complement to the conventional sub-6 GHz bands. The use of higher frequencies and higher bandwidths poses new implementation challenges, as for example in terms of hardware constraints or architectural features. Moreover, the propagation environment is adverse for smaller wavelength signals: compared with lower bands characteristics, diffraction tends to be lower while penetration or blockage losses can be much greater [36]. Therefore, mmWave signals experience a severe path-loss which hinders the establishment of a reliable communication link and requires high beamforming gain [37]. On the upside, millimeter wavelengths allow to stack a high number of antenna elements in a modest space [38] thus facilitating the exploitation of the superior beamforming performance stemming from mMIMO antennas [39].

In the mmWave band, configuring the mMIMO antennas entails an additional effort [40]. The high cost and power consumption of the radio components – in particular, the analog-to-digital converters – impact on the UEs and the small BSs, thus limiting the practical implementation of *fully-digital* beamforming architectures [41]. Therefore, low cost architectures are suggested, where the beam design is codebook-based (GoB), and implemented in analog fashion [42]. Another trend lies in the so-called *hybrid* beamforming architectures, where a low-dimensional digital processor is concatenated with an RF analog beamformer [43, 44]. In all of these solutions, a bottleneck is found in the mMIMO regime while searching for the analog beam combinations at transmitter and receiver which offer the best channel gain, a problem referred to as *beam alignment* in the literature [45, 46]. In particular, beam alignment becomes critical when the communication is between two mMIMO devices [16], where the number of beam combinations is huge and represents a significant pilot and time resources overhead.

The current literature reflects the interesting trade-off between *latency* and beamforming performance that is found in beam alignment [47, 48]. Narrower beamwidths lead to increased alignment overhead, but provide a higher transmission rate, as a result of higher directive gains and lower interference. On the other hand, larger beamwidths expedite the alignment process, though smaller beam gains reduce rate and coverage.

One approach for reducing alignment overhead – without compromising performance – has been proposed in [49]. It consists in exploiting location side-information so as to reduce the effective beam search areas in the presence of Line-of-Sight (LOS) propagation. Similar approaches are found in [50–52], where spatial information – obtained

through radars, automotive sensors or Out-of-Band (OOB) information – has been confirmed as a useful source of side-information, capable of assisting beam alignment and selection in mmWave communications. As we have anticipated in Section 1.2.1, selecting the transmit-receive beams is a non-trivial problem and is further exacerbated in multi-user settings, where the best beams depend on several factors, including the Signal-to-Interference-and-Noise Ratio (SINR), which require *full coordination* among the devices. Moreover, exploiting side-information to meet the limited feedback constraint imposes the design of *robust* approaches to coordinated beam selection, as such information might give nothing but a *partial* view on the actual state of the network. How to deal with those additional uncertainties is a *key element* of this thesis.

1.2.3 Massive MIMO and D2D

The advances in Device-to-Device (D2D) communications allow to exchange information among neighboring UEs with negligible resource overhead [53]. The standardization of network-assisted D2D communications within the 3GPP group [54] has sparked interest in exploring the possibilities arising from D2D-aided techniques in modern mobile networks. Several works have shown promising results on D2D-enabled interference management and radio resource allocation [55–57]. Despite an extensive literature on D2D implementation in mobile networks [58], just a few works investigate the potential integration of D2D and mMIMO techniques. In [59, 60], the authors introduce an intermediate CSI exchange phase in the classical FDD closed-loop feedback. Once the channel is acquired at the UEs, local CSI is exchanged through D2D side-links so that the global CSI is available to all UEs. As a consequence, a *coordinated* design of the feedback data can be derived towards feedback overhead reduction. [61] considers a two-phase multi-casting scheme where the mMIMO BS precodes the common message to target an appropriate subset of devices, which in turn cooperate to spread the information across the rest of the network via D2D retransmissions. The precoding gain at the BS and the D2D side-links helps in achieving the maximum multi-cast rate. In this thesis, we focus on D2D-enabled information exchange protocols which can achieve device coordination with limited information, much smaller than the local CSI. The methods that we present in Chapters 4, 5 and 6 are based in part on the sharing of a low-rate beam-related information that can assist with beam-domain coordination strategies.

Coordination can be achieved via centralized or decentralized approaches. In the next section, we show the pros and cons of such opposite – but perhaps *complementary* – approaches and motivate why future mobile networks should be *partly* decentralized.

1.3 Decentralized Coordination

The conventional approach for enabling coordination in mobile networks is based on concentrating all feedback and measurement data, as well as computational power, at a central node, as e.g. the BS or the *cloud*. For example, the Cloud-Radio Access Network (C-RAN) is a popular centralized framework for delivering efficient resource allocation and solving advanced multi-cell coordination algorithms [62]. In this respect, the devices at the network edge – such as the UEs and the BSs – push their measured data into an optical backhaul-supported cloud where dedicated servers run the required network optimization algorithms. The solutions of such algorithms, i.e. the transmission decisions, are then sent back to the edge devices for application. Although the centralized approach is still prevailing in mobile networks design, pure cloud-centric architectures are rather expensive and come with their own technical limitations. For example, the centralized processing increases the *latency*, which is killer for critical 5G applications such as the tactile-internet [63], and decreases the timeliness of the CSI, a crucial information for multi-antenna transmission. The exponential increase in the number of connected devices [64] heighten these drawbacks, with potential spill-over effects on the network performance. We are therefore witnessing a growing interest in designing a more adaptable network of devices that can cooperate *autonomously* without the help of a central node. The devices should leverage their local computing, sensing and communication capabilities to interact with each other and increase the network performance. Thus, the cooperating devices run *decentralized* algorithms that are designed to maximize a *global* network performance metric as e.g. the network throughput, through adjusting *local* transmission parameters such as the power level, the precoder, etc. However, each local parameter decision is made using local information *only*, which is often a *noisy* and partial estimate of the global state information, different at each device. In this respect, the decentralized approach involves an inevitable performance loss compared to the centralized approach with ideal backhaul links.

In this thesis, we refer as "decentralized" or "distributed" any coordination mechanism for which the coordinating devices have only a partial view over the global network state information that would otherwise be required for a centralized solution. Here, "partial" may allude to the availability of limited, noisy, or possibly long-term statistical information.

1.4 Focus of the Thesis

In this thesis, we focus on decentralized coordination methods in the context of massive multi-antenna transmission. In the massive antenna regime, the leading forms of distributed coordination that can be envisioned are *i)* the beam selection and alignment across multiple devices – in particular, at mmWave frequencies [41] – and *ii)* the cooperation among BSs for user scheduling. The centralized solutions of both these coordination frameworks require significant coordination and resource overhead. In this thesis, we exploit beam-domain coordination among the devices to address these problems, which can be most often recast as *Team Decision (TD)* problems. In general, the results presented in this thesis are not built upon results in the TD literature, due to computational and practical constraints. Instead, we exploit the particular properties of each considered problem to derive heuristic solutions. However, keeping the TD formulation in mind will prove helpful to obtain interesting insights and understand the fundamentals of the problems. We introduce the TD framework in the next section.

1.5 Coordination with Decentralized Information

The lack of reliable observed data at each decision-making device calls for robust decentralized coordination algorithms, whose purpose is to minimize the loss with respect to the centralized solutions. The emphasis on a *common* performance goal and the *latency* constraints for inter-device communication requires a different approach from classical device cooperation frameworks. For example, in egoistic game-theoretical approaches [65], the radio devices are conflicting with each other and potential equilibria do not *automatically* translate into global network gains. In this case, the imperfect coordination which hinder the maximization of the global performance metric arises from the distributed nature of the observed data, based upon which the decisions are made.

The theoretical roots behind *one-shot* decentralized coordination can instead be found in the so-called *Team Decision theory* [66], which is known for a long time and often involves solving a non-trivial distributed functional optimization problem. Yet, the strong development of the computational capabilities in the past decade has opened up new avenues for solving such difficult problems. In the following, we show how the TD formulation unfolds in the context of beam-domain coordination.

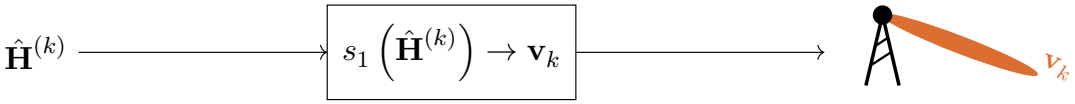

Figure 1.1 – Beam decision with distributed information. The k-th device makes its decision on the basis of its own global network state estimate $\hat{\mathbf{H}}^{(k)}$.

1.5.1 Decentralized Beam-Domain Coordination

Let us consider a network with K cooperating devices, which will be instantiated as BSs or UEs in the chapters of this thesis (see Table 1.1). We assume that the k-th device adopts the *strategy* $s_k : \mathbb{C}^m \rightarrow \mathcal{S}_k \subseteq \mathbb{C}^{d_k}$, based on local estimates, where $\mathcal{S}_k$ is its decision sub-space, i.e. its beam or precoder *codebook* in beam-domain coordination (refer to Fig. 1.1). The general TD problem, whose goal is to maximize the global network performance metric $f : \mathbb{C}^m \times \prod_{k=1}^{K} \mathbb{C}^{d_k} \rightarrow \mathbb{R}$, can be formulated as follows:

$$\left(s_1^*, \ldots, s_K^*\right) = \underset{s_1,\ldots,s_K}{\operatorname{argmax}} \mathbb{E}_{\mathbf{H},\hat{\mathbf{H}}^{(1)},\ldots,\hat{\mathbf{H}}^{(K)}} \left[f\left(s_1\left(\hat{\mathbf{H}}^{(1)}\right), \ldots, s_K\left(\hat{\mathbf{H}}^{(K)}\right), \mathbf{H}\right)\right], \tag{1.1}$$

where

- $\mathbf{H} \in \mathbb{C}^m$ is the global state of the network[1];
- $\hat{\mathbf{H}}^{(k)} \in \mathbb{C}^m$ is the local estimate of $\mathbf{H}$ which is available at the k-th device.

The formulation in (1.1) refers to a static setting where each of the K devices designs transmission policies in order to coordinate with the other devices, based on the expectation over the *joint Probability Density Function (PDF)* of the actual network state and all local estimates, defined as

$$p_{\mathbf{H},\hat{\mathbf{H}}^{(1)},\ldots,\hat{\mathbf{H}}^{(K)}}. \tag{1.2}$$

Thus, the mutual correlation between $\hat{\mathbf{H}}^{(1)}, \ldots, \hat{\mathbf{H}}^{(K)}$ and the correlation between these estimates and the actual state $\mathbf{H}$ set a limit to the coordination performance. In particular, the solution to (1.1) depends on the associated information structure, i.e. the nature of the observations made at each device and how such local information relates to the actual global state. In the following, we will introduce and motivate the decentralized information structures that will be considered throughout this thesis.

[1] We stress that $\mathbf{H}$ can be either CSI or related to CSI, as e.g. location information (refer to Table 1.1).

1.5.2 Distributed Information Structures

The information structure underpinning the TD problem in (1.1) describes how the local information $\hat{\mathbf{H}}^{(k)}$ available at the k-th device relates to the local estimates at the other devices $\hat{\mathbf{H}}^{(j)}$, $\forall j \neq k$, as well as to the actual global state information vector $\mathbf{H}$. Note that the configuration in (1.1) precludes explicit interactions between the cooperating devices, which is consistent with *low-latency* applications. In this respect, the large number of devices in future mobile networks represents a favorable circumstance as devices that are located closer to each other have greater chance for *low-latency* direct D2D communication (refer to Section 1.2.3). Thus, some rounds of information exchanges between the devices can be assumed, leading to specific information configurations and easier, more practical, TD problems. In this section, we first describe an intuitive and tractable information model which consists in considering Gaussian noise-corrupted global information at each device. Then, we describe a hierarchical information setup which arises in networks where some devices are endowed with greater information gathering capabilities.

Distributed Gaussian Information Configuration

The distributed Gaussian configuration assumes that some Gaussian noise with device-dependent covariance matrix $\mathbf{\Sigma}_k \in \mathbb{C}^{m\times m}$ corrupts the estimate $\hat{\mathbf{H}}^{(k)}$ at the k-th device. In particular, we can write the estimate $\hat{\mathbf{H}}^{(k)}$ at the k-th device as

$$\hat{\mathbf{H}}^{(k)} = \sqrt{1-\mathbf{\Sigma}_k^2}\mathbf{H} + \mathbf{\Sigma}_k^2\mathbf{N}, \qquad \forall k = \{1,\dots,K\}, \tag{1.3}$$

where $\mathbf{N} \sim \mathcal{CN}(0, \mathbf{I}_m)$ is Gaussian-distributed noise.

Under this model, the knowledge of the noise variances at the other devices is sufficient to derive the joint PDF in (1.2). In practical scenarios, some devices can have greater sensing and estimation capabilities with respect to other devices, as e.g. high-end devices compared to low-end devices. Such cases are well-captured in (1.3), where greater noise variances can be assumed for the low-end devices. Some examples on practical applications of such configuration can be found in [67–69]. In general, this model can be extended to *any* kind of noise, as for example uniform bounded noise. In Chapter 3, we assume a bounded error model for the location side-information, such that the location estimates at each device fall inside a disk around the actual locations.

Hierarchical Distributed Configuration

The hierarchical distributed information structure is obtained when the devices can be ordered such that the k-th device has access to the information – so, the transmission decision – at the j-th device, where $j < k$, in addition to its local information. This configuration implies that the first device is the least informed one while the K-th device is the most informed one and knows the information at all *lower-ranked* devices. In a mathematical sense, it means that there exist some functions $h_{k,j} : \mathbb{C}^m \to \mathbb{C}^m$ such that

$$\hat{\mathbf{H}}^{(j)} = h_{k,j}\left(\hat{\mathbf{H}}^{(k)}\right), \qquad \forall j < k. \tag{1.4}$$

The advantage of the hierarchical distributed configuration is that – unlike the information structure in (1.3) – the devices can follow a chain of strategies where the better informed k-th device can adapt its own strategies to the known strategies taken at the lower-ranked less-informed j-th device, where $j < k$, in order to improve the common performance metric. The hierarchical distributed configuration is obtainable through e.g. multi-level quantization schemes [70] or also D2D side-links (refer to Section 1.2.3). A remaining obstacle resides in the fact the k-th device is not able to predict with exactitude the strategies of the better informed j-th devices, where $j > k$. Low-complex sub-optimal solutions are possible. For instance, the k-th device can assume that the higher-ranked devices have access to the same local information $\hat{\mathbf{H}}^{(k)}$. Following this approximation, the (hierarchical) TD at the k-th device is obtained as follows:

$$\begin{aligned}&\left(s_k^{\mathrm{HC}}, \bar{s}_{k+1}, \ldots, \bar{s}_K\right)\\ &\qquad = \underset{s_k,\ldots,s_K}{\operatorname{argmax}} \mathbb{E}_{\mathbf{H}|\hat{\mathbf{H}}^{(k)}}\left[f\left(s_1^*, \ldots, s_{k-1}^*, s_k\left(\hat{\mathbf{H}}^{(k)}\right), \ldots, s_K\left(\hat{\mathbf{H}}^{(k)}\right), \mathbf{H}\right)\right].\end{aligned} \tag{1.5}$$

Remark 1.1. The decisions $\bar{s}_{k+1}^*, \ldots, \bar{s}_K^*$ in (1.5) are *auxiliary* variables which are not used for actual transmission. The higher-ranked j-th device, where $j > k$, will use more accurate information to derive its own decision. □

Under the hierarchical information setting, the TD optimization problem reduces to a conventional robust optimization problem. Indeed, the optimal decision at the k-th device in (1.5) depends *solely* on its local estimate $\hat{\mathbf{H}}^{(k)}$, i.e. the generic k-th device do not need to estimate the information and the decisions at the other devices.

The hierarchical configuration has been exploited in [71] to design a robust precoder for distributed Network MIMO. In Chapters 4, 5 and 6, the hierarchical setup will prove beneficial for achieving beam-domain coordination with *low-complexity*.

Cooperation among	Nature of the Information	Coordination Goal	Chapter
BS and **UE** (Fig. 1.2a)	Location	Single-User Beam Alignment	3
K UEs (Fig. 1.2b)	Out-of-Band and Statistical	Multi-User Beam Selection	4, 5
K BSs (Fig. 1.2c)	Beam Index	Scheduling in Spectrum Sharing	6

Table 1.1 – The coordination scenarios which are studied throughout this thesis.

1.6 Thesis Outline

In this section, we give a brief outline of this dissertation, which gathers, unifies, and extends the work carried out over the duration of the PhD. Table 1.1 summarizes the cooperating scenarios that are studied throughout the thesis. Some example diagrams are provided in Fig. 1.2. This dissertation is composed of 7 chapters, whose short description is given in the following list.

Chapter 1: We have given here an overview on coordination in 5G mobile networks and introduced the motivations for a partial *decentralization* of the future mobile networks. The so-called *Team Decision* formulation helps in raising decentralized coordination problems to the appropriate level of abstraction. Such problems are in general hard to crack and, in most cases, solving them remains an open problem. Nevertheless, we have shown that some distributed information structures of practical relevance can approximate and ease the TD problems.

Chapter 2: In this chapter, we introduce the channel and beam codebook models that will be used throughout the thesis. Furthermore, we highlight the main differences between mmWave and conventional sub-6 GHz propagation environments.

Chapter 3: In this chapter, we consider the first case of Table 1.1, where the BS and the UE aims at performing beam alignment in the mmWave band, exploiting location side-information. To exhibit resilience with respect to the imperfections in the estimation process, we formulate the optimum TD problem and introduce a suite of low-complex algorithms to approximate such non-trivial problem. The proposed robust decentralized beam alignment algorithm closes the gap with the centralized approach, obtained with perfect information. These results were published in:

[72] F. Maschietti, D. Gesbert, P. de Kerret, and H. Wymeersch, "Robust location-aided beam alignment in millimeter wave massive MIMO," *Proc. IEEE GLOBECOM*, Dec. 2017.

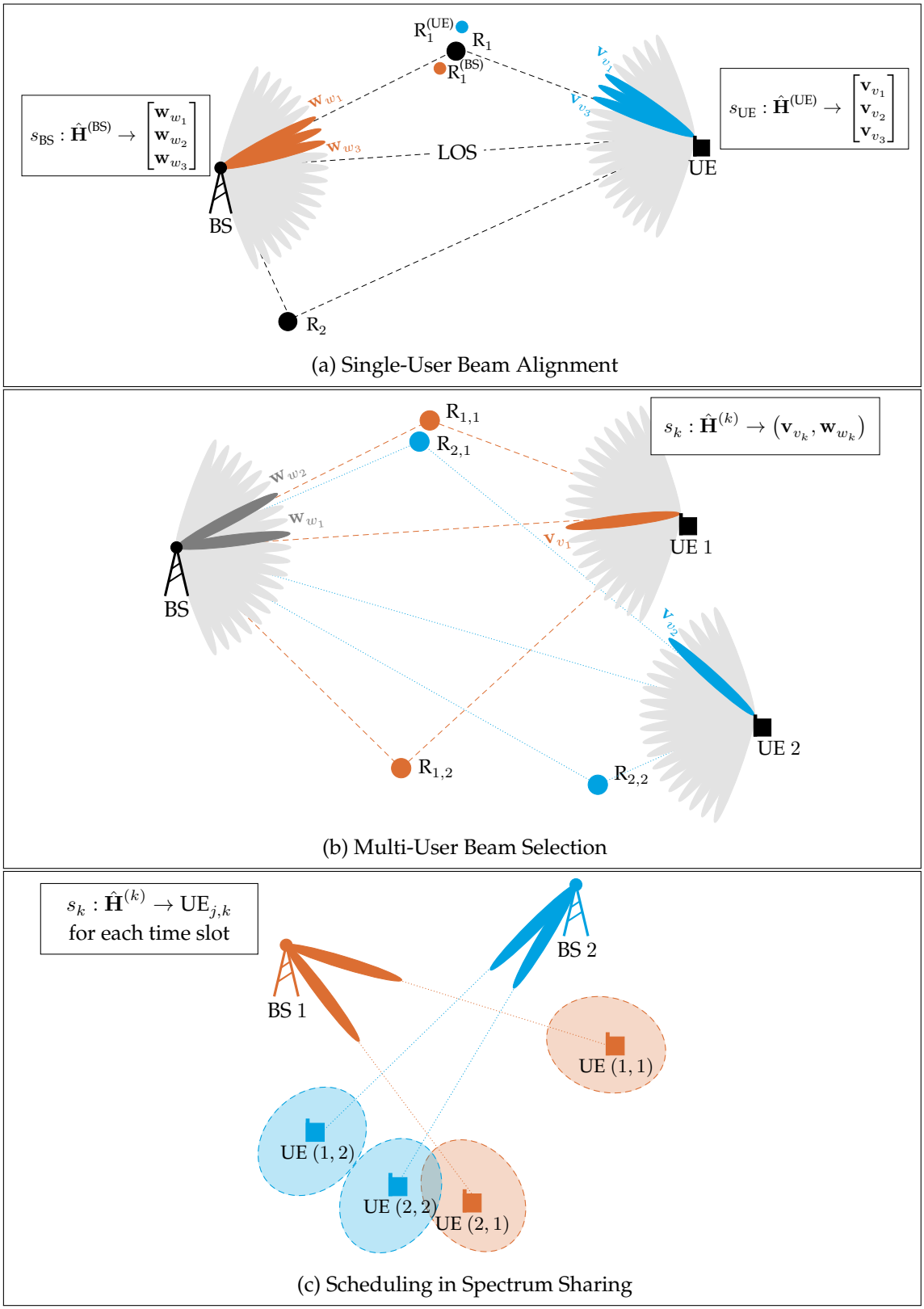

Figure 1.2 – Scenario example for the considered decentralized coordination problems.

Chapter 4: Considering the practical limitations in obtaining location estimates for several UEs, we propose in this chapter an OOB information-aided beam selection algorithm for a mmWave UL scenario, where K UEs coordinate to maximize the sum-rate (refer to Fig. 1.2b). In particular, we exploit the spatial information extracted from the lower (sub-6 GHz) bands in order to assist with an inter-user coordination scheme. The decentralized coordination mechanism allows the suppression of the so-called *co-beam* interference, which would otherwise lead to irreducible interference at the BS side. These results can be found in:

[73] F. Maschietti, D. Gesbert, and P. de Kerret, "Coordinated beam selection in millimeter wave multi-user MIMO using out-of-band information," *Proc. IEEE ICC*, May 2019.

Chapter 5: In this chapter, we expose the existence of an interesting *trade-off* that arises in multi-user beam selection DL scenarios between maximizing the SINR and minimizing the training overhead. This is evident in networks where the *scalability* of the RSs represents one of the main bottlenecks, as e.g. FDD mMIMO networks. We show that such trade-off can be explored through beam-domain coordination among the UEs. In particular, we introduce a suite of coordinated beam selection algorithms in increasing order of *coordination complexity*. The proposed algorithms are capable to strike a balance between CSI acquisition overhead and multi-user interference management using statistical information, through the so-called *covariance shaping*. Simulation results demonstrate the effectiveness of the proposed algorithms, compared to other approaches in the literature, in particular under *rapidly-varying* channels with short coherence time. These results are contained in:

[74] F. Maschietti, G. Fodor, D. Gesbert, and P. de Kerret, "Coordinated beam selection for training overhead reduction in FDD massive MIMO," *Proc. IEEE ISWCS*, Aug. 2019,

and

[75] ——, "User coordination for fast beam training in FDD multi-user massive MIMO," *submitted to IEEE Trans. Wireless Commun.*, Dec. 2019.

Chapter 6: In this chapter, we consider the scenario in Fig. 1.2c, where K BSs belonging to competing mobile operators aim to improve the rate performance of mmWave

spectrum sharing via coordinated user scheduling. We expose an additional, but different trade-off between *coordination* and *privacy* that arises in this context, due to the clear correlation between the exchanged CSI and the location of the UEs. We propose an algorithm capable to strike a balance between spectrum sharing performance and *privacy-preservation* based on the sharing of a low-rate obfuscated beam index information among the BSs. These results were published in:

> [76] F. Maschietti, P. de Kerret, and D. Gesbert, "Exploring the trade-off between privacy and coordination in millimeter wave spectrum sharing," *Proc. IEEE ICC*, May 2019.

Chapter 7: The conclusion chapter, with the results of this thesis and the discussion of the potential research avenues. The manuscript ends with the appendices (proofs), the résumé of the thesis in French and the complete list of the references.

Chapter 2

Models for Massive MIMO and mmWave Communications

In this chapter, we describe the channel and beam codebook models that are used throughout the thesis (except when otherwise mentioned), and introduce the beam-domain representation of the channel that is obtained under such models. The beam-domain representation is a natural choice to cope with the large-dimension of the channels and meet the requirements for *low-latency* Channel State Information (CSI) sharing. Furthermore, we highlight the main differences between the propagation environments in sub-6 GHz and Millimeter Wave (mmWave) (30-300 GHz) bands, and outline how those differences translate into the statistical description of the channel model.

2.1 Geometric Channel Model

We consider the popular two-dimensional geometric channel model in Fig. 2.1, which assumes the existence of L distinct *physical paths* between the Transmitter (TX) and the Receiver (RX)[1]. Let us assume that the TX (resp. the RX) is equipped with N_{TX} (resp. N_{RX}) antennas. The channel matrix $\mathbf{H} \in \mathbb{C}^{N_{\text{RX}} \times N_{\text{TX}}}$ is then expressed as follows [77]:

$$\mathbf{H} \triangleq \sqrt{N_{\text{TX}} N_{\text{RX}}} \sum_{\ell=1}^{L} \alpha_\ell \mathbf{a}_{\text{RX}}(\phi_\ell) \mathbf{a}_{\text{TX}}^{\text{H}}(\theta_\ell), \tag{2.1}$$

where $\alpha_\ell \sim \mathcal{CN}(0, \sigma_\ell^2)$ denotes the complex gain of the ℓ-th path, including the shaping filter and the large-scale path-loss, and where the variables $\phi_\ell \in [0, 2\pi)$ and $\theta_\ell \in [0, 2\pi)$ are the Angle-of-Departure (AoD) and the Angle-of-Arrival (AoA) for the ℓ-th path.

[1] For e.g. Uplink (UL) transmissions, we will have TX = UE and RX = BS.

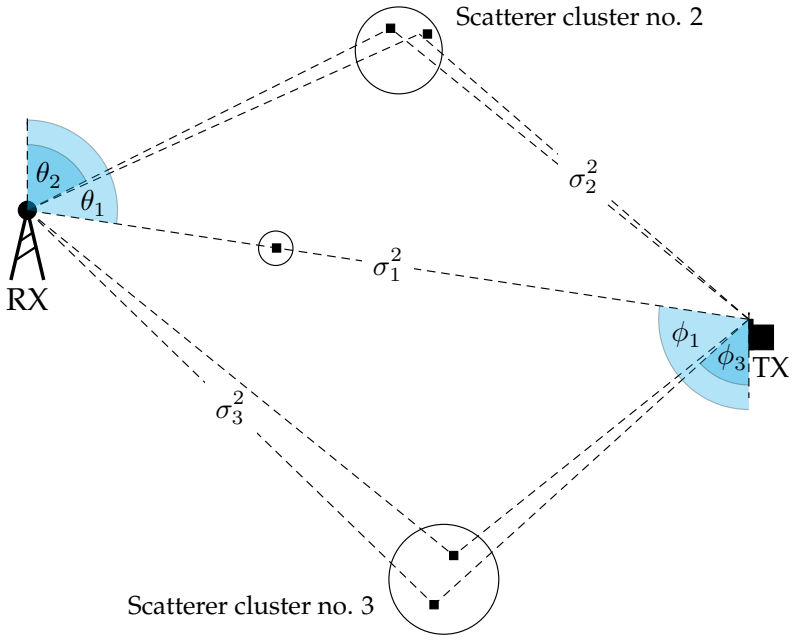

Figure 2.1 – Geometric channel model and notations with 3 clusters of paths.

The vectors $\mathbf{a}_{\text{TX}}(\phi_\ell) \in \mathbb{C}^{N_{\text{TX}} \times 1}$ and $\mathbf{a}_{\text{RX}}(\theta_\ell) \in \mathbb{C}^{N_{\text{RX}} \times 1}$ denote the *unitary* antenna steering vectors at the TX and the RX, for which we consider the well-known *Uniform Linear Array (ULA)* with $\lambda/2$ inter-element spacing. This assumption implies that [78]

$$\mathbf{a}_{\text{TX}}(\phi_\ell) \triangleq \sqrt{\frac{1}{N_{\text{TX}}}} \left[1, e^{-i\pi \cos(\phi_\ell)}, \ldots, e^{-i\pi(N_{\text{TX}}-1)\cos(\phi_\ell)}\right]^{\text{T}}, \tag{2.2}$$

$$\mathbf{a}_{\text{RX}}(\theta_\ell) \triangleq \sqrt{\frac{1}{N_{\text{RX}}}} \left[1, e^{-i\pi \cos(\theta_\ell)}, \ldots, e^{-i\pi(N_{\text{RX}}-1)\cos(\theta_\ell)}\right]^{\text{T}}. \tag{2.3}$$

The channel paths often tend to appear as clusters, i.e. groups of *closely-located* multi-path components that propagate along a similar path (see Fig. 2.1) [78]. One of the biggest advantages of the geometric models is that a large number of different scenarios can be modeled with the same framework, using appropriate input parameters. The parameters of the model can be categorized into statistical and environmental parameters. The statistical parameters describe e.g. the distribution of the clusters in the environment, as well as how the multi-path components are placed within each cluster. The environmental characteristics includes e.g. the dimension of the radio cell and the antenna heights at both ends. In the following, we outline the main propagation differences between sub-6 GHz and mmWave channels, and show how those differences translate into the statistical description of the geometric channel model.

2.1.1 Channel Parameters in Sub-6 GHz Communications

Several measurement campaigns have been carried out to characterize sub-6 GHz Massive MIMO (mMIMO) channels [79]. Although i.i.d. *Rayleigh fading* channels are often considered in the mMIMO literature, such rich-scattering environment is hard to find in practical scenarios, except when large aperture antennas are used. Indeed, some UEs have strong Line-of-Sight (LOS) components and can undergo *spatially-correlated* small-scale fading, with common propagation paths [18]. The geometric channel model is thus appropriate for simulating the sub-6 GHz radio environment, with recommended statistical parameters as in the COST 2100 [80] or the WINNER II frameworks [81].

2.1.2 Channel Parameters in mmWave Communications

The measuring of mmWave channels have received considerable attention, leading to a solid understanding of how these channels differ from sub-6 GHz channels [36, 79, 82]. In general, the propagation environment is adverse for smaller wavelengths: compared with lower bands characteristics, diffraction tends to be lower while penetration or blockage losses can be much greater, due to e.g. foliage and rain [36]. Table I in [82] provides a comprehensive overview on the statistical description of the large-scale channel parameters at 28 and 73 GHz, including the path-loss model and the distribution for the clusters. The measured data in [82] shows that mmWave channels exhibit limited scattering, with few one-bounce reflected paths contributing to the propagation. In this respect, the suggested distribution for the number of clusters follows $\max(\text{Poisson}(1.8), 1)$. Another accurate statistical description for the generation of mmWave channels based on the geometric model is given in [83].

Not all channel characteristics *vary greatly with the frequency*. High correlation has been observed between the temporal and angular characteristics of the LOS path in sub-6 GHz and mmWave channels [84]. The correlation diminishes as the LOS condition is lost, as small scattering objects participating in the radio propagation emerge at higher frequencies [85]. Nevertheless, it has been shown in [86] that, in an outdoor scenario with strong reflectors (buildings), the paths with uncommon AoA at frequencies far apart[2] are less than 10% of the overall paths. The high spatial congruence between sub-6 GHz and mmWave channels can help in deriving low-complex decentralized beam selection strategies, as we will see in Chapter 4.

[2] In [86], 5 carrier frequencies ranging between 900 MHz and 90 GHz have been compared.

2.2 Beam Codebook

Beam-domain representations of the mMIMO channels can be obtained through the use of the Grid-of-Beams (GoB), which slices the actual channels in fixed trasmit-receive spatial directions (refer to Section 1.2). We define the beam codebooks as follows:

$$\mathcal{V} \triangleq \{\mathbf{v}_1, \ldots, \mathbf{v}_{M_{\text{TX}}}\}, \qquad \mathcal{W} \triangleq \{\mathbf{w}_1, \ldots, \mathbf{w}_{M_{\text{RX}}}\}, \tag{2.4}$$

where $\mathbf{v}_v \in \mathbb{C}^{N_{\text{TX}} \times 1}$, $v \in [\![1, M_{\text{TX}}]\!]$, denotes the v-th beamforming vector (or beam) in $\mathcal{V}$, and $\mathbf{w}_w \in \mathbb{C}^{N_{\text{RX}} \times 1}$, $w \in [\![1, M_{\text{RX}}]\!]$, denotes the w-th beamforming vector (or beam) in $\mathcal{W}$.

In the 3GPP standards [34], it is suggested to use Discrete Fourier Transform (DFT) beams for codebook-based transmission, i.e. (at the TX side) $\mathbf{v}_v \in \text{row}\left(\mathbf{F}_{\text{TX}}\right), \forall v$, where $\mathbf{F}_{\text{TX}} \in \mathbb{C}^{N_{\text{TX}} \times N_{\text{TX}}}$ is an N_{TX}-dimensional DFT matrix [78]. Under ULAs, another suitable design for the fixed elements in the codebook consists in selecting the steering vectors in (2.2) and (2.3) over a discrete grid of angles, as follows [87]:

$$\mathbf{v}_v \triangleq \mathbf{a}_{\text{TX}}(\bar{\phi}_v), \quad v \in [\![1, M_{\text{TX}}]\!], \tag{2.5}$$

$$\mathbf{w}_w \triangleq \mathbf{a}_{\text{RX}}(\bar{\theta}_w), \quad w \in [\![1, M_{\text{RX}}]\!], \tag{2.6}$$

where the quantized angles $\bar{\phi}_v$ and $\bar{\theta}_w$ can be chosen according to different sampling strategies of the $[0, \pi]$ range [78].

2.2.1 Beam-Domain Channel Representation

We now introduce the beam-domain representation of the MIMO channel in (2.1). Let us define the matrices $\mathbf{V} \in \mathbb{C}^{N_{\text{TX}} \times M_{\text{TX}}}$ and $\mathbf{W} \in \mathbb{C}^{N_{\text{RX}} \times M_{\text{RX}}}$ as follows:

$$\mathbf{V} \triangleq \begin{bmatrix} \mathbf{v}_1 & \ldots & \mathbf{v}_{M_{\text{TX}}} \end{bmatrix}, \tag{2.7}$$

$$\mathbf{W} \triangleq \begin{bmatrix} \mathbf{w}_1 & \ldots & \mathbf{w}_{M_{\text{RX}}} \end{bmatrix}. \tag{2.8}$$

The beam-domain representation of $\mathbf{H}$, also known as *effective channel* $\bar{\mathbf{H}} \in \mathbb{C}^{M_{\text{RX}} \times M_{\text{TX}}}$ is written as follows:

$$\bar{\mathbf{H}} \triangleq \mathbf{W}^{\text{H}} \mathbf{H} \mathbf{V}. \tag{2.9}$$

An example of beam-domain representation of the channel in (2.1) is shown in Fig. 2.2. The multi-path clusters are *clearly visible* in the beam-domain. In this respect, the coordinated selection of transmit-receive beam pairs can help capturing the strong channel

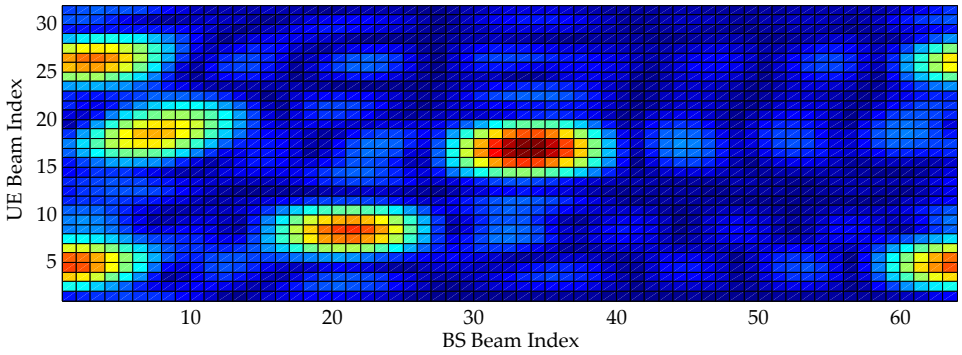

Figure 2.2 – Beam-domain representation of a geometric channel.

gain deriving from one or multiple multi-path clusters. This problem is tackled in the next chapter for the single-user case and in Chapters 4 (UL) and 5 (DL) for the multi-user case.

Chapter 3

Location-Aided Beam Alignment in Single-User mmWave mMIMO

3.1 Introduction

In this chapter, we address the first case of Table 1.1, where the pair Base Station (BS)-User Equipment (UE) aims at performing *beam alignment* so as to establish communication in the Millimeter Wave (mmWave) band. To cope with the constraints exposed in Section 1.2.2, location-aided beam alignment has been proposed for fast link establishment in mmWave [49]. The intuition consists in exploiting location information so as to reduce the effective beam search areas. In this respect, 5G devices are expected to access ubiquitous location information through several technologies [88].

In this work, we consider some important limitation factors which hinder the performance of location-aided beam alignment. First, the UE and the BS are *unlikely* to acquire location information with the same *degree of accuracy*. On the one hand, the location of the BS can be inferred with high precision, being the BS static. In contrast, the location of the UE, due to *mobility*, is harder to infer. In particular, the UE can be expected to have more precise information about its own location compared to the BS, although *unavoidably noisy*. Moreover, practical propagation environments include the presence of some strong reflectors, leading to additional propagation paths. The location information for such reflectors can be assumed available, although with some uncertainties that are most often lower at the BS than at the UE.

We propose a framework for utilizing location side-information in a *doubly* Massive MIMO (mMIMO) setup (i.e. both UE and BS devices are equipped with massive antennas [16]) while accounting for unequal levels of uncertainties on this information at

both the BS and the UE sides. Based on this probabilistic location information setting, the BS and the UE weigh their beam decision upon the *quality* of their local location information and *simultaneously* on the quality level expected at the other end. We recast this problem as a decentralized Team Decision problem where no explicit exchange of information is considered and propose a suite of practical algorithms exploring various *complexity-performance* trade-off levels.

3.2 Models and Scenario

Consider the scenario in Figure 3.1. A BS equipped with $N_{\text{BS}} \gg 1$ antennas aims to establish communication with a single UE with $N_{\text{UE}} \gg 1$ antennas[1]. In order to extract the best possible beamforming gain, a *beam alignment* phase is carried out. The BS aims to select a precoding vector $\mathbf{w} \in \mathcal{W} \subset \mathbb{C}^{N_{\text{BS}} \times 1}$, while the UE aims to select an appropriate receive-side combining vector $\mathbf{v} \in \mathcal{V} \subset \mathbb{C}^{N_{\text{UE}} \times 1}$. Both beamforming vectors (or beams) are from predefined beam codebooks, as defined in Section 2.2.

Exhaustive beam alignment consists in pilot-training all the possible combinations of transmit and receive beams (out of $M_{\text{BS}} M_{\text{UE}}$ pairs) and selecting the pair which exhibits the highest Signal-to-Noise Ratio (SNR). In the mMIMO regime, this requires prohibitive pilot, power and time resources. As a result, a method for pruning out *unlikely* beam combinations is desirable. To this end, we assume that the BS (resp. the UE) pre-selects a subset of $D_{\text{BS}} \ll M_{\text{BS}}$ (resp. $D_{\text{UE}} \ll M_{\text{UE}}$) beams for subsequent pilot training. When the pre-selection phase is over, the BS trains the pre-selected beams through sending Reference Signal (RS) for each one of the D_{BS} beams, while the UE is allowed to make SNR measurements over each of its D_{UE} beams.

In this work, we are interested in deriving beam subset pre-selection strategies that do not require *any* active channel sounding but can be carried out on the basis of long-term statistical information including location-dependent information for the BS and the UE as introduced in [49]. In contrast with [49], we consider potential reflector location information and, in particular, we place the emphasis on robustness with respect to location uncertainties in a *high-mobility* scenario. The model for the long-term location information, and corresponding uncertainties, are introduced in the following. The channel model is the geometric model defined in Section 2.1.

[1] In the rest of this chapter, we assume an Uplink (UL) transmission, although all concepts and algorithms are applicable to the Downlink (DL) as well.

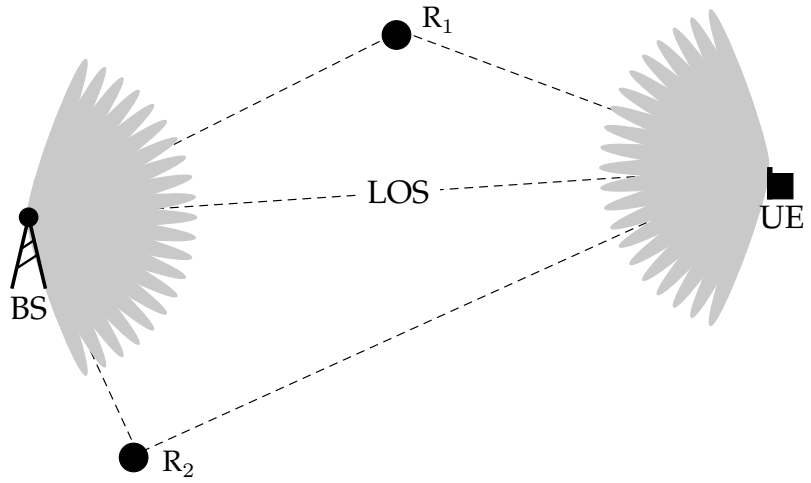

Figure 3.1 – Scenario example with one LOS path and two reflected NLOS paths.

3.3 Information Model

As discussed above, we are interested in exploiting long-term statistical information to perform beam pre-selection. Unlike prior work, the emphasis of this work lies in the accounting for uncertainties in the acquisition of such information at the BS and the UE. In what follows, we introduce the information model emphasizing the decentralized nature of information available at both the BS and UE sides. In particular, we will consider the *noisy* distributed model, described in Section 1.5.2 and outlined in Fig. 3.2.

3.3.1 Definition of the Model

In order to establish a reference case, we consider the setting where the available information allows to define the average SNR that would be obtained under *any* transmit-receive beam selection. To this end, we define the average beam gain matrix.

Definition 3.1. The average beam gain matrix $\mathbf{G} \in \mathbb{R}^{M_{\text{UE}} \times M_{\text{BS}}}$ contains the power level associated with each combined choice of transmit-receive beam pair after averaging over small scale fading. The (v, w)-th element of $\mathbf{G}$ is defined as

$$G_{v,w} \triangleq \mathbb{E}_{\boldsymbol{\alpha}} \left[\left| \mathbf{w}_w^{\text{H}} \mathbf{H} \mathbf{v}_v \right|^2 \right], \tag{3.1}$$

where the expectation is carried out over the channel coefficients $\boldsymbol{\alpha} = [\alpha_1, \ldots, \alpha_L]$.

We now introduce the position matrix, containing the location information for all the entities in the considered scenario.

Definition 3.2. The position matrix $\mathbf{P} \in \mathbb{R}^{2\times(L+1)}$ contains the two-dimensional location coordinates $\mathbf{p}_n = [x_n \quad y_n]^{\mathrm{T}}$ for node n, where n refers to either the BS, the UE or one of the reflectors $\mathrm{R}_m, m = 1, \ldots, L-1$. It is defined as follows:

$$\mathbf{P} \triangleq \begin{bmatrix} \mathbf{p}_{\mathrm{BS}} & \mathbf{p}_{\mathrm{R}_1} & \cdots & \mathbf{p}_{\mathrm{R}_{L-1}} & \mathbf{p}_{\mathrm{UE}} \end{bmatrix}. \tag{3.2}$$

The following lemma characterizes the average beam gain matrix $\mathbf{G}$ as a function of the position matrix $\mathbf{P}$, considering the channel and codebook models in Chapter 2.

Lemma 3.1. *We can write the (v, w)-th element of the average beam gain matrix $\mathbf{G}$ as*

$$G_{v,w}(\mathbf{P}) = \sum_{\ell=1}^{L} \sigma_\ell^2 \left| L_{\mathrm{UE}}(\Delta_{\ell,v}) \right|^2 \left| L_{\mathrm{BS}}(\Delta_{\ell,w}) \right|^2, \tag{3.3}$$

where we remind the reader that σ_ℓ^2 denotes the variance of the channel coefficients α_ℓ in (2.1) and we have defined:

$$L_{\mathrm{BS}}(\Delta_{\ell,w}) \triangleq \sqrt{\frac{1}{N_{\mathrm{BS}}}} \frac{e^{i(\pi/2)\Delta_{\ell,w}}}{e^{i(\pi/2)N_{\mathrm{BS}}\Delta_{\ell,w}}} \frac{\sin((\pi/2)N_{\mathrm{BS}}\Delta_{\ell,w})}{\sin((\pi/2)\Delta_{\ell,w})}, \tag{3.4}$$

$$L_{\mathrm{UE}}(\Delta_{\ell,v}) \triangleq \sqrt{\frac{1}{N_{\mathrm{UE}}}} \frac{e^{i(\pi/2)\Delta_{\ell,v}}}{e^{i(\pi/2)N_{\mathrm{UE}}\Delta_{\ell,v}}} \frac{\sin((\pi/2)N_{\mathrm{UE}}\Delta_{\ell,v})}{\sin((\pi/2)\Delta_{\ell,v})}, \tag{3.5}$$

and

$$\Delta_{\ell,w} \triangleq (\cos(\bar{\theta}_w) - \cos(\theta_\ell)), \tag{3.6}$$

$$\Delta_{\ell,v} \triangleq (\cos(\phi_\ell) - \cos(\bar{\phi}_v)), \tag{3.7}$$

with the angles $\phi_\ell, \ell = 1, \ldots, L$ and $\theta_\ell, \ell = 1, \ldots, L$ obtained from the position matrix $\mathbf{P}$ using simple algebra (the detailed steps are relegated to Appendix A.1).

Proof. Refer to Appendix A.1. □

Note that it is possible to ignore the second terms in (3.4) and (3.5), as we aim to compute the squared absolute value in (3.3).

3.3.2 Distributed Information Model

In a realistic setting where both BS and UE *separately* acquire location information via a *noisy* process of Global Navigation Satellite System (GNSS)-based estimation, Angle-of-Arrival (AoA) estimation (for reflector position estimation) and *latency-prone* BS-UE feedback, a distributed position information model ensues where the positioning accuracies are *device-dependent*, i.e. different at BS and UE.

Noisy information model at the BS: The position matrix $\hat{\mathbf{P}}^{(\mathrm{BS})}$ available at the BS is modeled as follows:

$$\hat{\mathbf{P}}^{(\mathrm{BS})} \triangleq \mathbf{P} + \mathbf{E}^{(\mathrm{BS})} \tag{3.8}$$

where $\mathbf{E}^{(\mathrm{BS})}$ is

$$\mathbf{E}^{(\mathrm{BS})} \triangleq \begin{bmatrix} \mathbf{e}_{\mathrm{BS}}^{(\mathrm{BS})} & \mathbf{e}_{\mathrm{R}_1}^{(\mathrm{BS})} & \dots & \mathbf{e}_{\mathrm{R}_{L-1}}^{(\mathrm{BS})} & \mathbf{e}_{\mathrm{UE}}^{(\mathrm{BS})} \end{bmatrix}, \tag{3.9}$$

containing the random position estimation error made by the BS on $\mathbf{p}_n$, with known *arbitrary* Probability Density Function (PDF) $f_{\mathbf{e}_n^{(\mathrm{BS})}}$.

Noisy information model at the UE: Akin to the BS side, the UE obtains the estimate $\hat{\mathbf{P}}^{(\mathrm{UE})}$, where:

$$\hat{\mathbf{P}}^{(\mathrm{UE})} \triangleq \mathbf{P} + \mathbf{E}^{(\mathrm{UE})} \tag{3.10}$$

where $\mathbf{E}^{(\mathrm{UE})}$ is defined as $\mathbf{E}_{(\mathrm{BS})}$ in (3.9), but containing the random position estimation error made by the UE on $\mathbf{p}_n$, with a known *arbitrary* PDF $f_{\mathbf{e}_n^{(\mathrm{UE})}}$.

3.3.3 Shared Information

In what follows, we assume that both the BS and the UE knows the number of dominant paths L, and their average path powers $\sigma_\ell^2, \ell = 1, \dots, L$ based on prior averaged measurements. Likewise, the statistical distributions $f_{\mathbf{e}_n^{(\mathrm{BS})}},\ \forall n$ and $f_{\mathbf{e}_n^{(\mathrm{UE})}},\ \forall n$ are supposed to be quasi-static and as such are supposed to be available (or estimated) at both the BS and UE sides. In other words, the BS (resp. the UE) is aware of the *quality* for position estimates which it and the UE (resp. BS) have at their disposal. For instance, the BS might know less about the UE location than the UE itself, as e.g. due to *latency* in communicating the UE position to the BS in a mobile scenario or due to the use of different position technologies (*Global Positioning System (GPS)* at the UE, *Time Difference of Arrival (TDOA)* localization at the BS). In contrast, the BS might have greater capabilities to estimate the position of the reflectors accurately compared to the UE, due to a larger number of antennas at the BS or due to interactions with multiple UEs. Both the BS and the UE are aware of this situation and wish to exploit it for greater coordination performance. The central question of this work is "*how?*".

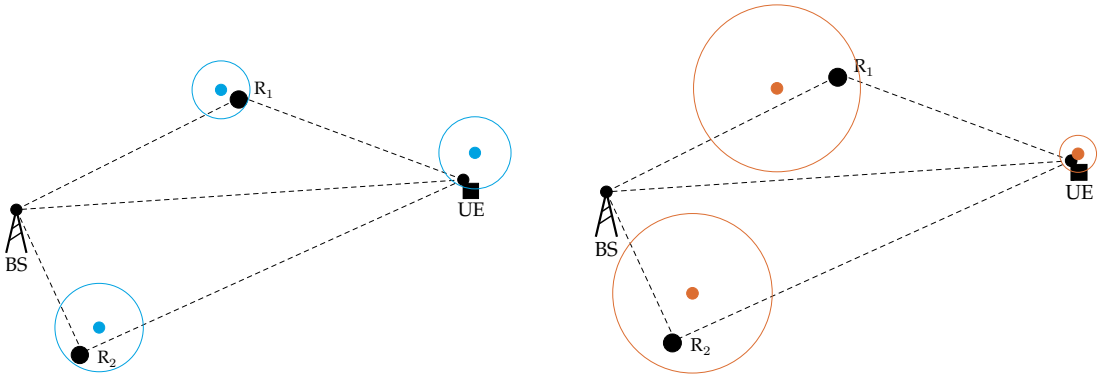

(a) View at the BS (b) View at the UE

Figure 3.2 – Example of the distributed location information setting. The estimated location information is denoted with blue (at the BS side) and orange (at the UE side) points, along with their *uncertainty* circles. The black points represent the actual locations. In this sketch, a bounded error model is assumed.

3.4 Coordinated Beam Alignment Methods

In this section, we present several strategies for coordinated beam alignment. The aim of such strategies is to restore robustness in the beam pre-selection phase in the face of the estimation noise in the location estimates at both sides, as shown in (3.8) and (3.10).

Let $\mathcal{D}_{\text{BS}} \subset \mathcal{W}$ (resp. $\mathcal{D}_{\text{UE}} \subset \mathcal{V}$) be the set of $D_{\text{BS}} = |\mathcal{D}_{\text{BS}}|$ (resp. $D_{\text{UE}} = |\mathcal{D}_{\text{UE}}|$) pre-selected beams at the BS (resp. the UE). In order to pre-select the beams, we will use the following figure of merit $\mathbb{E}[\mathcal{R}(\mathcal{D}_{\text{BS}}, \mathcal{D}_{\text{UE}}, \mathbf{P})]$, where:

$$\mathcal{R}(\mathcal{D}_{\text{BS}}, \mathcal{D}_{\text{UE}}, \mathbf{P}) \triangleq \max_{v \in \mathcal{D}_{\text{UE}}, w \in \mathcal{D}_{\text{BS}}} \log_2 \left(1 + \frac{G_{v,w}(\mathbf{P})}{\sigma_n^2}\right) \tag{3.11}$$

where N_0 is the thermal noise power[2].

3.4.1 Beam Alignment under Perfect Information

Before introducing the distributed approaches to this problem, we focus on the idealized benchmark, where both the BS and the UE obtain the perfect position matrix $\mathbf{P}$.

The optimal beam sets $(\mathcal{D}_{\text{BS}}^{\text{up}}, \mathcal{D}_{\text{UE}}^{\text{up}})$ which maximize the transmission rate are then found as follows:

$$(\mathcal{D}_{\text{BS}}^{\text{up}}, \mathcal{D}_{\text{UE}}^{\text{up}}) = \underset{\mathcal{D}_{\text{BS}} \subset \mathcal{W}, \mathcal{D}_{\text{UE}} \subset \mathcal{V}}{\text{argmax}} \mathcal{R}(\mathcal{D}_{\text{BS}}, \mathcal{D}_{\text{UE}}, \mathbf{P}). \tag{3.12}$$

[2]We assume for simplification an interference-free network.

3.4.2 Optimal Bayesian Beam Alignment

Let us now consider the core of this work where the BS and the UE must make beam pre-selection decisions in a decentralized manner, based on their respective location information in (3.8) and (3.10). We recast this problem as a Team Decision problem, where the team members, i.e. the BS and the UE seek to coordinate their actions so as to maximize their transmission rate, while not being able to *accurately* predict each other decision due to distributed observations. For instance, let us consider the example scenario in 3.1 and $D_{\text{BS}} = D_{\text{UE}} = 2$. The BS might decide to beam in the direction of the UE and R_1, while the UE might decide to beam in the direction of the BS but also R_2 (for example, if its information on the position of R_1 is not accurate enough). As a result, a strong mismatch would be obtained for one of the pre-selected beam pairs. Moreover, due to the noise in the information, beaming towards e.g. the presumed location of the UE might not achieve high beamforming gain at the actual UE. The goal of the robust decentralized algorithm is hence to avoid such inefficient behavior.

Beam pre-selection at the BS is equivalent to the following mapping:

$$s_{\text{BS}}: \quad \mathbb{R}^{2\times(L+1)} \to \mathcal{W} \tag{3.13}$$

$$\hat{\mathbf{P}}^{(\text{BS})} \mapsto s_{\text{BS}}\left(\hat{\mathbf{P}}^{(\text{BS})}\right), \tag{3.14}$$

whereas at the UE, we have:

$$s_{\text{UE}}: \quad \mathbb{R}^{2\times(L+1)} \to \mathcal{V} \tag{3.15}$$

$$\hat{\mathbf{P}}^{(\text{UE})} \mapsto s_{\text{UE}}\left(\hat{\mathbf{P}}^{(\text{UE})}\right) \tag{3.16}$$

Let $\mathcal{S}$ denote the space containing all the possible choices of pairs of such functions. The *optimally-robust* team decision strategies $\left(s^*_{\text{BS}}, s^*_{\text{UE}}\right) \in \mathcal{S}$ which maximize the expected rate can be found through solving the following optimization problem:

$$\left(s^*_{\text{BS}}, s^*_{\text{UE}}\right) = \underset{(s_{\text{BS}}, s_{\text{UE}})\in\mathcal{S}}{\operatorname{argmax}} \mathbb{E}_{\mathbf{P},\hat{\mathbf{P}}^{(\text{BS})},\hat{\mathbf{P}}^{(\text{UE})}}\left[\mathcal{R}\left(s_{\text{BS}}\left(\hat{\mathbf{P}}^{(\text{BS})}\right), s_{\text{UE}}\left(\hat{\mathbf{P}}^{(\text{UE})}\right), \mathbf{P}\right)\right], \tag{3.17}$$

where the expectation operator is carried out over the joint PDF $f_{\mathbf{P},\hat{\mathbf{P}}^{(\text{BS})},\hat{\mathbf{P}}^{(\text{UE})}}$.

The optimization in (3.17) is a non-trivial stochastic functional optimization problem [89]. In order to circumvent this problem, we now examine several approximation strategies which offer a range of trade-offs between the *optimal robustness* of (3.17) and the *implementation complexity*.

3.4.3 Naive-Coordinated Beam Alignment

A simple, yet naive, implementation of decentralized coordination mechanisms consists in having each side making its decision by treating (mistaking) local information as perfect and global. Thus, the BS and the UE solve for (3.12), where the BS assumes $\hat{\mathbf{P}}^{(\text{BS})} = \mathbf{P}$ and the UE assumes $\hat{\mathbf{P}}^{(\text{UE})} = \mathbf{P}$. We denote the resulting mappings as $\left(s_{\text{BS}}^{\text{naive}}, s_{\text{UE}}^{\text{naive}}\right) \in \mathcal{S}$, which are found as follows:

- Optimization at the BS:

$$s_{\text{BS}}^{\text{naive}}\left(\hat{\mathbf{P}}^{(\text{BS})}\right) = \underset{\mathcal{D}_{\text{BS}}\subset\mathcal{W}}{\text{argmax}} \max_{\mathcal{D}_{\text{UE}}\subset\mathcal{V}} \mathcal{R}\left(\mathcal{D}_{\text{BS}}, \mathcal{D}_{\text{UE}}, \hat{\mathbf{P}}^{(\text{BS})}\right); \tag{3.18}$$

- Optimization at the UE:

$$s_{\text{UE}}^{\text{naive}}\left(\hat{\mathbf{P}}^{(\text{UE})}\right) = \underset{\mathcal{D}_{\text{UE}}\subset\mathcal{V}}{\text{argmax}} \max_{\mathcal{D}_{\text{BS}}\subset\mathcal{W}} \mathcal{R}\left(\mathcal{D}_{\text{BS}}, \mathcal{D}_{\text{UE}}, \hat{\mathbf{P}}^{(\text{UE})}\right), \tag{3.19}$$

which can be solved through exhaustive set search or a low-complex *greedy* approach (see details later). The basic limitation of the naive approach is that it fails to account for both *i)* the noise in the location estimates at the decision makers, and *ii)* the discrepancies in the uncertainties of such estimates. Indeed, the BS (resp. the UE) assumes that the UE (resp. the BS) receives the same estimate and take its decision on this basis.

3.4.4 1-Step Robust Coordinated Beam Alignment

Taking one step towards robustness requires from the BS and the UE to account for their own local information noise. In particular, each decision-making device can assume that its local estimate, while not perfect, is at least *globally shared*, i.e. that $\hat{\mathbf{P}}^{(\text{BS})} = \hat{\mathbf{P}}^{(\text{UE})}$ for the purpose of algorithm derivation. We denote the resulting beam pre-selection as *1-Step robust* – obtained through the mappings $\left(s_{\text{BS}}^{\text{1-s}}, s_{\text{UE}}^{\text{1-s}}\right) \in \mathcal{S}$ as follows:

- Optimization at the BS:

$$s_{\text{BS}}^{\text{1-s}}\left(\hat{\mathbf{P}}^{(\text{BS})}\right) = \underset{\mathcal{D}_{\text{BS}}\subset\mathcal{W}}{\text{argmax}} \max_{\mathcal{D}_{\text{UE}}\subset\mathcal{V}} \mathbb{E}_{\mathbf{P}|\hat{\mathbf{P}}^{(\text{BS})}}\Big[\mathcal{R}\left(\mathcal{D}_{\text{BS}}, \mathcal{D}_{\text{UE}}, \mathbf{P}\right)\Big]; \tag{3.20}$$

- Optimization at the UE:

$$s_{\text{UE}}^{\text{1-s}}\left(\hat{\mathbf{P}}^{(\text{UE})}\right) = \underset{\mathcal{D}_{\text{UE}}\subset\mathcal{V}}{\text{argmax}} \max_{\mathcal{D}_{\text{BS}}\subset\mathcal{W}} \mathbb{E}_{\mathbf{P}|\hat{\mathbf{P}}^{(\text{UE})}}\Big[\mathcal{R}\left(\mathcal{D}_{\text{BS}}, \mathcal{D}_{\text{UE}}, \mathbf{P}\right)\Big]. \tag{3.21}$$

Optimization (3.17) is therefore replaced with a more standard stochastic optimization problem for which a vast literature is available [90]. Considering w.l.o.g. the optimization at the BS, one standard approach consists in approximating the expectation through Monte-Carlo iterations according to the PDF $f_{\mathbf{P}|\hat{\mathbf{P}}^{(\mathrm{BS})}}$. Once the discrete summation replaces the expectation operator, the optimal solution of the optimization problem can be again obtained through sequential search. Indeed, the nature of the problem is such that it is possible to split (3.20) and (3.21) in multiple maximizations – over the single beams in $\mathcal{V}$ and $\mathcal{W}$ – *without loosing optimality*. The proposed 1-Step robust approach is summarized in Algorithm 1, showing what is done at the BS side. The UE runs the same algorithm with inputs $\hat{\mathbf{P}}^{(\mathrm{UE})}$ and $f_{\mathbf{e}_n^{(\mathrm{UE})}}$, $\forall n$, where in line 5 the max is instead operated over columns.

Algorithm 1 1-Step Robust Beam Alignment (BS side)

INPUT: $\hat{\mathbf{P}}^{(\mathrm{BS})}$, $f_{\mathbf{e}_n^{(\mathrm{BS})}}$, $\forall n$

1: **for** $i = 1 : \mathrm{MCT}$ **do** ▷ Approximate the expectation over $\mathbf{P}|\hat{\mathbf{P}}^{(\mathrm{BS})}$ with MCT Monte-Carlo iterations

2: Compute possible position matrix $\hat{\mathbf{P}} = \hat{\mathbf{P}}^{(\mathrm{BS})} - \mathbf{E}^{(\mathrm{BS})}$, with $\mathbf{E}^{(\mathrm{BS})}$ generated according to $f_{\mathbf{e}^{(\mathrm{BS})}}$

3: Compute possible gain matrix $\hat{\mathbf{G}}$ through (A.3) and (3.3)

4: $\mathbf{M}(:, i) = \max(\hat{\mathbf{G}}^{(\mathrm{BS})}, \text{“rows"})$ ▷ Find the max for each column

5: **end for**

6: $\mathrm{Idx} = \mathrm{sort}(\mathrm{mean}(\mathbf{M}, \text{“columns"}), \text{“descending"})$ ▷ Order the beams after averaging over the for loop

7: $\mathcal{D}_{\mathrm{BS}} = \mathrm{Idx}(1 : D_{\mathrm{BS}})$ ▷ The first D_{BS} beams are pre-selected for pilot transmission

The proposed greedy approach has much less computational cost than the exhaustive search, which requires to search over all the combinations resulting from picking D_{BS} (resp. D_{UE}) beams at a time among M_{BS} (resp. M_{UE}). Note that the approach above provides robustness with respect to the local noise at the decision makers; it however fails to account for discrepancies in location uncertainties across the BS and the UE.

3.4.5 2-Step Robust Coordinated Beam Alignment

An *optimality condition* for the robust Bayesian beam alignment in (3.17) is that it is *person-by-person* (PP) optimal, i.e. the decision makers take the best strategies given the strategies at the other devices [89]. The PP optimal solution $\left(s_{\text{BS}}^{\text{PP}}, s_{\text{UE}}^{\text{PP}}\right) \in \mathcal{S}$ satisfies the following fixed point equations:

- Optimization at the BS:

$$s_{\text{BS}}^{\text{PP}}\left(\hat{\mathbf{P}}^{(\text{BS})}\right) = \underset{\mathcal{D}_{\text{BS}} \subset \mathcal{W}}{\operatorname{argmax}}\, \mathbb{E}_{\mathbf{P}, \hat{\mathbf{P}}^{(\text{UE})} | \hat{\mathbf{P}}^{(\text{BS})}} \left[\mathcal{R}\left(\mathcal{D}_{\text{BS}}, s_{\text{UE}}^{\text{PP}}\left(\hat{\mathbf{P}}^{(\text{UE})}\right), \mathbf{P}\right) \right]; \tag{3.22}$$

- Optimization at the UE:

$$s_{\text{UE}}^{\text{PP}}\left(\hat{\mathbf{P}}^{(\text{UE})}\right) = \underset{\mathcal{D}_{\text{UE}} \subset \mathcal{V}}{\operatorname{argmax}}\, \mathbb{E}_{\mathbf{P}, \hat{\mathbf{P}}^{(\text{BS})} | \hat{\mathbf{P}}^{(\text{UE})}} \left[\mathcal{R}\left(s_{\text{BS}}^{\text{PP}}\left(\hat{\mathbf{P}}^{(\text{BS})}\right), \mathcal{D}_{\text{UE}}, \mathbf{P}\right) \right]. \tag{3.23}$$

The interdependence between (3.22) and (3.23) makes solving the PP optimum challenging. Thus, we propose an approximate solution in which this dependence is removed. In particular, we replace the PP mapping inside the expectation operator with the 1-Step robust mapping defined in Section 3.4.4.

The intuition is that the BS (resp. the UE) makes its beam selection using the belief that the UE (resp. the BS) is using the 1-Step robust mapping at its side. Such mapping can be computed thanks to (3.20) and (3.21). In the 2-Step algorithm, both local noise statistics and differences between the uncertainties at both sides are thus exploited. We denote with $\left(s_{\text{BS}}^{\text{2-s}}, s_{\text{UE}}^{\text{2-s}}\right) \in \mathcal{S}$ the 2-Step robust approach, which reads as:

- Optimization at the BS:

$$s_{\text{BS}}^{\text{2-s}}\left(\hat{\mathbf{P}}^{(\text{BS})}\right) = \underset{\mathcal{D}_{\text{BS}} \subset \mathcal{W}}{\operatorname{argmax}}\, \mathbb{E}_{\mathbf{P}, \hat{\mathbf{P}}^{(\text{UE})} | \hat{\mathbf{P}}^{(\text{BS})}} \left[\mathcal{R}\left(\mathcal{D}_{\text{BS}}, s_{\text{UE}}^{\text{1-s}}\left(\hat{\mathbf{P}}^{(\text{UE})}\right), \mathbf{P}\right) \right]; \tag{3.24}$$

- Optimization at the UE:

$$s_{\text{UE}}^{\text{2-s}}\left(\hat{\mathbf{P}}^{(\text{UE})}\right) = \underset{\mathcal{D}_{\text{UE}} \subset \mathcal{V}}{\operatorname{argmax}}\, \mathbb{E}_{\mathbf{P}, \hat{\mathbf{P}}^{(\text{BS})} | \hat{\mathbf{P}}^{(\text{UE})}} \left[\mathcal{R}\left(s_{\text{BS}}^{\text{1-s}}\left(\hat{\mathbf{P}}^{(\text{BS})}\right), \mathcal{D}_{\text{UE}}, \mathbf{P}\right) \right]. \tag{3.25}$$

The proposed 2-Step algorithm is summarized in Algorithm 2. Compared to the 1-Step approach, the statistics of both the BS and the UE are taken into account in Algorithm 2.

Remark 3.1. This approach could then be extended through the insertion of the 2-Step robust mapping inside the expectation operator, so as to get the 3-step robust approach, and so forth. Of course, it comes with an increased computational cost. □

Algorithm 2 2-Step Robust Beam Alignment (BS side)

INPUT: $\hat{\mathbf{P}}^{(\text{BS})}$, $f_{\mathbf{e}_n^{(\text{BS})}}$, $\forall n$, $f_{\mathbf{e}_n^{(\text{UE})}}$, $\forall n$

for $i = 1 : \text{MCT}$ **do** ▷ Approximate the expectation over $\mathbf{P}|\hat{\mathbf{P}}^{(\text{BS})}$ with MCT Monte-Carlo iterations
  Compute possible position matrix $\hat{\mathbf{P}} = \hat{\mathbf{P}}^{(\text{BS})} - \mathbf{E}^{(\text{BS})}$, with $\mathbf{E}^{(\text{BS})}$ generated according to $f_{\mathbf{e}^{(\text{BS})}}$
  Compute possible gain matrix $\hat{\mathbf{G}}$ through (A.3) and (3.3)
  for $l = 1 : \text{MCT}$ **do** ▷ MCT Monte-Carlo iterations over $\hat{\mathbf{P}}^{(\text{UE})}|\hat{\mathbf{P}}^{(\text{BS})}$
    Compute possible position matrix $\hat{\hat{\mathbf{P}}} = \hat{\mathbf{P}} + \mathbf{E}^{(\text{UE})}$, with $\mathbf{E}^{(\text{UE})}$ generated according to $f_{\mathbf{e}^{(\text{UE})}}$
    Compute possible gain matrix $\hat{\hat{\mathbf{G}}}$ through (A.3) and (3.3)
    $\tilde{\mathbf{M}}(:, l) = \max(\hat{\hat{\mathbf{G}}}, \text{“columns"})$ ▷ Find the max for each row
  end for
  $\text{Idx} = \text{sort}(\text{mean}(\tilde{\mathbf{M}}, \text{“columns"}), \text{“descending"})$ ▷ Order the beams after averaging over the loop
  $\mathbf{M}(:, i) = \max(\hat{\mathbf{G}}(\text{Idx}(1 : D_{\text{UE}}), :), \text{“rows"})$ ▷ Find the max over the columns associated to $s_{\text{UE}}^{\text{1-s}}$
end for
$\text{Idx} = \text{sort}(\text{mean}(\mathbf{M}, \text{“columns"}), \text{“descending"})$ ▷ Order the beams after averaging over the for loop
$\mathcal{D}_{\text{BS}} = \text{Idx}(1 : D_{\text{BS}})$ ▷ The first D_{BS} beams are pre-selected for pilot transmission

3.5 Simulation Results for the Single-User Scenario

We consider the scenario in Fig. 3.1, with $L = 3$ multi-path components. A distance of 100 m is assumed from the BS to the UE. Both the BS and the UE are equipped with $N_{\text{BS}} = N_{\text{UE}} = 64$ antennas. We assume that the devices have to choose D_{BS} and D_{UE} beams among the $M_{\text{BS}} = M_{\text{UE}} = 64$ in the codebooks. The plotted transmission rates are the averaged – over 10000 Monte-Carlo iterations – instantaneous rates.

3.5.1 Beam Codebook Design

Since ULAs produce unequal beamwidths depending on the pointing direction – wider through the endfire direction, tighter through the broadside direction [78] – we separate the grid angles $\bar{\phi}_p$ and $\bar{\theta}_q$ according to the inverse cosine function, as follows:

$$\bar{\phi}_v = \arccos\left(1 - \frac{2(v-1)}{M_{\text{UE}} - 1}\right), \quad v \in [\![1, M_{\text{UE}}]\!], \tag{3.26}$$

$$\bar{\theta}_w = \arccos\left(1 - \frac{2(w-1)}{M_{\text{BS}} - 1}\right), \quad w \in [\![1, M_{\text{BS}}]\!]. \tag{3.27}$$

As a result, and in order to guarantee equal gain losses among the adjacent angles, more of the latter are considered as the broadside direction is reached.

3.5.2 Location Information Model

In the simulations, we use a uniform bounded error model for the location information [91]. In particular, we assume that all the location estimates lie somewhere inside disks centered in the actual positions $\mathbf{p}_n$, $\forall n$. Let $S(r)$ be the two-dimensional closed ball centered at the origin and of radius r, i.e.

$$S(r) = \left\{ \mathbf{p} \in \mathbb{R}^2 : \|\mathbf{p}\|_2 \leq r \right\}. \tag{3.28}$$

We model the random estimation errors as follows:

- $\mathbf{e}_n^{(\mathrm{BS})}$ *uniformly distributed* in $S\left(r_n^{(\mathrm{BS})}\right)$;
- $\mathbf{e}_n^{(\mathrm{UE})}$ *uniformly distributed* in $S\left(r_n^{(\mathrm{UE})}\right)$,

where $r_n^{(\mathrm{BS})}$ and $r_n^{(\mathrm{UE})}$ are the maximum positioning error for node n as seen from the BS and the UE.

3.5.3 Results and Discussion

According to measurement campaigns [82,92], LOS propagation is the prominent propagation driver in mmWave bands. As a consequence, we consider a stronger (on average) LOS path, with respect to the reflected paths. The latter are assumed to have the same average power. Moreover, we consider the following degrees of precision for the location information and denote them as the set of settings $\mathcal{A}$:

- $r_{\mathrm{UE}}^{(\mathrm{BS})} = 13$ m, $r_{\mathrm{UE}}^{(\mathrm{UE})} = 7$ m;
- $r_{\mathrm{R}_1}^{(\mathrm{BS})} = 11$ m, $r_{\mathrm{R}_1}^{(\mathrm{UE})} = 18$ m;
- $r_{\mathrm{R}_2}^{(\mathrm{BS})} = 15$ m, $r_{\mathrm{R}_2}^{(\mathrm{UE})} = 17$ m;
- $r_{\mathrm{BS}}^{(\mathrm{BS})} = 0$ m, $r_{\mathrm{BS}}^{(\mathrm{UE})} = 0$ m.

In general, those values are tied up together so that it is unrealistic to have e.g. small uncertainties for the reflectors (reflecting points) associated to big uncertainties for the UE. Indeed, the location of the reflecting point depends on the location of the devices. Given that 5G devices are expected to access position information with a guaranteed precision of about 1 m in open areas [88], those settings are robust with respect to the *mobility* of the devices or to possible discontinuous location awareness.

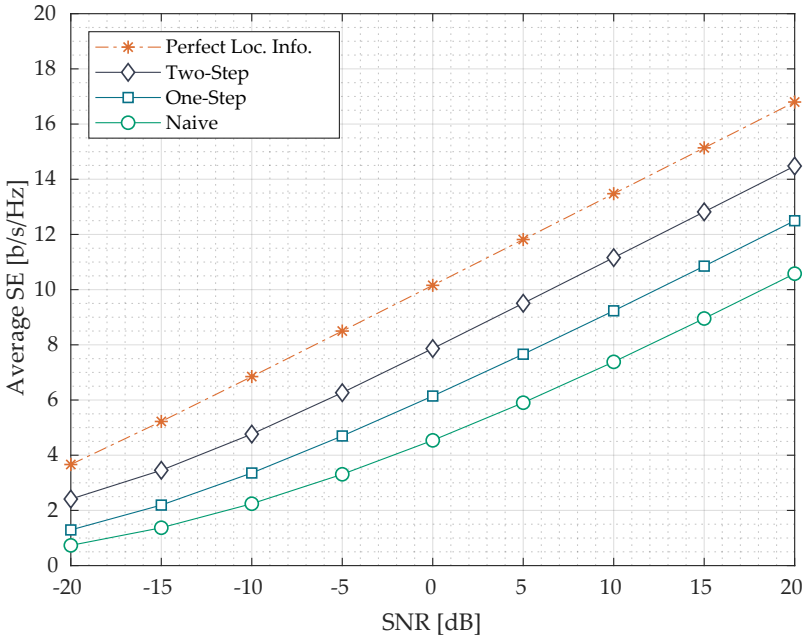

Figure 3.3 – SE vs SNR. Stronger LOS path, settings $\mathcal{A}$ and $D_{\text{BS}} = D_{\text{UE}} = 4$.

Fig. 3.3 compares the proposed algorithms in the settings $\mathcal{A}$, showing the Spectral Efficiency (SE) as a function of the SNR. The 2-Step robust approach outperforms the other distributed solutions, being able to consider the noise statistics at both ends.

In Fig. 3.4, we show the rate performance of the proposed algorithms as a function of the number of pre-selected beams – assuming a fixed SNR of 10 dB. As expected, a higher number of pre-selectable beams leads to increased performance, as there is more chance to capture the beam combination providing the best channel gain. The simulations show that the 2-Step robust algorithm almost reaches the centralized approach, obtained with *perfect information* with already $D_{\text{BS}} = D_{\text{UE}} = 5$ beams.

In order to better understand the actual behavior of the proposed algorithms, we plot in Fig 3.6 their selected beam sets, for a given realization. In particular, the naive-coordinated beam alignment pre-selects beams pointing towards the presumed locations of the entities in the network, thus leading to strong alignment disagreements between the BS and the UE. The 1-Step approach introduces some robustness with respect to the local noise, i.e. more beams are selected for covering the spatial sectors where the location knowledge comes with more noise. The 2-Step approach provides complete robustness, with *fully-coordinated* beam pre-selections, aimed at maximizing the chance to capture the best beam combination, given the information setting.

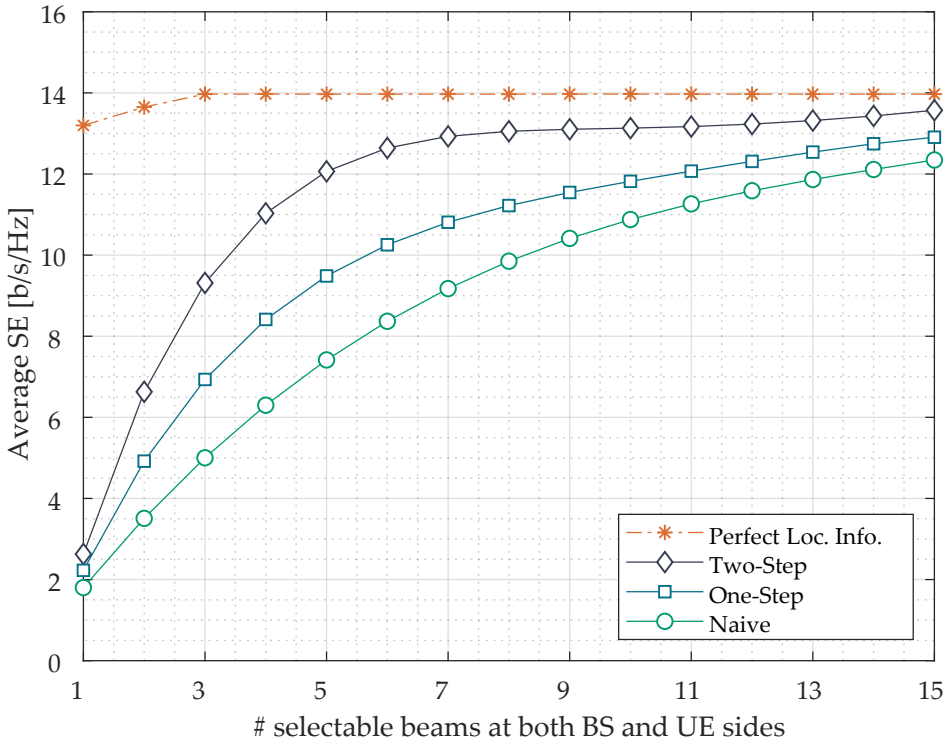

Figure 3.4 – SE vs number of pre-selected beams at the BS and the UE (among $M_{\text{BS}} = M_{\text{UE}} = 64$). Stronger LOS path, settings $\mathcal{A}$, for an SNR $= 10$ dB.

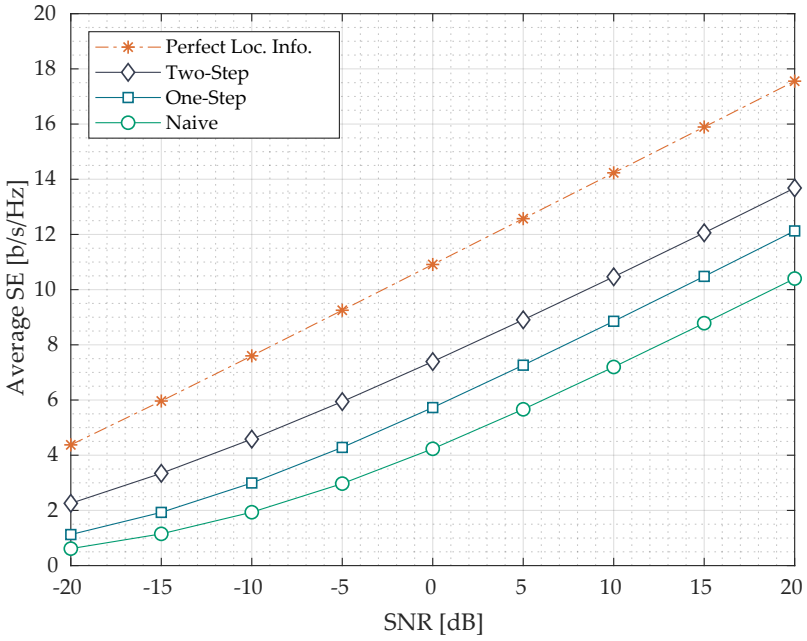

Figure 3.5 – SE vs SNR. Stronger LOS path, settings $\mathcal{B}$ and $D_{\text{BS}} = D_{\text{UE}} = 4$.

It is also interesting to observe how the proposed algorithms behave in case of LOS blockage. We consider thus an LOS path with $\sigma^2_{\text{LOS}} = 0$, and reflected paths with the same average power. Moreover, we consider another set of degrees of precision for location information – settings $\mathcal{B}$ – as follows:

- $r^{(\text{BS})}_{\text{UE}} = 7$ m, $r^{(\text{UE})}_{\text{UE}} = 3$ m;
- $r^{(\text{BS})}_{\text{R}_1} = 8$ m, $r^{(\text{UE})}_{\text{R}_1} = 11$ m;
- $r^{(\text{BS})}_{\text{R}_2} = 18$ m, $r^{(\text{UE})}_{\text{R}_2} = 8$ m;
- $r^{(\text{BS})}_{\text{BS}} = 0$ m, $r^{(\text{UE})}_{\text{BS}} = 0$ m.

In this case as well, as it can be seen in Fig. 3.5, the 2-Step robust algorithm outperforms the other distributed solutions, with a smaller gap compared to the case with settings $\mathcal{A}$, due to the *higher accuracy* of the estimated location information. The chosen beams for the settings $\mathcal{B}$ can be seen in Fig. 3.7, for a given realization.

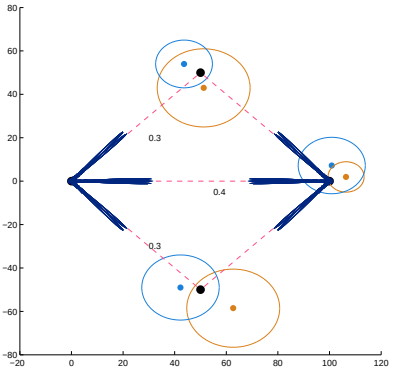

(a) BA with perfect information

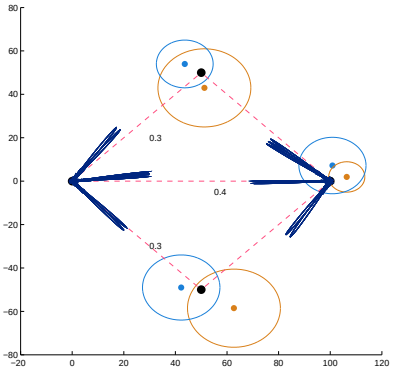

(b) Naive BA

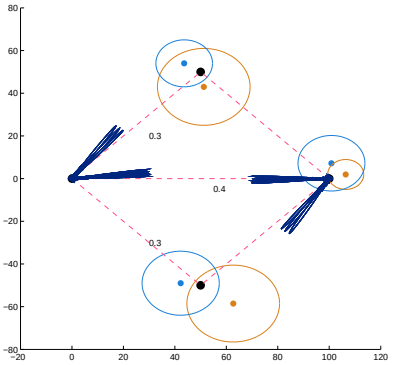

(c) 1-Step Robust BA

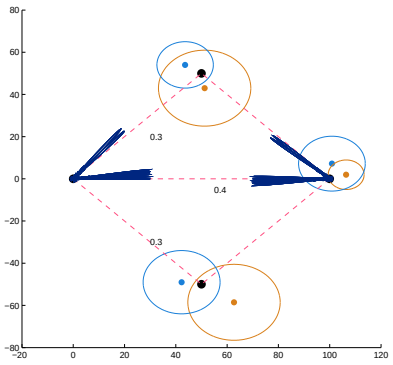

(d) 2-Step Robust BA

Figure 3.6 – Beam sets selected for pilot transmission with the proposed beam alignment (BA) algorithms, for a given realization. Stronger LOS path, i.e. $\sigma^2_{\text{LoS}} = 0.4$ as shown, settings $\mathcal{A}$, and $D_{\text{BS}} = D_{\text{UE}} = 7$.

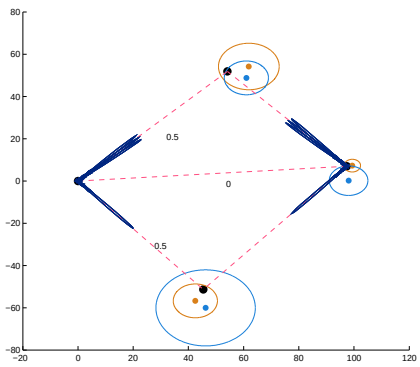

(a) BA with perfect information

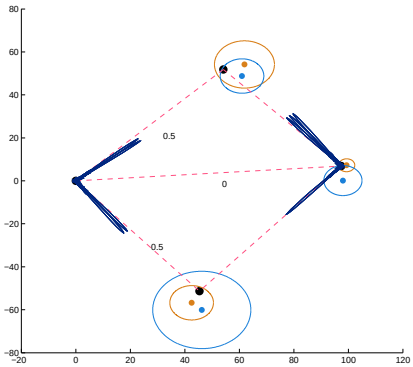

(b) Naive BA

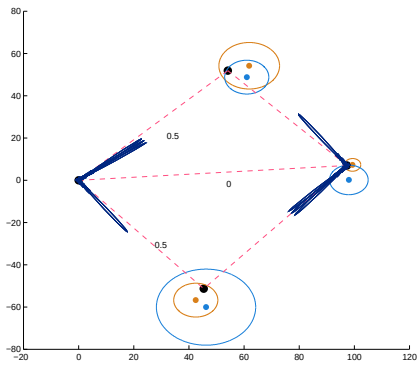

(c) 1-Step Robust BA

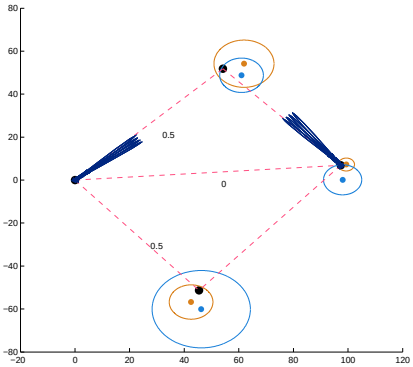

(d) 2-Step Robust BA

Figure 3.7 – Beam set selected for pilot transmission with the proposed beam alignment (BA) algorithms, for a given realization. LOS blockage, i.e. $\sigma^2_{\text{LoS}} = 0$ as shown, settings $\mathcal{B}$, and $D_{\text{BS}} = D_{\text{UE}} = 4$.

3.6 Conclusions

Exploiting location information allows to reduce alignment overhead while impacting *only slightly* on the actual rate performance. Dealing with the imperfect location knowledge is challenging as such information is not shared between the cooperating devices, leading to disagreements affecting the performance. In this chapter, we have introduced a suite of algorithms which take into account the imperfect location information and improve the coordination between the devices through the exploitation of their shared statistical knowledge of the estimation noise. Numerical results have indicated that great performance can be achieved with the proposed 2-Step robust algorithm. Finding closed forms of the proposed algorithms is an interesting and challenging research problem which is still open.

Chapter 4

Multi-User Beam Selection in mmWave mMIMO Using Out-of-Band Information

4.1 Introduction

In *hybrid* Millimeter Wave (mmWave) schemes, multi-user beam selection refers to the joint selection of analog transmit-receive beams across all User Equipments (UEs). One can decide to leave all the interference-rejection processing at the digital stage of the receiver. For example, in [87], the analog stage is intended to find the best beam directions at each UE, i.e. based on the local Signal-to-Noise Ratio (SNR). The strength of this approach lies in the fact that it is possible to use the existing *low-latency* beam training algorithms for single-user links – such as the 2-Step robust algorithm in Section 3.4.5 – in the analog stage. Yet, multiple *closely-located* UEs bear certain risk to share one or more common reflectors, causing the potential alignment of the Angles-of-Arrival (AoA) of some strong paths at the Base Station (BS) [18,82], which leads to the so-called *co-beam* interference (refer to Fig. 4.1). In this case, the interference-rejection processing in the digital domain might not be effective.

In this chapter, we address the second case in Table 1.1, where coordinated beam selection is performed among multiple UEs in an Uplink (UL) scenario. Extending the information model of Chapter 3 to multi-user settings is straightforward, but implies that each device obtains location estimates of the other devices, which is rather unpractical. To go around this problem, we propose to enforce coordination through statistical Out-of-Band (OOB) information. The coordination mechanism is based on the idea of

each UE *autonomously* selecting an analog beam for transmission so as to strike a trade-off between *i)* capturing enough channel gain and *ii)* ensuring the UE signals impinge on distinct beams at the BS side. The intuition behind point *ii)* is to ensure that the resulting effective channel matrix at the BS preserves full rank properties, thus enabling inter-UE interference mitigation in the digital domain.

4.2 Models and Problem Formulation

We consider a multi-band scenario, where a wireless network using sub-6 GHz bands coexists with a mmWave network. The channel and codebook models used in the following are as in Chapter 2. In line with [51], the sub-6 GHz model is likewise defined, with all variables underlined to distinguish them.

4.2.1 Uplink mmWave Signal Model

Consider the single-cell uplink multi-user scenario in Fig. 4.1. The BS is equipped with $N_{\text{BS}} \gg 1$ antennas and serves K UEs with $N_{\text{UE}} \gg 1$ antennas each. The UEs are assumed to reside in a disk with given radius r, which is used to control the inter-UE average distance. We assume that each UE sends one data stream to the BS, and that the BS has $N_{\text{RF}} = K$ RF chains available, each one connected to all the N_{BS} antennas, assuming a *fully-connected hybrid* architecture [41].

The k-th UE precodes the data $s_k \in \mathbb{C}$ through the analog precoding vector (or beam) $\mathbf{v}_{v_k} \in \mathcal{V} \subset \mathbb{C}^{N_{\text{UE}} \times 1}$. We assume that the UEs have one RF chain each, i.e. UEs are limited to analog beamforming via phase shifters (constant-magnitude elements) [43]. In addition, $\mathbb{E}[\|\mathbf{v}_{v_k} x_k\|^2] \leq 1$, assuming normalized power constraints. The reconstructed signal after mixed analog/digital combining at the BS can be expressed as follows – assuming no timing and carrier mismatches:

$$\hat{\mathbf{x}} = \sum_{k=1}^{K} \bar{\mathbf{W}}^{\text{H}} \mathbf{W}^{\text{H}} \mathbf{H}_k \mathbf{v}_{v_k} x_k + \bar{\mathbf{W}}^{\text{H}} \mathbf{W}^{\text{H}} \mathbf{n} \tag{4.1}$$

where $\mathbf{H}_k \in \mathbb{C}^{N_{\text{BS}} \times N_{\text{UE}}}$ is the channel matrix from the k-th UE to the BS and $\mathbf{n} \in \mathbb{C}^{N_{\text{BS}} \times 1}$ is the thermal noise vector, with zero mean and covariance matrix $\sigma_n^2 \mathbf{I}_{N_{\text{BS}}}$. $\mathbf{W} \in \mathbb{C}^{N_{\text{BS}} \times N_{\text{RF}}}$ is the analog combining matrix, containing the beams $\mathbf{w}_{w_k} \in \mathcal{W} \subset \mathbb{C}^{N_{\text{BS}} \times 1}$ relative to each of the K RF chains, while $\bar{\mathbf{W}} \in \mathbb{C}^{N_{\text{RF}} \times K}$ denotes the digital combining matrix.

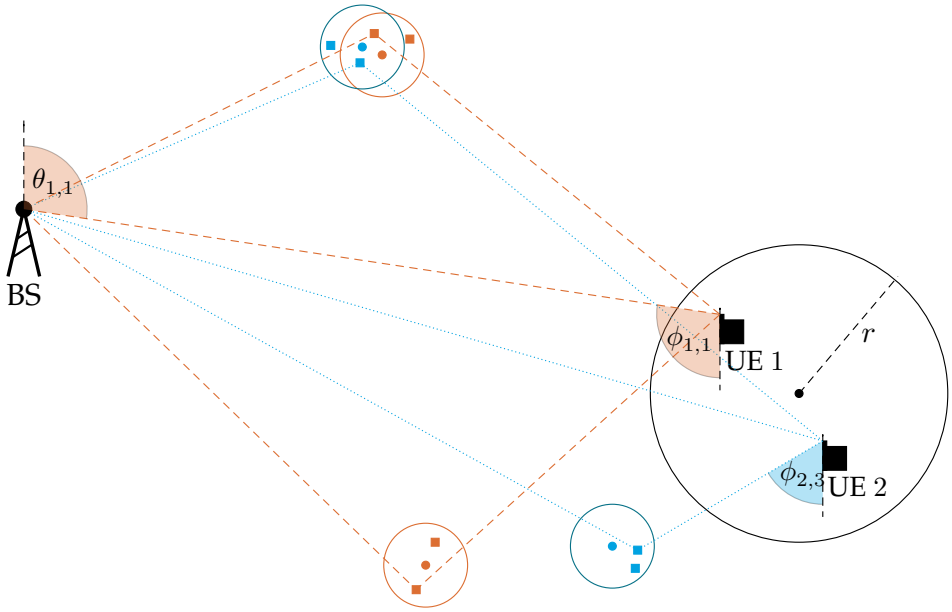

Figure 4.1 – Scenario example with $K = 2$ UEs and 3 clusters per UE. The UEs are assumed to reside in a disk of radius r. In this illustration, two *closely-located* UEs share some reflectors and the signal waves reflecting on the top ones arrive quasi-aligned at the BS, leading to severe interference and degraded sum-rate.

4.2.2 Problem Formulation

Let us introduce the *effective channel* $\bar{\mathbf{h}}_k \triangleq \mathbf{W}^{\mathrm{H}}\mathbf{H}_k\mathbf{v}_{v_k} \in \mathbb{C}^{K\times 1}$ of the k-th UE. The multi-user beam selection problem in mmWave communications consists in selecting the analog transmit-receive beams from the codebooks $\mathcal{V}$ and $\mathcal{W}$[1] in order to maximize the sum-rate defined as follows:

$$\mathcal{R}\left(v_{1:K}, w_{1:K}\right) \triangleq \sum_{k=1}^{K} \log_2\left(1+\gamma_k(v_{1:K}, w_{1:K})\right), \tag{4.2}$$

where $v_{1:K}$ (resp. $w_{1:K}$) are the indexes of the selected beams at the UE side (resp. BS side), while γ_k is the received Signal-to-Interference-and-Noise Ratio (SINR) for the k-th UE, defined as

$$\gamma_k\left(v_{1:K}, w_{1:K}\right) \triangleq \frac{|\bar{\mathbf{w}}_k^{\mathrm{H}}\bar{\mathbf{h}}_k|^2}{\sum_{j\neq k}|\bar{\mathbf{w}}_k^{\mathrm{H}}\bar{\mathbf{h}}_j|^2 + \|\bar{\mathbf{w}}_k\|^2\sigma_{\tilde{n}}^2}, \tag{4.3}$$

with $\bar{\mathbf{w}}_k \in \mathbb{C}^{K\times 1}$ denoting the k-th column of the digital combiner $\bar{\mathbf{W}}$, and where we used the notation $\sigma_{\tilde{n}}^2$ to denote the variance of the filtered noise $\mathbf{W}^{\mathrm{H}}\mathbf{n}$.

[1] We assume that $\mathcal{W}$ is the same across all the UEs.

Remark 4.1. The dependence of $\gamma_k\left(v_{1:K}, w_{1:K}\right)$ on the selected beams at both sides is hidden in the definition of the effective channel $\bar{\mathbf{h}}_k = \mathbf{W}^{\mathrm{H}}\mathbf{H}_k\mathbf{v}_{v_k}$, where we recall that $\mathbf{W}$ is the analog combiner containing the selected beams $\mathbf{w}_{w_k}$, $\forall k \in [\![1, K]\!]$. □

In order to maximize (4.2), the mutual optimization of both analog and digital components must be considered. A common viable approach consists in decoupling the design, as the analog precoder can be optimized through long-term statistical information, whereas the digital one can be made dependent on instantaneous one [87]. The same approach is followed here.

In particular, we consider Zero-Forcing (ZF) combining, so that we have

$$\bar{\mathbf{W}} \triangleq \left(\bar{\mathbf{H}}^{\mathrm{H}}\bar{\mathbf{H}}\right)^{-1}\bar{\mathbf{H}}^{\mathrm{H}}. \tag{4.4}$$

The received SINR for the k-th UE is then simplified as

$$\gamma_k\left(v_{1:K}, w_{1:K}\right) = \frac{1}{\sigma_{\tilde{n}}^2\left\{\left(\bar{\mathbf{H}}^{\mathrm{H}}\bar{\mathbf{H}}\right)^{-1}\right\}_{k,k}}, \tag{4.5}$$

with $\{\cdot\}_{k,k}$ denoting the k-th element on the diagonal of $\left(\bar{\mathbf{H}}^{\mathrm{H}}\bar{\mathbf{H}}\right)^{-1}$.

In general, the *perfect* knowledge of the effective channels is needed to maximize (4.2). As seen in Section 1.2.2, such information is not available without a significant resource overhead. In the next section, we propose some strategies to exploit sub-6 GHz information for a distributed and low-overhead approach to the problem.

4.3 Out-of-Band-Aided Beam Selection

Let us consider the existence of a sub-6 GHz channel $\underline{\mathbf{H}}_k \in \mathbb{C}^{\underline{N}_{\mathrm{BS}} \times \underline{N}_{\mathrm{UE}}}$ between the k-th UE and the BS. We assume that each UE is able to compute a *spatial spectrum* $\mathbb{E}[|\underline{\mathbf{S}}_k|^2] \in \mathbb{C}^{\underline{M}_{\mathrm{BS}} \times \underline{M}_{\mathrm{UE}}}$ of the sub-6 GHz channel, where [51]

$$\underline{\mathbf{S}}_k = \underline{\mathbf{W}}^{\mathrm{H}}\underline{\mathbf{H}}_k\underline{\mathbf{V}}. \tag{4.6}$$

The matrices $\underline{\mathbf{W}} \in \mathbb{C}^{\underline{N}_{\mathrm{BS}} \times \underline{M}_{\mathrm{BS}}}$ and $\underline{\mathbf{V}} \in \mathbb{C}^{\underline{N}_{\mathrm{UE}} \times \underline{M}_{\mathrm{UE}}}$ collect all the sub-6 GHz beamforming vectors at the BS and UE sides, sampled at the same angles as the mmWave ones. In particular, we assume $\underline{N}_{\mathrm{BS}} \ll \underline{M}_{\mathrm{BS}} = M_{\mathrm{BS}}$ and $\underline{N}_{\mathrm{UE}} \ll \underline{M}_{\mathrm{UE}} = M_{\mathrm{UE}}$. The (v, w)-th element of $\mathbb{E}[|\underline{\mathbf{S}}_k|^2]$ contains thus the sub-6 GHz channel gain obtained with the $\underline{v}$-th beam at the k-th UE and the $\underline{w}$-th one at the BS.

Remark 4.2. The computation of $\mathbb{E}[|\underline{\mathbf{S}}_k|^2]$ is *merely* bound to the knowledge of the average sub-6 GHz channel, as $\underline{\mathbf{W}}$ and $\underline{\mathbf{V}}$ are predefined fixed matrices. Note that the acquisition of the CSI matrix for conventional sub-6 GHz communications is a standard operation [33]. In this respect, sub-6 GHz channel measurements can be collected and stored *periodically* – e.g. within the channel coherence time – to be *readily* available for evaluating $\mathbb{E}[|\underline{\mathbf{S}}_k|^2]$. In other words, obtaining the spatial spectrum $\mathbb{E}[|\underline{\mathbf{S}}_k|^2]$ requires no additional training overhead [51]. □

4.3.1 Exploiting Sub-6 GHz Information

The available sub-6 GHz spatial information can be exploited to obtain a rough estimate of the angular characteristics of the mmWave channel. Indeed, due to the larger beamwidth of sub-6 GHz beams, one sub-6 GHz beam can be associated to a set of mmWave beams, as defined below.

> **Definition 4.1.** For a given sub-6 GHz beam pair $(\underline{v}, \underline{w})$, we introduce the set $\mathcal{S}(\underline{v}, \underline{w}) \triangleq \mathcal{S}_{\text{UE}}(\underline{v}) \times \mathcal{S}_{\text{BS}}(\underline{w})$ where $\mathcal{S}_{\text{UE}}(\underline{v})$ (resp. $\mathcal{S}_{\text{BS}}(\underline{w})$) contains all the mmWave beams belonging to the 3-dB beamwidth of the $\underline{v}$-th (resp. $\underline{w}$-th) sub-6 GHz beam.

It is important to remark that we focus on the selection of sub-6 GHz beams to further refine. We indeed adhere to the well-known two-stage beamforming and training operation, where *fine-grained* training (called beam refinement) follows *coarse-grained* training (called sector sweeping). In our approach, coarse-grained beam selection is achieved without *actually* training the beams with reference signals, but using instead beam information extracted from lower channels, so as to speed up the process. Once these coarse sub-6 GHz beams are chosen, the small subset of associated mmWave beams is trained. We refer to [93] for more details on this standard step. In what follows, we propose some multi-user beam selection strategies leveraging the described OOB-related side-information.

4.3.2 Uncoordinated Beam Selection

We first review here the approach given in [87], where the authors proposed to design the analog beamformers to maximize the SNR at each UE, neglecting multi-user interference.

When OOB information is available, the beam selection ($\underline{v}_k^{\text{un}} \in \underline{\mathcal{V}}, \underline{w}_k^{\text{un}} \in \underline{\mathcal{W}}$) at the k-th UE – which we will denote as *uncoordinated* (un) – can be expressed as follows:

$$\left(\underline{v}_k^{\text{un}}, \underline{w}_k^{\text{un}}\right) = \underset{\underline{v}_k, \underline{w}_k}{\operatorname{argmax}} \log_2 \left(1 + \mathbb{E}_{v_k, w_k | \underline{v}_k, \underline{w}_k} \left[\gamma_k^{\text{su}}(v_k, w_k)\right]\right), \tag{4.7}$$

where we have approximated the average rate through *Jensen's inequality* and we have defined the single-user expected SNR, conditioned on a given sub-6 GHz beam pair $(\underline{v}_k, \underline{w}_k) \in \underline{\mathcal{V}} \times \underline{\mathcal{W}}$, as follows:

$$\mathbb{E}_{v_k, w_k | \underline{v}_k, \underline{w}_k} \left[\gamma_k^{\text{su}}(v_k, w_k)\right] = \sum_{(v_k, w_k) \in \mathcal{S}(\underline{v}_k, \underline{w}_k)} \frac{g_{k, v_k, w_k}}{S_k \sigma_{\tilde{n}}^2}, \tag{4.8}$$

with

$$g_{k, v_k, w_k} \triangleq \mathbb{E}\left[\left|\mathbf{w}_{w_k} \mathbf{H}_k \mathbf{v}_{v_k}\right|^2\right] \tag{4.9}$$

$$= \mathbb{E}\left[\left|\mathbf{S}_{k, v_k, w_k}\right|^2\right], \tag{4.10}$$

being the average beamforming gain obtained at the k-th UE with the transmit-receive beam pair (v_k, w_k), and where $S_k \triangleq \text{card}(\mathcal{S}(\underline{v}_k, \underline{w}_k))$.

To solve (4.8), the k-th UE needs to know the mmWave gain g_{k, v_k, w_k} $\forall (v_k, w_k) \in \mathcal{S}(\underline{v}_k, \underline{w}_k)$. This information is not available but can be replaced for algorithm derivation purposes[2] with the gain observed in the sub-6 GHz channel over the beam pair $(\underline{v}_k, \underline{w}_k)$. In other words, we assume

$$g_{k, v_k, w_k} \approx \mathbb{E}\left[\left|\underline{\mathbf{S}}_{k, \underline{v}_k, \underline{w}_k}\right|^2\right], \quad \forall (v_k, w_k) \in \mathcal{S}(\underline{v}_k, \underline{w}_k). \tag{4.11}$$

Note that the average gain information derived from $\underline{\mathbf{S}}$ will *unlikely* match with its mmWave counterpart in absolute terms, due to multipath, noise effects and path-loss discrepancies. Still, high spatial congruence has been observed between the mmWave and sub-6 GHz radio environments, as seen in Section 2.1.2. In this respect, (4.11) allows to spot a valuable candidate set for mmWave beams in most of the situations. Yet, an important limitation of this approach is that each UE solves its own beam selection problem *independently* of the other UEs, thus ignoring the possible impairments in terms of interference. Therefore, *as the inter-UE average distance decreases*, the performance of this procedure is expected to degrade since the UEs have much more chance to share their best propagation paths – which results in co-beam interference at the BS.

[2]The proposed algorithms are then evaluated in Section 4.4 under realistic multi-band channel conditions as proposed in [51], where the described behavior and consequent randomness is taken into account.

4.3.3 Hierarchical Coordinated Beam Selection

In order to achieve coordination, we propose to use a hierarchical information structure requiring small overhead. In particular, an *(arbitrary)* order among the UEs is established[3], for which the k-th UE has access to the beam decisions carried out at the lower-ranked UEs $1, \dots, k-1$. We further assume that such exchanged beam information is *perfectly* decoded at the intended UEs.

Remark 4.3. Exchanging sub-6 GHz beams rather than mmWave ones introduces some *uncertainty*, but allows to save time as no UE has to wait for another one to perform actual beam training. □

Assuming that the sub-6 GHz beam indices $\underline{w}_{1:k-1}$ have been received, the *coordinated* (co) sub-6 GHz beam pair $(\underline{v}_k^{\text{co}} \in \underline{\mathcal{V}}, \underline{w}_k^{\text{co}} \in \underline{\mathcal{W}})$ relative to the k-th UE is obtained through solving the following optimization problem:

$$(\underline{v}_k^{\text{co}}, \underline{w}_k^{\text{co}}) = \underset{\underline{v}_k, \underline{w}_k}{\operatorname{argmax}} \ \log_2 \left(1 + \mathbb{E}_{v_{1:K}, w_{1:K} | \underline{v}_k, \underline{w}_{1:k+1}} \left[\gamma_k(v_{1:K}, w_{1:K})\right]\right). \tag{4.12}$$

Solving (4.12) is not trivial, being a subset selection problem for which a Monte-Carlo approach to approximate the expectation with a discrete summation leads to unpractical computational time. Interestingly, for large N_{BS} and N_{UE}, we are able to derive an approximation for the expectation in (4.12) which will be useful for algorithm derivation. We start with showing such intermediate result.

Proposition 4.1. *In the limit of large N_{BS} and N_{UE}, the expected SINR (averaged over small-scale fading) of the k-th UE obtained after ZF combining at the BS is*

$$\mathbb{E}\left[\gamma_k(v_{1:K}, w_{1:K})\right] = \begin{cases} \dfrac{g_{k,v_k,w_k}}{\sigma_{\tilde{n}}^2} & \text{if } w_k \neq w_j \ \forall j \in [\![1, K]\!] \backslash \{k\} \\ 0 & \text{if } \exists\, j \in [\![1, K]\!] \backslash \{k\} : w_j = w_k \end{cases}. \tag{4.13}$$

Proof. Refer to Appendix A.2. □

Remark 4.4. In the large-dimensional regime, the dependence of the SINR in (4.3) on the transmit beams of the other UEs vanishes. In particular, catastrophic co-beam interference is experienced through intersections at the BS receive beam *only*. We kept the dependence in (4.13) to avoid introducing additional notation. □

[3]The hierarchical information exchange is proposed here to facilitate the coordination mechanism at reduced overhead. In this work, we shall leave aside further analysis on how such a *hierarchy* is defined and maintained.

Using Proposition 4.1, the expectation in (4.12) can be approximated as follows:

$$\mathbb{E}_{v_{1:K},w_{1:K}|\underline{v}_k,\underline{w}_{1:k}}\left[\gamma_k(v_{1:K},w_{1:K})\right] \approx \sum_{\substack{(v_k,w_k)\in\mathcal{S}(\underline{v}_k,\underline{w}_k)\\ w_k\notin\cup_{j=1}^{k-1}\mathcal{S}_{\text{BS}}(\underline{w}_j)}} \frac{g_{v_k,w_k}}{S_k\sigma_{\tilde{n}}^2}. \tag{4.14}$$

Using (4.14) in (4.12) to choose the sub-6 GHz beams at the k-th UE allows to take into account the *potential* co-beam interference transferred to the lower-ranked UEs with *low complexity*.

Remark 4.5. The K-th (highest-ranked) UE has to consider via (4.14) the coarse-grained beam decisions of all the other (lower-ranked) UEs to avoid generating potential co-beam interference. Therefore, such UE might be forced to exchange high data rate for less leakage, as the best non-interfering paths might have been already exploited. Therefore, it is essential to *change the hierarchy* at regular intervals to ensure an average acceptable rate per UE. □

We summarize the proposed coordinated beam selection in Algorithm 3. The algorithm is compatible with vectorization and parallelization, which minimize computational time.

Algorithm 3 OOB-Aided Hierarchical Coordinated Beam Selection at the k-th UE

INPUT: $\mathbb{E}\left[|\underline{\mathbf{S}}_k|^2\right]$, $\underline{w}_{1:k-1}$

Step 1: Exploiting OOB side-information

if $u = 1$ **then** ▷ The k-th UE is the lowest in the *hierarchy*
  $\mathbb{E}\left[\boldsymbol{\gamma}_k\right] = \mathbb{E}\left[|\underline{\mathbf{S}}_k|^2\right]/\sigma_{\tilde{n}}^2$ ▷ Solve (4.7) via (4.8)
else ▷ The k-th UE is *not* the lowest in the *hierarchy*
  for $\underline{v} = 1 : M_{\text{UE}}$ **do**
    for $\underline{w} = 1 : M_{\text{BS}}$ **do**
      $X = \text{card}\big(\mathcal{S}(\underline{v},\underline{w}) \setminus \mathcal{S}_{\text{BS}}(\underline{w}_1) \cup \cdots \cup \mathcal{S}_{\text{BS}}(\underline{w}_{k-1})\big)$
      $S = \text{card}\big(\mathcal{S}(\underline{v},\underline{w})\big)$
      $T = \mathbb{E}\left[|\underline{\mathbf{S}}_{k,\underline{v},\underline{w}}|^2\right]/\sigma_{\tilde{n}}^2$
      $\mathbb{E}\left[\gamma_k(\underline{v},\underline{w})\right] = XT/S$ ▷ Solve (4.12) via (4.14)
    end for
  end for
end if
return $(\underline{v}_k^{\text{co}},\underline{w}_k^{\text{co}}) \leftarrow \text{argmax}_{\underline{v},\underline{w}}\ \mathbb{E}\left[\boldsymbol{\gamma}_k\right]$

Step 2: Pilot-training the subset of mmWave beams

$(v_k^{\text{co}},w_k^{\text{co}}) \leftarrow \text{argmax}_{v,w}\left|\mathbf{w}_{k,w}\mathbf{H}_k\mathbf{v}_{k,v}\right|^2\ \forall v,w \in \mathcal{S}(\underline{v}_k^{\text{co}},\underline{w}_k^{\text{co}})$

4.4 Simulation Results

We evaluate here the performance of the proposed algorithm for $K = 5$ *closely-located* UEs. We assume $N_{\text{BS}} = 64$, $N_{\text{UE}} = 16$ for mmWave communications, and $N_{\text{BS}} = 8$ and $N_{\text{UE}} = 4$ for sub-6 GHz ones. As for the carrier frequencies, we consider 28 GHz and 3 GHz for mmWave and sub-6 GHz operation, respectively. All the plotted data rates are the averaged – over 10000 Monte-Carlo iterations – instantaneous sum-rates, obtained after ZF combining at the digital stage (BS side).

4.4.1 Multi-Band Channels

The performance of the proposed OOB-aided algorithms depends on the *spatial congruence* between sub-6 GHz and mmWave channels. The authors in [51] proposed a simulation environment for generating sub-6 GHz and mmWave channels based on the model in (2.1). The MATLAB®code used to simulate those channels is open-source and available on IEEEXplore [51]. We use the same model except that we consider a narrowband channel model, for which path time spread and beam squint effect can be neglected [82]. Note that *frequency-selective* filters at the BS side helps discriminating (in time) among UEs which generate co-beam interference, and thus might results in giving an extra performance in average wide-band channels. In this work, we consider a worst case scenario. In principle, models and algorithms could be extended to a wideband setting.

4.4.2 Results and Discussion

We consider a stronger (on average) Line-of-Sight (LOS) path with respect to the reflected ones [82]. In particular, we adopt the following large-scale path-loss model:

$$\text{PL}(\delta) = \alpha + \beta \log_{10}(\delta) + \xi \qquad [\text{dB}] \tag{4.15}$$

where δ is the path length and where the path-loss parameters α, β and ξ are taken from Table I in [82] for both LOS and Non-Line-of-Sight (NLOS) contributions. Since the model in [51] is for a single-user scenario, we consider the model in [94] to extend it so as to generate correlated channel clusters for all the neighboring UEs in the disk. In [94], the position of the reflectors is made also dependent on the position of the UEs, and as a result, the possible sharing of reflectors and scatterers for neighboring UEs is taken into account. An example of the available sub-6 GHz spatial spectrum at two UEs is shown in Fig. 4.2.

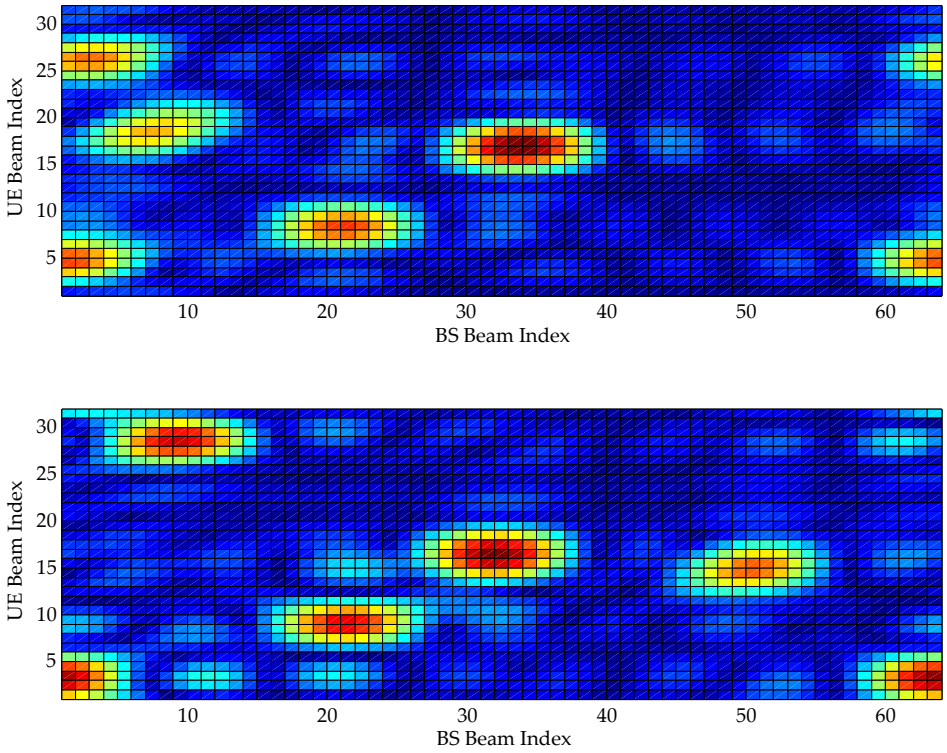

Figure 4.2 – Simulated example of the available $\mathbb{E}[|\underline{\mathbf{S}}_k|^2]$ at two neighboring UEs, with $r = 11$ m. Some strong reflectors are being shared, while others are uncommon. The average power of the paths – based on (4.15) – can be different across the UEs.

In Fig. 4.3, we show the sum-Spectral Efficiency (SE) of the proposed algorithms as a function of the SNR, where the average distance between the UEs is 13 meters. For reference, we also plot the curve related to the upper bound achieved with no multi-user interference. The proposed OOB-aided coordinated algorithm outperforms the uncoordinated one, which neglects co-beam interference. The coordination gain increases with the SNR.

In Fig. 4.4, we show the sum-SE of the proposed algorithms as a function of the average inter-UE distance, for a mmWave SNR of 1 dB. The coordination among the UEs allows for huge SE gains for inter-UE distances below 15 meters. As the average inter-UE distance increases – and so, there is less chance for the co-beam interference to occur – the performance gap between the two algorithms narrows.

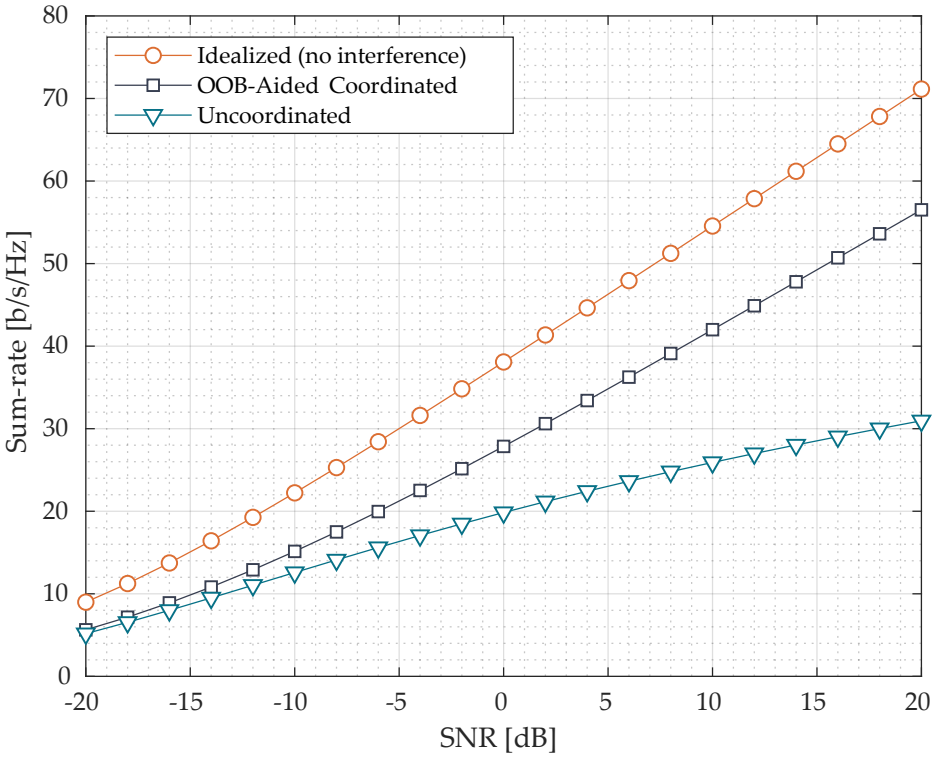

Figure 4.3 – Sum-SE vs (mmWave) SNR. The average inter-UE distance is 13 m. The OOB-aided coordinated algorithm outperforms the uncoordinated one.

4.5 Conclusions

In this chapter, we introduced a low-overhead OOB-aided decentralized beam selection algorithm for a mmWave uplink multi-user scenario, leading to improved interference management. The core of the proposed algorithm resides in the hierarchical information exchange, which allows for a low-overhead approach to the multi-user beam selection problem, exploiting the massive antenna limit. Finding clear relationships between mmWave and lower bands radio environments is essential for OOB-aided approaches – in particular, towards robust algorithms taking channels discrepancies into account – and it is an interesting open research problem.

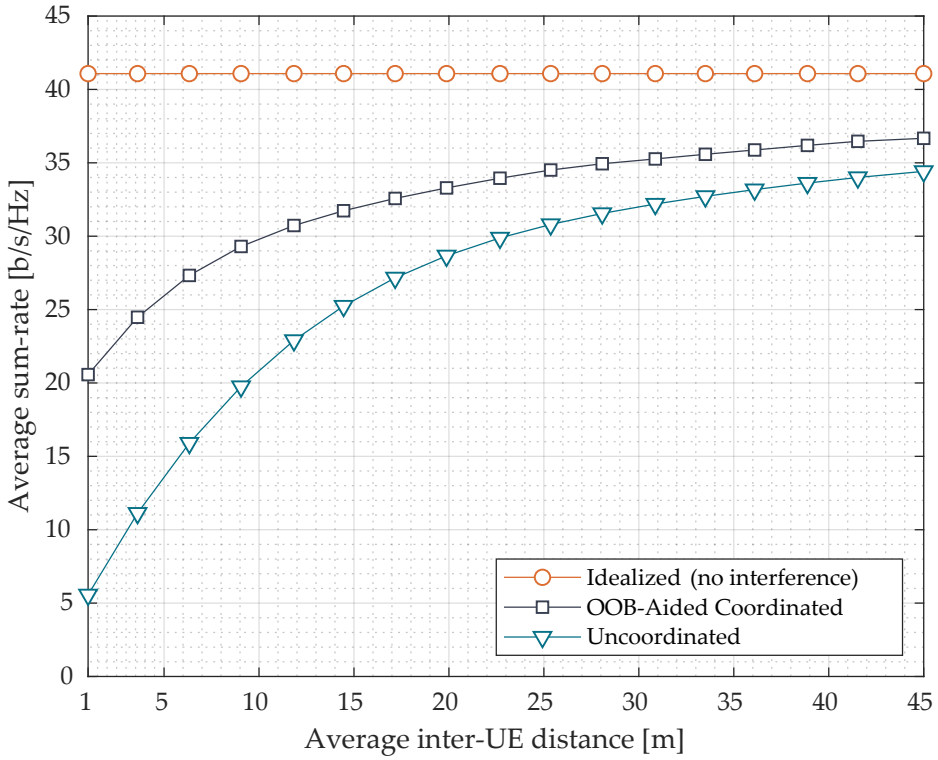

Figure 4.4 – Sum-SE vs average inter-UE distance. The SNR is fixed to 1 dB. The performance gain achieved through coordination decreases with the inter-UE distance.

Chapter 5

Multi-User Beam Selection for Training Overhead Reduction

5.1 Introduction

In this chapter, we introduce a coordination mechanism between multiple User Equipments (UEs) to facilitate statistical beam selection for effective throughput maximization in networks where the *scalability* of the Reference Signals (RSs) constitutes a main bottleneck. We consider multi-beam selection at the UE side with multi-stream Downlink (DL) Massive MIMO (mMIMO) transmission. Compared to Chapter 4, we show that beam selection in such scenarios must deal with a novel interesting *trade-off* between *i)* selecting the beams that capture the largest channel gains for each UE, and *ii)* selecting the beams that might capture somewhat weaker paths but are *common* to multiple UEs, so as to reduce the training overhead. The essence of such trade-offs is captured in Fig. 5.1, where UE 2 can capitalize on its weaker paths to reduce the number of activated beams at the Base Station (BS) side.

In order to design the long-term Grid-of-Beams (GoB) beamformers, we propose a suite of decentralized coordinated beam selection algorithms exploring various *complexity-performance* trade-offs. In particular, the coordination between the UEs is enforced through an exchange protocol exploiting low-rate Device-to-Device (D2D) communications. In this respect, we leverage from the forthcoming 3GPP Release 16, which is expected to support *side-links* which facilitate cooperative communications among neighboring UEs with low resource consumption [53, 54].

5.2 Models and Problem Formulation

Consider a single-cell mMIMO network (refer to Fig. 5.1), where the BS is equipped with $N_{\text{BS}} \gg 1$ antennas and serves (in downlink transmission) $K \ll N_{\text{BS}}$ UEs with N_{UE} antennas each. We assume that the BS uses linear precoding techniques to process the signals before transmitting to all UEs. We consider Frequency Division Duplex (FDD) operation, i.e. the DL and the Uplink (UL) channels are not reciprocal. The codebook model is as in Chapter 2. In the following, we describe the training and data signal models for this chapter. In particular, we consider pilot-aided channel estimation with *beamformed* RSs, as *recently standardized* in 3GPP New Radio (NR) [34].

Before we detail our mathematical model, let us focus on the example shown in Fig. 5.1, which carries the essence of the intuition behind the proposed trade-off between *i) channel gain, ii) spatial separability*, and *iii) training overhead*.

Consider Fig. 5.1 and the problem of which beams should each UE activate and how it affects which beams are lit up at the BS and the subsequent training overhead. Conventional uncoordinated max-SNR based beam selection would collect the *highest amount of energy* but would result in $M_{\text{BS}} = 5$ beams to train at the BS. Instead, UE 2 can opt for the weaker (non-bold light blue beams) $\mathbf{w}_{2,1}$ and $\mathbf{w}_{2,3}$ while UE 1 continues to activate its three beams. Note that this *beam strategy* collects *less energy*, yet it reduces the training overhead by 40% as the number of activated beams at the BS falls to $M_{\text{BS}} = 3$, since beams $\mathbf{v}_1$, $\mathbf{v}_2$ and $\mathbf{v}_5$ at the BS side serve both UE 1 and UE 2 and maintain *separability* between the UEs. In the following, we are interested in designing a coordinated beam selection algorithm that optimizes this trade-off from a throughput perspective. We introduce now our mathematical model.

5.2.1 Channel Estimation with Grid-of-Beams

A NR-like OFDM-based modulation scheme is assumed [34]. We consider a resource grid consisting of T resource elements. Among those, τD_{BS} are allocated to RSs, and $T - \tau D_{\text{BS}}$ to data, where D_{BS} denotes the number of beams that are trained among the ones in $\mathcal{V}$ and τ is the duration measured in *number of OFDM symbols* of their associated RSs (one RS for each beam [34], refer to Fig. 5.2). The received training signal $\mathbf{Y}_k \in \mathbb{C}^{D_{\text{UE}} \times \tau}$ at the k-th UE, where D_{UE} is the number of activated beams at the UE side, can be expressed as

$$\mathbf{Y}_k = \rho \mathbf{W}_k^{\text{H}} \mathbf{H}_k \mathbf{V} \mathbf{S} + \mathbf{W}_k^{\text{H}} \mathbf{N}_k, \qquad \forall k \in [\![1, K]\!], \tag{5.1}$$

where $\mathbf{S} \in \mathbb{C}^{D_{\text{BS}} \times \tau}$ contains the orthogonal (known) RSs, with $\mathbf{S}\mathbf{S}^{\text{H}} = \mathbf{I}_{D_{\text{BS}}}$, $\mathbf{V} \triangleq \left[\mathbf{v}_1 \dots \mathbf{v}_{D_{\text{BS}}}\right] \in \mathbb{C}^{N_{\text{BS}} \times D_{\text{BS}}}$ is the normalized training (GoB) precoder common to all the

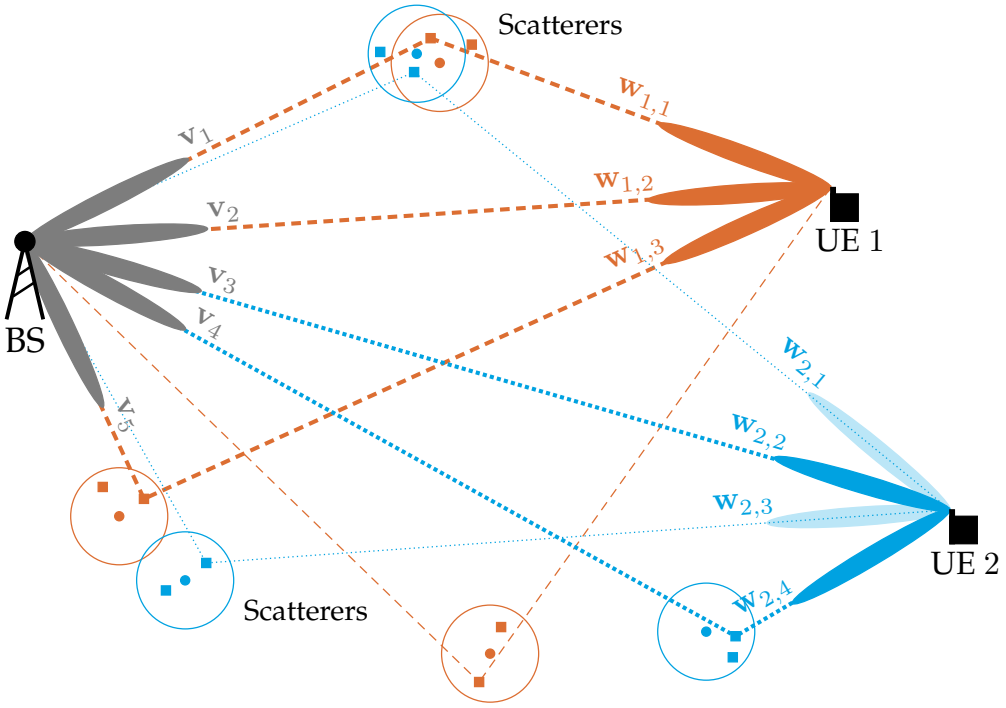

Figure 5.1 – Intuitive example with $K = 2$ UEs highlighting the trade-off between *i) energy* (i.e. activating strong paths), *ii) spatial separability*, and *iii) training overhead* (i.e. lighting up a smaller set of beams at the BS). The blue and orange circles represent the multi-path clusters, *possibly* shared among the UEs. Stronger paths are marked in bold.

UEs, $\mathbf{H}_k \in \mathbb{C}^{N_{\text{UE}} \times N_{\text{BS}}}$ is the channel between the BS and the k-th UE, with $\text{vec}(\mathbf{H}_k) \sim \mathcal{CN}(\mathbf{0}, \mathbf{\Sigma}_k)$ and $\mathbf{\Sigma}_k \in \mathbb{C}^{N_{\text{BS}}N_{\text{UE}} \times N_{\text{BS}}N_{\text{UE}}}$ the respective channel covariance (assumed to be known), and $\mathbf{W}_k \triangleq \left[\mathbf{w}_{k,1} \dots \mathbf{w}_{k,D_{\text{UE}}}\right] \in \mathbb{C}^{N_{\text{UE}} \times D_{\text{UE}}}$ is the training combiner at the k-th UE. Note that both $\mathbf{V}$ and $\mathbf{W}_k$ $\forall k$ contain beamformers belonging to the predefined GoB codebooks $\mathcal{V}$ and $\mathcal{W}$[1]. The matrix $\mathbf{N}_k \in \mathbb{C}^{N_{\text{UE}} \times \tau}$, whose elements are i.i.d. $\mathcal{CN}(0, \sigma_n^2)$, denotes the receiver noise at the k-th UE, while $\rho \triangleq \sqrt{\frac{P}{T}}$, where P is the total transmit power available at the BS in the considered coherent (over both time and sub-carriers) frame.

Following the training stage, the UEs are able to estimate their instantaneous GoB effective channels, defined as

$$\bar{\mathbf{H}}_k \triangleq \mathbf{W}_k^{\text{H}} \mathbf{H}_k \mathbf{V} \in \mathbb{C}^{D_{\text{UE}} \times D_{\text{BS}}}, \qquad \forall k \in [\![1, K]\!], \tag{5.2}$$

and whose covariance is denoted with $\bar{\mathbf{\Sigma}}_k \in \mathbb{C}^{D_{\text{BS}}D_{\text{UE}} \times D_{\text{BS}}D_{\text{UE}}}$, $\forall k \in [\![1, K]\!]$.

[1] To lighten the notation, we assume that $\mathcal{W}$ is the same across all the UEs. The algorithms we present in Section 5.5 can be *easily* generalized to different codebooks $\mathcal{W}_k$, $\forall k \in [\![1, K]\!]$ at the UE side.

We introduce now the block diagonal matrix $\mathbf{W} \in \mathbb{C}^{KN_{\text{UE}} \times KD_{\text{UE}}}$ containing all the GoB combiners $\mathbf{W}_k$, $\forall k \in [\![1, K]\!]$, as follows:

$$\mathbf{W} \triangleq \begin{bmatrix} \mathbf{W}_1 & & \mathbf{0} \\ & \ddots & \\ \mathbf{0} & & \mathbf{W}_K \end{bmatrix}. \tag{5.3}$$

The entire multi-user effective channel matrix $\bar{\mathbf{H}} \in \mathbb{C}^{KD_{\text{UE}} \times D_{\text{BS}}}$ can then be expressed as

$$\bar{\mathbf{H}} \triangleq \mathbf{W}^{\text{H}} \mathbf{H} \mathbf{V}, \tag{5.4}$$

where $\mathbf{H} \triangleq \left[\mathbf{H}_1^{\text{T}} \dots \mathbf{H}_K^{\text{T}}\right]^{\text{T}} \in \mathbb{C}^{KN_{\text{UE}} \times N_{\text{BS}}}$ is the overall multi-user channel.

To close the CSI acquisition loop, each UE feeds back its estimated effective channel to the BS. As a consequence, the BS obtains an estimate $\hat{\bar{\mathbf{H}}} \in \mathbb{C}^{KD_{\text{UE}} \times D_{\text{BS}}}$ of the multi-user effective channel $\bar{\mathbf{H}}$ which can be used to design the mMIMO data precoder (refer to Section 5.3). In this work, we assume that the UEs use the popular Linear Minimum Mean Square Error (LMMSE) estimator, given in the next lemma.

Lemma 5.1 ([95]). *The LMMSE effective channel estimate $\hat{\bar{\mathbf{H}}}_k \in \mathbb{C}^{D_{\text{UE}} \times D_{\text{BS}}}$ at the k-th UE can be obtained as follows:*

$$\text{vec}\left(\hat{\bar{\mathbf{H}}}_k\right) = \rho \bar{\mathbf{\Sigma}}_k \mathbf{A}^{\text{H}} \left(\rho^2 \mathbf{A} \bar{\mathbf{\Sigma}}_k \mathbf{A}^{\text{H}} + \sigma_n^2 \mathbf{\Gamma}\mathbf{\Gamma}^{\text{H}}\right)^{-1} \text{vec}\left(\mathbf{Y}_k\right), \tag{5.5}$$

where $\mathbf{A} \triangleq \left(\mathbf{S}^{\text{T}} \otimes \mathbf{I}_{D_{\text{UE}}}\right) \in \mathbb{C}^{\tau D_{\text{UE}} \times D_{\text{BS}} D_{\text{UE}}}$ and $\mathbf{\Gamma} \triangleq \left(\mathbf{I}_\tau \otimes \mathbf{W}_k^{\text{H}}\right) \in \mathbb{C}^{\tau D_{\text{UE}} \times \tau N_{\text{UE}}}$.

The channel estimation error vector $\mathbf{e}_k \triangleq \text{vec}\left(\bar{\mathbf{H}}_k\right) - \text{vec}\left(\hat{\bar{\mathbf{H}}}_k\right)$ at the k-th UE has zero mean elements [95] and associated covariance matrix as given in the next lemma.

Lemma 5.2. *The covariance $\mathbf{\Sigma}_{\mathbf{e}_k} \in \mathbb{C}^{D_{\text{BS}} D_{\text{UE}} \times D_{\text{BS}} D_{\text{UE}}}$ of the LMMSE channel estimation error at the k-th UE can be expressed as follows:*

$$\mathbf{\Sigma}_{\mathbf{e}_k} = \left(\bar{\mathbf{\Sigma}}_k^{-1} + \kappa \mathbf{A}^{\text{H}} \left(\mathbf{\Gamma}\mathbf{\Gamma}^{\text{H}}\right)^{-1} \mathbf{A}\right)^{-1}, \tag{5.6}$$

having defined the scalar $\kappa \triangleq \rho^2 / \sigma_n^2$.

Proof. Refer to Appendix A.3. □

In the following, we introduce the data signal model for this chapter. In particular, compared to the previous Chapter 4, we consider multi-stream transmission.

5.2.2 Data Signal Model

The data transmission phase (over the effective channels) follows the training and UE feedback stages. Let us denote with $\mathbf{x}_k \triangleq \left[x_{1,1} \dots x_{1,L_k}\right] \in \mathbb{C}^{L_k \times 1}$ the data vector transmitted to the k-th UE. Thus, $\mathbf{x} \triangleq \left[\mathbf{x}_1 \dots \mathbf{x}_K\right] \in \mathbb{C}^{L \times 1}$ is the overall data vector, where $L \triangleq \sum_k L_k$ is the total number of transmitted data symbols and $\mathbb{E}[\mathbf{x}\mathbf{x}^{\mathrm{H}}] = \mathbf{I}_L$. The received data signal $\hat{\mathbf{x}}_k$ at the k-th UE can be expressed as

$$\begin{aligned}\hat{\mathbf{x}}_k &= \rho \bar{\mathbf{W}}_k^{\mathrm{H}} \bar{\mathbf{H}}_k \bar{\mathbf{V}} \mathbf{x} + \bar{\mathbf{W}}_k^{\mathrm{H}} \bar{\mathbf{n}}_k, \qquad \forall k \in [\![1, K]\!] \\ &= \rho \bar{\mathbf{W}}_k^{\mathrm{H}} \bar{\mathbf{H}}_k \bar{\mathbf{V}}_k \mathbf{x}_k + \sum_{j \neq k} \rho \bar{\mathbf{W}}_k^{\mathrm{H}} \bar{\mathbf{H}}_k \bar{\mathbf{V}}_j \mathbf{x}_j + \bar{\mathbf{W}}_k^{\mathrm{H}} \bar{\mathbf{n}}_k, \end{aligned} \tag{5.7}$$

where $\bar{\mathbf{V}} \triangleq \left[\bar{\mathbf{V}}_1 \dots \bar{\mathbf{V}}_K\right] \in \mathbb{C}^{D_{\mathrm{BS}} \times L}$ is the normalized mMIMO (digital) data precoder, with $\bar{\mathbf{V}}_k \triangleq \left[\bar{\mathbf{v}}_{k,1} \dots \bar{\mathbf{v}}_{k,L_k}\right]$, $\bar{\mathbf{H}}_k$ is the effective channel between the BS and the k-th UE after GoB precoding and combining, $\bar{\mathbf{W}}_k \in \mathbb{C}^{D_{\mathrm{UE}} \times L_k}$ is the mMIMO (digital) data combiner at the k-th UE, and $\bar{\mathbf{n}}_k \triangleq \mathbf{W}_k^{\mathrm{H}} \mathbf{n}_k \in \mathbb{C}^{D_{\mathrm{UE}} \times 1}$ denotes the filtered receiver noise at the k-th UE.

The instantaneous Spectral Efficiency (SE) $\mathcal{R}_k(\mathbf{V}, \bar{\mathbf{V}}, \mathbf{W}, \bar{\mathbf{W}})$ relative to the k-th UE can then be expressed as follows:

$$\mathcal{R}_k\left(\mathbf{V}, \bar{\mathbf{V}}, \mathbf{W}, \bar{\mathbf{W}}\right) \triangleq \log_2 \det\left(\mathbf{I}_{L_k} + \rho^2 \bar{\mathbf{K}}_k^{-1} \bar{\mathbf{W}}_k^{\mathrm{H}} \bar{\mathbf{H}}_k \bar{\mathbf{V}}_k \bar{\mathbf{V}}_k^{\mathrm{H}} \bar{\mathbf{H}}_k^{\mathrm{H}} \bar{\mathbf{W}}_k\right), \tag{5.8}$$

where $\bar{\mathbf{K}}_k \triangleq \rho^2 \sum_{j \neq k} \bar{\mathbf{W}}_k^{\mathrm{H}} \bar{\mathbf{H}}_k \bar{\mathbf{V}}_j \bar{\mathbf{V}}_j^{\mathrm{H}} \bar{\mathbf{H}}_k^{\mathrm{H}} \bar{\mathbf{W}}_k + \sigma_n^2 \bar{\mathbf{W}}_k^{\mathrm{H}} \mathbf{W}_k^{\mathrm{H}} \mathbf{W}_k \bar{\mathbf{W}}_k$ is the interference plus noise covariance relative to the k-th UE, and where we recall that the dependence on $\mathbf{V}$ and $\mathbf{W}$ is because $\bar{\mathbf{H}} \triangleq \mathbf{W}^{\mathrm{H}} \mathbf{H} \mathbf{V}$.

5.2.3 Optimal Precoders and Combiners

In order to design a processing scheme which achieves the optimal effective network throughput, the mutual optimization of the (constrained) GoB and (unconstrained) mMIMO data beamformers should be considered. Let us first define the overall training overhead as follows.

Definition 5.1. Let $\mathbf{V} \in \mathbb{C}^{N_{\mathrm{BS}} \times D_{\mathrm{BS}}}$ be the GoB precoder at the BS. The training overhead $\omega(\mathbf{V}) \in [0, 1]$ in terms of pilot resource elements is defined as follows:

$$\omega(\mathbf{V}) \triangleq \frac{\tau}{T} \mathrm{card}\left(\mathrm{col}\left(\mathbf{V}\right)\right). \tag{5.9}$$

Note that the training overhead depends on how the GoB precoder $\mathbf{V}$ is designed. Indeed, $\mathrm{col}\left(\mathbf{V}\right)$ consist of the beams to train in the channel estimation phase (refer to Eq. (5.1) and Fig. 5.2).

Therefore, the achievable effective network throughput $\mathcal{R}$ can be expressed as

$$\mathcal{R}\left(\mathbf{V},\bar{\mathbf{V}},\mathbf{W},\bar{\mathbf{W}}\right) \triangleq \left(1-\omega\left(\mathbf{V}\right)\right)\sum_{k=1}^{K}\mathcal{R}_k\left(\mathbf{V},\bar{\mathbf{V}},\mathbf{W},\bar{\mathbf{W}}\right). \tag{5.10}$$

The optimal beamformers $\left(\mathbf{V}^*,\bar{\mathbf{V}}^*,\mathbf{W}^*,\bar{\mathbf{W}}^*\right)$ are then found as follows:

$$\begin{aligned}\left(\mathbf{V}^*,\bar{\mathbf{V}}^*,\mathbf{W}^*,\bar{\mathbf{W}}^*\right) = \underset{\mathbf{V},\bar{\mathbf{V}},\mathbf{W},\bar{\mathbf{W}}}{\operatorname{argmax}}\ & \mathbb{E}_{\mathbf{H}}\Big[\mathcal{R}\left(\mathbf{V},\bar{\mathbf{V}},\mathbf{W},\bar{\mathbf{W}}\right)\Big], \\ \text{subject to } & \mathrm{col}\left(\mathbf{V}\right)\in\mathcal{V} \\ & \mathrm{col}\left(\mathbf{W}_k\right)\in\mathcal{W},\ \forall k=[\![1,K]\!].\end{aligned} \tag{P$\star$}$$

Finding the global optimum for the optimization problem (P$\star$) is not trivial and often found to be intractable, even without considering the pre-log factor relative to the training overhead [87,96]. In this work, we follow the same approach of the previous Chapter 4 consisting in decoupling the precoder/combiner design, as the GoB beamformers can be optimized through long-term statistical information, whereas the mMIMO data beamformers can depend on the instantaneous CSI [87]. In particular, we consider two different timescales:

- **Small timescale** *(channel coherence time)*: within which the instantaneous channel realization $\mathbf{H}_k,\ \forall k$ is assumed to be constant and a single training phase is carried out for CSI acquisition at the BS;
- **Large timescale** *(beam coherence time)*: within which the covariance matrices $\mathbf{\Sigma}_k,\ \forall k$ – i.e. the spatial characteristics of the channels – are assumed to be constant and the long-term GoB beamformers are designed *(beam selection)*[2].

In the following section, we will focus on the design of the mMIMO data precoder and combiners with given multi-user effective channel $\bar{\mathbf{H}}$. Later, the design of the long-term GoB beamformers will be considered assuming fixed mMIMO data beamformers.

[2]The beam coherence time T_{beam} – which depends on the beam width, the UE speed and other factors – has been shown to be much longer than the channel coherence time T_{coh} [97].

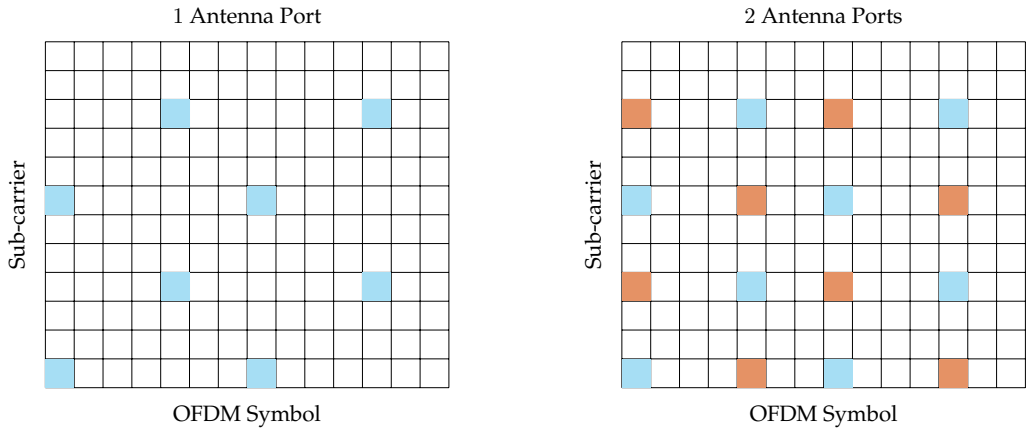

Figure 5.2 – CSI-RS locations in a DL NR resource block. When GoB precoding is used, the effective channels are mapped to one precoded RS each (or antenna port each, according to 3GPP) sent over τD_{BS} non-overlapping resource elements (here in light blue and orange). Therefore, less resource elements are available for transmitting data to the UEs, leading to throughput degradation.

5.3 Data Beamformers Design

Since we consider multi-beam processing at the UE side, i.e. $D_{\text{UE}} > 1$, the complete diagonalization of the effective channel $\bar{\mathbf{H}}$ at the BS side is suboptimal [98]. The Block Diagonalization (BD) approach is a popular method to design near-optimal beamformers that eliminate the multi-user interference in such scenarios. In particular, the mMIMO data precoder $\bar{\mathbf{V}}$ at the BS side aims to produce a block-diagonal $\bar{\mathbf{H}}\bar{\mathbf{V}}$ where no multi-user interference is experienced. The eventual remaining inter-stream interference can then be suppressed at the UE side through a proper combining operation. In this section, we review the complete procedure to perform the BD [98], which will allow for a simplified SE expression depending on the long-term GoB beamformers *only*.

To ensure a block-diagonal $\bar{\mathbf{H}}\bar{\mathbf{V}}$, the precoder $\bar{\mathbf{V}}_k$ has to be designed such that

$$\bar{\mathbf{H}}_j \bar{\mathbf{V}}_k = \mathbf{0}, \ \forall j \neq k. \tag{5.11}$$

Introducing the matrix $\bar{\mathbf{H}}_{/k} \in \mathbb{C}^{(K-1)D_{\text{UE}} \times D_{\text{BS}}}$ as

$$\bar{\mathbf{H}}_{/k} \triangleq \left[\bar{\mathbf{H}}_1^{\text{T}} \dots \bar{\mathbf{H}}_{k-1}^{\text{T}} \bar{\mathbf{H}}_{k+1}^{\text{T}} \dots \bar{\mathbf{H}}_K^{\text{T}}\right]^{\text{T}}, \tag{5.12}$$

the condition in (5.11) is enforced through letting $\bar{\mathbf{V}}_k$ lie in null $\left(\bar{\mathbf{H}}_{/k}\right)$. Whenever card $\left(\text{null}\left(\bar{\mathbf{H}}_{/k}\right)\right) \neq 0$, the BS can send interference-free data to the k-th UE.

As a first step, the Singular Value Decomposition (SVD) is performed on $\bar{\mathbf{H}}_{/k}$:

$$\bar{\mathbf{H}}_{/k} = \bar{\mathbf{U}}_{/k}\bar{\mathbf{S}}_{/k}\left[\bar{\mathbf{M}}_{/k}^{(1)}\bar{\mathbf{M}}_{/k}^{(0)}\right]^{\mathrm{H}}, \tag{5.13}$$

where $\bar{\mathbf{M}}_{/k}^{(1)}$ contains the first $\bar{M}_{/k} \triangleq \text{rank}\left(\bar{\mathbf{H}}_{/k}\right)$ right singular vectors of $\bar{\mathbf{H}}_{/k}$, while $\bar{\mathbf{M}}_{/k}^{(0)}$ contains the last $(D_{\text{BS}} - \bar{M}_{/k})$ ones. Thus, we know that

$$\bar{\mathbf{H}}_j\bar{\mathbf{M}}_k^{(0)} = \mathbf{0},\ \forall j \neq k. \tag{5.14}$$

The BD of the overall multi-user effective channel $\bar{\mathbf{H}}$ can then be expressed as

$$\bar{\mathbf{H}}_{\text{BD}} = \begin{bmatrix} \bar{\mathbf{H}}_1\bar{\mathbf{M}}_{/1}^{(0)} & & \mathbf{0} \\ & \ddots & \\ \mathbf{0} & & \bar{\mathbf{H}}_K\bar{\mathbf{M}}_{/K}^{(0)} \end{bmatrix}. \tag{5.15}$$

To achieve optimal SE, further SVD-based processing is carried out [98]. Since $\bar{\mathbf{H}}_{\text{BD}}$ is block diagonal, we can perform an individual SVD for each UE rather than decomposing the overall large matrix $\bar{\mathbf{H}}_{\text{BD}}$. In particular, we can write

$$\bar{\mathbf{H}}_k\bar{\mathbf{M}}_{/k}^{(0)} = \left[\bar{\mathbf{U}}_k^{(1)}\bar{\mathbf{U}}_k^{(0)}\right]\begin{bmatrix}\bar{\mathbf{S}}_k & \mathbf{0} \\ \mathbf{0} & \mathbf{0}\end{bmatrix}\left[\bar{\mathbf{M}}_k^{(1)}\bar{\mathbf{M}}_k^{(0)}\right]^{\mathrm{H}}. \tag{5.16}$$

The product $\bar{\mathbf{M}}_{/k}^{(0)}\bar{\mathbf{M}}_k^{(1)}$ produces an orthogonal basis with dimension $L_k \triangleq \text{rank}\left(\bar{\mathbf{H}}_k\bar{\mathbf{M}}_{/k}^{(0)}\right)$ and can be used as the interference-nulling precoder for the k-th UE, i.e. $\mathbf{V}_k = \bar{\mathbf{M}}_{/k}^{(0)}\bar{\mathbf{M}}_k^{(1)}$. In order to send interference-free data to the k-th UE, $\text{rank}\left(\bar{\mathbf{H}}_k\bar{\mathbf{M}}_{/k}^{(0)}\right) \geq 1$ is needed. The receive combiner $\bar{\mathbf{W}}_k$ relative to the k-th UE is then designed as $\bar{\mathbf{W}}_k = \bar{\mathbf{U}}_k^{(1)}$.

Lemma 5.3. *The condition rank* $\left(\bar{\mathbf{H}}_k\bar{\mathbf{M}}_{/k}^{(0)}\right) \geq 1$ *is respected when there exists at least one vector in row* $\left(\bar{\mathbf{H}}_k\right)$ *that is Linearly Independent (LI) of row* $\left(\bar{\mathbf{H}}_{/k}\right)$.

Proof. Let us assume that $\exists\ \mathbf{k} \in \text{row}\left(\bar{\mathbf{H}}_k\right)$ that is LI of row $\left(\bar{\mathbf{H}}_{/k}\right)$. Then, since $\bar{\mathbf{M}}_{/k}^{(0)}$ is a basis for null $\left(\bar{\mathbf{H}}_{/k}\right)$, we have $\mathbf{k}\bar{\mathbf{M}}_{/k}^{(0)} \neq \mathbf{0}$. Therefore, rank $\left(\bar{\mathbf{H}}_k\bar{\mathbf{M}}_{/k}^{(0)}\right) \geq 1$. □

Note that inverting the entire $\bar{\mathbf{H}}$ at the BS side through e.g. Zero-Forcing (ZF) precoding requires that each vector in row $\left(\bar{\mathbf{H}}_k\right)$ is LI of row $\left(\bar{\mathbf{H}}_{/k}\right)$. The BD approach offers thus more freedom for designing the GoB beamformers $\mathbf{V}$ and $\mathbf{W}$.

Proposition 5.1 ([98]). *When all the interference cancellation conditions are met, the instantaneous SE after BD precoding $\mathcal{R}_k^{\mathrm{BD}}(\mathbf{V},\mathbf{W})$ relative to the k-th UE can be written as follows:*

$$\mathcal{R}_k^{\mathrm{BD}}(\mathbf{V},\mathbf{W}) \triangleq \log_2 \det\left(\mathbf{I}_{L_k} + \kappa \bar{\mathbf{S}}_k^{\mathrm{H}} \bar{\mathbf{S}}_k\right), \tag{5.17}$$

where the dependence on $\mathbf{V}$ and $\mathbf{W}$ is hidden in the linear transformation (5.16).

Therefore, fixing BD as the mMIMO data precoder allows to reformulate (P$\star$) as a long-term joint transmit-receive beam selection problem, where the optimum GoB beamformers $(\mathbf{V}^*,\mathbf{W}^*)$ are found as follows:

$$\begin{aligned}\left(\mathbf{V}^{(\mathrm{P0})},\mathbf{W}^{(\mathrm{P0})}\right) = \underset{\mathbf{V},\mathbf{W}}{\operatorname{argmax}}\ & \mathbb{E}_{\mathbf{H}}\Big[\left(1-\omega\left(\mathbf{V}\right)\right)\sum_{k=1}^{K}\mathcal{R}_k^{\mathrm{BD}}\left(\mathbf{V},\mathbf{W}\right)\Big], \qquad \text{(P0)}\\ \text{subject to } & \operatorname{col}\left(\mathbf{V}\right)\in\mathcal{V}\\ & \operatorname{col}\left(\mathbf{W}_k\right)\in\mathcal{W},\ \forall k=[\![1,K]\!].\end{aligned}$$

The problem (P0) is a discrete optimization problem with a non-convex objective function. The solution for this class of problems is often hard to find and requires alternating minimization algorithms or relaxation techniques, which are however demanding to put into practice. In this work, we aim instead to design heuristic beam selection algorithms. In the next section, we will thus deal with the design of the long-term GoB beamformers $\mathbf{V}$ and $\mathbf{W}$.

5.4 Grid-of-Beams Beamformers Design

In general, it can be seen through inspecting the objective function in (P0) that designing proper GoB beamformers $\mathbf{V}$ and $\mathbf{W}$ implies *i)* harvesting large effective channel gain, *ii)* avoiding catastrophic multi-user interference, and *iii)* minimizing the training overhead. In this section, we investigate such conditions in detail so as to set the requirements for an effective GoB beamformers design. In particular, for each condition, we introduce a related beam selection optimization problem which approximates (P0) and whose practical implementation will be discussed in Section 5.5. To this end, we define the notion of relevant channel components and take a closer look at the beam reporting procedure defined in the current 5G NR specifications. Furthermore, we highlight the role of coordinating UEs in reducing the multi-user interference and the training overhead in the considered FDD mMIMO scenario.

5.4.1 Harvesting Large Effective Channel Gain

In the classical GoB implementation all the beams in the grid are trained regardless of their actual relevance, i.e. $D_{\text{BS}} = M_{\text{BS}}$. As pointed out in Section 1.2.1, such an operating mode is feasible for small GoBs only (refer to Fig. 5.2), although employing a small GoB, in turn, leads to a high performance loss [99]. In order to avoid exchanging performance for overhead, the intuition is to use a large GoB and leverage the knowledge of the long-term statistical information to train a few *(accurately)* selected beams to train, so as to keep $\omega = (\tau/T)\, D_{\text{BS}}$ small. In particular, in order to gather as much beamforming gain as possible, the idea is to capitalize on the so-called *relevant channel components*, whose number depends on the propagation environment.

Remark 5.1. This intuition has been exploited, to a large extent, to optimize mmWave communications. Owing to the sparse mmWave environment, few beams are enough to obtain an accurate low-dimensional representation of the actual channel [41]. □

Definition 5.2. We define the set $\mathcal{M}_k$ containing the relevant channel components (or relevant beam pairs) of the k-th UE as follows:

$$\mathcal{M}_k \triangleq \left\{(v,w) : \mathbb{E}_{\mathbf{H}_k}\left[\left|\mathbf{w}_w^{\text{H}}\mathbf{H}_k\mathbf{v}_v\right|^2\right] \geq \xi\right\}, \tag{5.18}$$

where ξ is a predefined power threshold.

Remark 5.2. The set $\mathcal{M}_k$ is *solely* dependent on the second order statistics of the channel $\mathbf{H}_k$. In particular, we refer to the notion of *beam coherence time* to denote the coherence time of such statistics. □

The following lemma establishes the mathematical relation between the relevant channel components and the second order statistics of the channel (channel covariance).

Lemma 5.4. *Let* $\boldsymbol{\Sigma}_k \triangleq \mathbb{E}_{\mathbf{H}_k}\left[\text{vec}\left(\mathbf{H}_k\right)\text{vec}\left(\mathbf{H}_k\right)^{\text{H}}\right] \in \mathbb{C}^{N_{\text{BS}}N_{\text{UE}}\times N_{\text{BS}}N_{\text{UE}}}$ *be the channel covariance matrix relative to the* k*-th UE. The set* $\mathcal{M}_k$ *containing the relevant channel components can be equivalently expressed as*

$$\mathcal{M}_k = \left\{(v,w) : \mathbf{b}_{v,w}^{\text{H}}\boldsymbol{\Sigma}_k\mathbf{b}_{v,w} \geq \xi\right\}, \tag{5.19}$$

where $\mathbf{b}_{v,w} \triangleq \left(\text{conj}\left(\mathbf{v}_v\right) \otimes \mathbf{w}_w\right) \in \mathbb{C}^{N_{\text{BS}}N_{\text{UE}}\times 1}$.

Proof. Refer to Appendix A.3. □

The relevant channel components relative to the k-th UE can thus be found through linear search over $M_{\text{BS}}M_{\text{UE}}$ elements, provided that the second order statistics of $\mathbf{H}_k$ are known.

Note that when the UEs exploit multi-beam covariance shaping, the set of relevant channel components can be altered[3]. Indeed, applying some receive beams means focusing on specific relevant beam pairs and neglecting some others. To this end, we define the subset $\mathcal{M}_k^{\text{BS}} \subseteq \mathcal{M}_k$ as follows.

Definition 5.3. We define the set $\mathcal{M}_k^{\text{BS}} \subseteq \mathcal{M}_k$ containing the relevant channel components (or, equivalently, beam pairs) of the k-th UE, when the k-th UE adopts $\mathbf{W}_k$ as its receive GoB combiner, as follows:

$$\mathcal{M}_k^{\text{BS}}(\mathbf{W}_k) \triangleq \{(v, w) \in \mathcal{M}_k : \mathbf{w}_w \in \mathbf{W}_k\}, \tag{5.20}$$

where we have introduced the notation $\mathcal{M}_k^{\text{BS}}(\cdot)$ to highlight that the set $\mathcal{M}_k^{\text{BS}}$ depends on the selected GoB combiner $\mathbf{W}_k$.

In more detail, for given GoB beamformers $\mathbf{V}$ and $\mathbf{W}_k$, an effective channel covariance $\bar{\mathbf{\Sigma}}_k$ can be defined. Furthermore, $\bar{\mathbf{\Sigma}}_k$ can be expressed in closed form as a function of the channel covariance $\mathbf{\Sigma}_k$, as highlighted in the following lemma.

Lemma 5.5. *Let* $\bar{\mathbf{\Sigma}}_k \triangleq \mathbb{E}_{\mathbf{H}_k}\left[\text{vec}\left(\mathbf{W}_k^{\text{H}}\mathbf{H}_k\mathbf{V}\right)\text{vec}\left(\mathbf{W}_k^{\text{H}}\mathbf{H}_k\mathbf{V}\right)^{\text{H}}\right] \in \mathbb{C}^{D_{\text{BS}}D_{\text{UE}} \times D_{\text{BS}}D_{\text{UE}}}$ *be the effective channel covariance relative to the k-th UE. $\bar{\mathbf{\Sigma}}_k$ can be equivalently expressed as*

$$\bar{\mathbf{\Sigma}}_k = \mathbf{B}_k^{\text{H}}\mathbf{\Sigma}_k\mathbf{B}_k, \tag{5.21}$$

where $\mathbf{B}_k \triangleq (\text{conj}(\mathbf{V}) \otimes \mathbf{W}_k) \in \mathbb{C}^{N_{\text{BS}}N_{\text{UE}} \times D_{\text{BS}}D_{\text{UE}}}$.

Proof. Refer to Appendix A.3. □

Let us now consider the single-user optimal SVD precoding [78] over the effective channels.

[3] With the exception of *spatially-uncorrelated* channels, where the same gain is expected from all spatial directions.

We can express the achievable SE at the k-th UE as follows:

$$\mathcal{R}_k^{\text{SVD}}\left(\mathbf{V},\mathbf{W}\right) \triangleq \log_2 \det\left(\mathbf{I}_{D_{\text{UE}}} + \kappa \mathbf{\Lambda}_k^{\text{H}} \mathbf{\Lambda}_k\right), \tag{5.22}$$

where we recall that $\kappa \triangleq \rho^2/\sigma_n^2$ and where $\mathbf{\Lambda} \triangleq \text{diag}\left(\lambda_1,\ldots,\lambda_{D_{\text{UE}}}\right)$, with $\lambda_1,\ldots,\lambda_{D_{\text{UE}}}$ being the singular values of the effective channel $\bar{\mathbf{H}}_k \triangleq \mathbf{W}_k^{\text{H}}\mathbf{H}_k\mathbf{V}$.

Proposition 5.2. *The average SE achievable at the k-th UE in a single-user scenario with SVD precoding can be upper bounded as follows:*

$$\mathbb{E}_{\mathbf{H}_k}\left[\mathcal{R}_k^{\text{SVD}}\left(\mathbf{V},\mathbf{W}_k\right)\right] \leq D_{\text{UE}} \log_2\left(1+\kappa D_{\text{UE}}^{-1}\text{Tr}\left(\bar{\mathbf{\Sigma}}_k\right)\right), \tag{5.23}$$

where $\bar{\mathbf{\Sigma}}_k$ is the effective channel covariance relative to the k-th UE.

Proof. Refer to Appendix A.3. □

Corollary 5.1. *The upper bound of the average SE in (5.23) is maximized when the effective channel covariance $\bar{\mathbf{\Sigma}}_k$ is shaped through the relevant beams.* □

Proof. Refer to Appendix A.3. □

Fig. 5.3 shows that the upper bound in (5.23) is tight and can be used to approximate the actual average SE. Thus, as a first approximation towards the maximization of the overall effective network throughput as in (P0), we formulate the uncoordinated beam selection problem (P1) which aims to maximize instead the sum SE defined as $\sum_{k=1}^{K}\mathcal{R}_k^{\text{SVD}}\left(\mathbf{V},\mathbf{W}_k\right)$:

$$\begin{aligned}\left(\mathbf{V}^{(\text{P1})},\mathbf{W}^{(\text{P1})}\right) = \underset{\mathbf{V},\mathbf{W}}{\text{argmax}} \sum_{k=1}^{K} D_{\text{UE}}\log_2\left(1+\kappa D_{\text{UE}}^{-1}\text{Tr}\left(\bar{\mathbf{\Sigma}}_k\right)\right), \\ \text{subject to } \text{col}\left(\mathbf{V}\right)\in\mathcal{V} \\ \text{col}\left(\mathbf{W}_k\right)\in\mathcal{W},\ \forall k=[\![1,K]\!].\end{aligned} \tag{P1}$$

Since the objective function in (P1) is *disjoint* with the UEs, (P1) can be solved through letting each UE maximizing its own related term in the sum. In particular, the k-th UE shapes its channel covariance using the beams in $\mathcal{M}_k$. Such a task requires a linear search over the $M_{\text{BS}}M_{\text{UE}}$ elements in the GoB codebooks. The relevant channel components (or beams) offers thus a straightforward method to design the GoB beamformers.

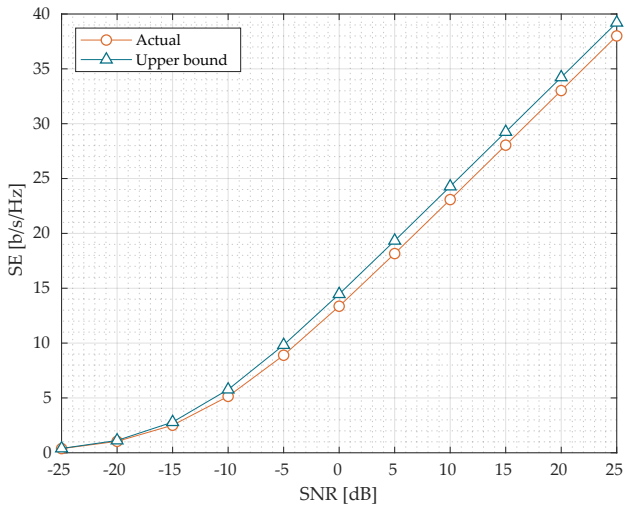

Figure 5.3 – Average SE vs SNR for a single-user case. Beam selection is based on the relevant beams. The upper bound in (5.23) can be used to approximate the actual SE.

5.4.2 Minimizing Multi-User Interference

As well-captured in Fig. 5.1, the uncoordinated selection of the GoB beamformers as in (P1) can lead to overall inefficient strategies in terms of training overhead and multi-user interference reduction. As opposed to uncoordinated approaches, clever coordinated beam selection strategies can help shaping the effective channel subspaces so as to optimize the multi-user transmission. In this section, we will show that a proper beam selection can be made so as to take multi-user interference into account within the covariance shaping process. To this end, we will introduce the so-called Generalized Correlation Matrix Distance (GCMD).

As seen in Section 5.3, the BD approach imposes two crucial conditions on the overall effective channel $\bar{\mathbf{H}} \triangleq \mathbf{W}^{\mathrm{H}}\mathbf{H}\mathbf{V}$ for transmitting data without multi-user interference:

- No inter-user interference $\iff \left|\text{null}\left(\bar{\mathbf{H}}_{/k}\right)\right| \neq 0$;
- No inter-stream interference $\iff \text{rank}\left(\bar{\mathbf{H}}_k \bar{\mathbf{M}}_{/k}^{(0)}\right) \geq 1$.

From Lemma 5.3, we know that the second condition requires at least one vector in row $\left(\bar{\mathbf{H}}_k\right)$ that is LI of row $\left(\bar{\mathbf{H}}_{/k}\right)$. Opposite to TDD mMIMO, where the LMMSE can return LI channel estimates depending on the propagation environment [15], the estimates in (5.5) are LI *almost surely*, due to independent channel realizations and estimation processes at the UE side. Therefore, the second condition for interference cancellation is *always* respected in the case of DL training with LMMSE at the UE side.

On the other hand, if $(K-1)D_{\text{UE}} < D_{\text{BS}}$, then $\left|\text{null}\left(\bar{\mathbf{H}}_{/k}\right)\right| \geq D_{\text{BS}} - (K-1)D_{\text{UE}} > 0$. Therefore, in such a case, it is *always* possible (for whatever $\mathbf{V}$ and $\mathbf{W}$) to find a matrix $\bar{\mathbf{M}}_{/k}^{(0)}$ in (5.13) different from the null matrix $\mathbf{0}$ and as such, to remove multi-user interference. In this case, the minimum training overhead becomes proportional to K and comparable to the one needed in TDD operation[4]. The bottom line is that $(K-1)\,D_{\text{UE}} < D_{\text{BS}}$ is the *only* condition that the BD precoding imposes on the GoB beamformers design in order to suppress multi-user interference.

Nevertheless, the BD precoding affects the received gain at the generic k-th UE. In particular, depending on how much the effective channels in $\bar{\mathbf{H}}$ are *spatially-separated*, the application of the precoding matrix $\bar{\mathbf{M}}_{/k}^{(0)}$ on $\bar{\mathbf{H}}_k$ can lead to a drastic gain loss compared to the single-user case (refer to Proposition 5.2). In order to infer such loss, the so-called Correlation Matrix Distance (CMD) can be used. The CMD has been introduced in [100] to measure the variation of the second-order statistics for fast-moving UEs. In a more recent work [22], the CMD has been exploited in mMIMO to increase the *spatial separability* among the UEs through covariance shaping at the UE side. The authors in [22] consider a two-user case. For multiple UEs, we introduce the Generalized Correlation Matrix Distance (GCMD) as follows.

Definition 5.4. We define the GCMD $\delta_k\left(\mathbf{\Sigma}_1, \ldots, \mathbf{\Sigma}_K\right) \in [0,1]$ between the channel covariance $\mathbf{\Sigma}_k$ of the k-th UE and the channel covariance $\mathbf{\Sigma}_j$ of the j-th UE, where $j \in [\![1, K]\!] \backslash \{k\}$ as

$$\delta_k\left(\mathbf{\Sigma}_1, \ldots, \mathbf{\Sigma}_K\right) \triangleq 1 - \frac{1}{K-1} \sum_{\substack{j=1 \\ j \neq k}}^{K} \frac{\text{Tr}\left(\mathbf{\Sigma}_k \mathbf{\Sigma}_j\right)}{\|\mathbf{\Sigma}_k\|_{\text{F}} \|\mathbf{\Sigma}_j\|_{\text{F}}}. \tag{5.24}$$

Note that the *spatial orthogonality* condition, i.e. $\text{Tr}\left(\mathbf{\Sigma}_k \mathbf{\Sigma}_j\right) = 0,\ \forall j \neq k$, which was exploited in several other studies related to FDD mMIMO optimization [11,12] is equivalent to $\delta_k\left(\mathbf{\Sigma}_1, \ldots, \mathbf{\Sigma}_K\right) = 1,\ \forall k$. This is a desirable spatial condition for which the BD incurs no reduction of the channel gain. On the other hand, the GCMD becomes zero when the covariance matrices of the UEs are equal up to a scaling factor. Both these extreme conditions are seldom experienced in practical scenarios [15,18]. Nevertheless, when the channel covariances are shaped through statistical beamforming, resulting in some *effective* channel covariances, the GCMD can be used as a metric to evaluate how the covariance shaping affects the *spatial separability* of the UEs.

[4] Although in TDD such overhead is generated in the UL channel.

In particular, we use the GCMD to introduce a *penalty factor* in $\mathcal{R}_k^{\text{SVD}}(\mathbf{V}, \mathbf{W}_k)$ so as to approximate the SE in (5.17) achieved after BD precoding. In this case, the optimal GoB beamformers $\left(\mathbf{V}^{(\text{P2})}, \mathbf{W}^{(\text{P2})}\right)$ are obtained through solving the coordinated beam selection problem (P2), as follows:

$$\left(\mathbf{V}^{(\text{P2})}, \mathbf{W}^{(\text{P2})}\right) = \underset{\mathbf{V},\mathbf{W}}{\text{argmax}} \sum_{k=1}^{K} D_{\text{UE}} \log_2 \left(1 + \kappa D_{\text{UE}}^{-1} \text{Tr}\left(\bar{\mathbf{\Sigma}}_k\right) \delta_k \left(\bar{\mathbf{\Sigma}}_1, \ldots, \bar{\mathbf{\Sigma}}_K\right)\right), \qquad \text{(P2)}$$

$$\text{subject to } (K-1) D_{\text{UE}} < D_{\text{BS}}$$

$$\text{col}(\mathbf{V}) \in \mathcal{V}$$

$$\text{col}(\mathbf{W}_k) \in \mathcal{W}, \ \forall k = [\![1, K]\!].$$

In (P2), the beam decision at the generic k-th UE influences the other beam decisions. Therefore, a central coordinator knowing all the large-dimensional channel covariances $\mathbf{\Sigma}_k, \ \forall k$ and which dictates the beam strategies to each UE is needed to solve this problem. In Section 5.5, we will propose a hierarchical approach to circumvent this issue. Note that in both (P1) and (P2) we have proposed approximations of the SE which neglect the pre-log factor relative to the training overhead. We will now look into the third condition required for an effective GoB beamformers design in the FDD mMIMO regime, which is the minimization of the training overhead.

5.4.3 Minimizing Training Overhead

There is a direct relation between the training overhead and the design of the GoB precoder $\mathbf{V}$ (refer to Definition 5.1). In particular, under the GoB assumption, the training overhead $\omega(\mathbf{V})$ ranges in $[1, (\tau/T)M_{\text{BS}}]$, where the right extreme is experienced when all the beams in the codebook $\mathcal{V}$ are trained. The more beams are trained, the more spatial degrees of freedom are obtained. However, when considering the training overhead, adding more and more beams is *likely* to result in diminishing returns [74].

The alternative is to train the relevant channel components [99, 101], as those relate to the spatial subspaces which give the strongest gain. In this case, the design of the precoder $\mathbf{V}$ is not separated from the design of the combiners $\mathbf{W}$, as well captured in (5.20). In the current 3GPP specifications, a beam reporting procedure is designed to assist the BS in the precoder selection [33]. Such procedure has a direct impact on the performance of the DL SE. In particular, the k-th UE reports to the BS the set $\mathcal{M}_k^{\text{BS}}(\mathbf{W}_k)$ – also known as Precoding Matrix Indicator (PMI) [33] – following an appropriate GoB combiner (beam) selection. To this end, we reformulate the definition of the training overhead, depending on the beam decisions carried out at the UE side.

Definition 5.5. Let $\mathbf{W} \in \mathbb{C}^{KN_{\text{UE}} \times KD_{\text{UE}}}$ be the overall GoB combiner as in (5.3). The training overhead $\omega(\mathbf{W})$ is defined as follows:

$$\omega(\mathbf{W}) \triangleq \frac{\tau}{T} \text{card}\left(\bigcup_{k=1}^{K} \mathcal{M}_k^{\text{BS}}(\mathbf{W}_k)\right). \tag{5.25}$$

In the 3GPP implementation, the beam decisions carried out at each UE have thus a central role in affecting the training overhead under the GoB approach. Note that $\omega(\mathbf{W})$ can increase and approach the extreme value $(\tau/T)M_{\text{BS}}$ in heterogeneous propagation environments with rich scattering, due to the growing number of relevant beams to activate at the BS side [99]. In this respect, adopting approaches such as (P1) or (P2) for selecting the beams can undermine the potential application of the GoB approach in multi-user scenarios. On the other hand, the largest training overhead reduction is achieved when the UEs coordinate in the beam domain so that (5.25) is minimized, which is

$$\min_{\mathbf{W}} \ \omega(\mathbf{W}). \tag{5.26}$$

In general, a balance between achievable beamforming gain and required training overhead, as well as multi-user interference, has to be considered in the beam decision process and combiner selection at the UEs. In the following, we formulate two optimization problems which take the pre-log factor relative to the training overhead into account. In the first one, the pre-log term is added in the objective function of the optimization problem (P1). Thus, we introduce thus the coordinated beam selection problem (P3), where both the achieved channel gain and the training overhead are taken into account, as follows:

$$\begin{aligned}\left(\mathbf{V}^{(\text{P3})}, \mathbf{W}^{(\text{P3})}\right) = \underset{\mathbf{V},\mathbf{W}}{\text{argmax}} \ & (1-\omega(\mathbf{W})) \sum_{k=1}^{K} D_{\text{UE}} \log_2\left(1 + \kappa D_{\text{UE}}^{-1} \text{Tr}\left(\bar{\mathbf{\Sigma}}_k\right)\right), \qquad \text{(P3)} \\ \text{subject to} \ & (K-1) D_{\text{UE}} < D_{\text{BS}} \\ & \text{col}(\mathbf{V}) \in \mathcal{V} \\ & \text{col}(\mathbf{W}_k) \in \mathcal{W}, \ \forall k = [\![1, K]\!].\end{aligned}$$

The last optimization problem that we introduce aims at balancing the three conditions for an effective GoB beamformers design that we have considered in this section. As such, the long-term beam selection problem (P4) includes the pre-log factor relative to the training overhead in the objective function of the problem (P2).

Problem	max *channel gain*	min *m.-u. interference*	min *training overhead*
Uncoordinated (P1)	☑	□	□
Coordinated (P2)	☑	☑	□
Coordinated (P3)	☑	□	☑
Coordinated (P4)	☑	☑	☑

Table 5.1 – The proposed optimization problems (P1)-(P4) with their considered sub-problems.

The optimum GoB beamformers $\left(\mathbf{V}^{(\mathrm{P4})}, \mathbf{W}^{(\mathrm{P4})}\right)$ are thus obtained as follows:

$$\begin{aligned}\left(\mathbf{V}^{(\mathrm{P4})}, \mathbf{W}^{(\mathrm{P4})}\right) \qquad & (\mathrm{P4})\\ = \underset{\mathbf{V},\mathbf{W}}{\operatorname{argmax}} \left(1-\omega\left(\mathbf{W}\right)\right) \sum_{k=1}^{K} D_{\mathrm{UE}} \log_2 \left(1+\kappa D_{\mathrm{UE}}^{-1} \mathrm{Tr}\left(\bar{\mathbf{\Sigma}}_k\right) \delta_k \left(\bar{\mathbf{\Sigma}}_1, \ldots, \bar{\mathbf{\Sigma}}_K\right)\right), \\ \text{subject to } \left(K-1\right) D_{\mathrm{UE}} < D_{\mathrm{BS}} \\ \mathrm{col}\left(\mathbf{V}\right) \in \mathcal{V} \\ \mathrm{col}\left(\mathbf{W}_k\right) \in \mathcal{W}, \ \forall k = [\![1, K]\!].\end{aligned}$$

The same conclusions drawn for the optimization problem (P2) are valid for (P4). In particular, to solve (P4), the central coordinator needs to know the PMIs $\mathcal{M}_k^{\mathrm{BS}}\left(\mathbf{W}_k\right), \forall k$ in addition to their channel covariances $\mathbf{\Sigma}_k, \forall k$.

Fig. 5.4 compares the effective network throughput $\mathcal{R}$ as in (P0) with its approximations in (P1)-(P4). The approximated objective function of the optimization problem (P4) gives the tightest upper bound to the actual effective network throughput as expected. We summarize the proposed optimization problems and their considered sub-problems as introduced above in Table 5.1.

In the next section, we will propose a framework exploiting D2D communications which will allow for a decentralized implementation of a series of beam selection algorithms based on the problems (P1)-(P4) described above. The nature of such problems is such that (P1)-(P4) offer and explore various *complexity-performance* trade-offs interesting from the implementation perspective.

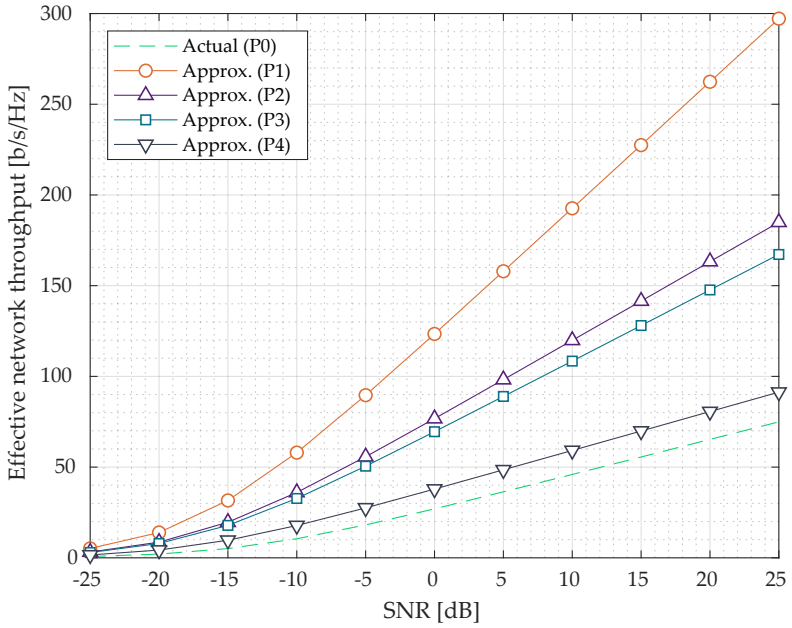

Figure 5.4 – Comparison of the actual effective network throughput $\mathcal{R}$ as in (5.10) and its approximations defined in (P0)-(P4). In this plot, $K = 7$ UEs. The beam selection at each UE is based on the local SNR. The approximation used for (P4) is the closest to the actual effective network throughput.

5.5 Decentralized Coordinated Beam Selection Algorithms

Although no instantaneous information is needed to solve (P1)-(P4), such problems still require a central coordinator that knows the channel covariances $\mathbf{\Sigma}_k \ \forall k$ and dictates the beam strategies to each UE. In this respect, collecting such large-dimensional statistical information at a central node as e.g. the BS involves additional resource overhead [2]. In order to achieve decentralized coordination, we propose to use the hierarchical information structure, introduced in Chapter 1.

The full signaling sequence of the proposed hierarchical beam selection is given in Fig. 5.5. The core part of the procedure resides in the beam decision made at each UE on a beam coherence time basis so that the respective objective function is maximized. Based on the objective functions in (P1)-(P4), we consider 4 different beam decision policies, as in (5.28). Such policies have different requirements concerning the statistical information to exchange through D2D side-links. In Table 5.2, we summarize the differences between the proposed beam selection policies based on (P1)-(P4) with respect to the required information at the k-th UE.

Algorithm	*Required local info.*	*Required info. to be exchanged through D2D*
Uncoordinated (P1)	$\mathbf{\Sigma}_k$	*Nothing*
Coordinated (P2)	$\mathbf{\Sigma}_k$	$\bar{\mathbf{\Sigma}}_j,\ j \in [\![1, k-1]\!]$
Coordinated (P3)	$\mathbf{\Sigma}_k$	$\mathcal{M}_j^{\text{BS}}(\mathbf{W}_j),\ j \in [\![1, k-1]\!]$
Coordinated (P4)	$\mathbf{\Sigma}_k$	$\bar{\mathbf{\Sigma}}_j,\ \mathcal{M}_j^{\text{BS}}(\mathbf{W}_j),\ j \in [\![1, k-1]\!]$

Table 5.2 – The proposed algorithms and their required information at the k-th UE. The information relative to the lower-ranked UEs $1, \dots, k-1$ is exchanged through D2D side-links.

Let us consider w.l.o.g. the beam selection at the k-th UE, i.e. at the k-th step of the algorithm, for the algorithm (P4). The algorithms (P1)-(P3) can be regarded as a sub-case of (P4). We define the set $\mathcal{W}_{k-1} \triangleq \{\mathbf{W}_1^*, \dots, \mathbf{W}_{k-1}^*\}$ containing the beam decisions which have been fixed prior to the k-th step. According to the hierarchical structure, the k-th UE knows the set $\mathcal{B}^{\text{fix}}(\mathcal{W}_{k-1}) \triangleq \cup_{j=1}^{k-1} \mathcal{M}_j^{\text{BS}}(\mathbf{W}_j^*)$ and the effective channel covariances $\bar{\mathbf{\Sigma}}_j,\ \forall j \in [\![1, k-1]\!]$. Therefore, the k-th UE can *i)* evaluate a *partial* GCMD $\delta_k\left(\bar{\mathbf{\Sigma}}_1, \dots, \bar{\mathbf{\Sigma}}_k\right)$ and *ii)* construct a *partial* GoB precoder $\mathbf{V}_{k-1}$ containing the precoding vectors relative to the indexes in $\mathcal{B}^{\text{fix}}(\mathcal{W}_{k-1})$. Likewise, the k-th UE can compute a *partial* $\omega(\mathcal{W}_{k-1})$.

The proposed decentralized beam selection $\mathbf{W}_k^*$ at the k-th UE can be then expressed in a recursive manner as follows:

$$\mathbf{W}_k^* = \underset{\mathbf{W}_k}{\text{argmax}}\ f_k\left(\left[\mathbf{V}_k \mathbf{V}_{k-1}\right], \{\mathbf{W}_k, \mathcal{W}_{k-1}\}\right), \tag{5.27}$$

where $\text{col}_m(\mathbf{V}_k) = \mathbf{v}_m\ \forall m \in \mathcal{M}_k^{\text{BS}}(\mathbf{W}_k)$, and

$$f_k(\mathbf{V}, \mathcal{W}) \triangleq \begin{cases} D_{\text{UE}} \log_2\left(1 + \kappa D_{\text{UE}}^{-1} \text{Tr}\left(\bar{\mathbf{\Sigma}}_k\right)\right) & \text{(P1)} \\ D_{\text{UE}} \log_2\left(1 + \kappa D_{\text{UE}}^{-1} \text{Tr}\left(\bar{\mathbf{\Sigma}}_k\right) \delta_k\left(\bar{\mathbf{\Sigma}}_1, \dots, \bar{\mathbf{\Sigma}}_k\right)\right) & \text{(P2)} \\ \left(1 - \omega(\mathcal{W})\right) D_{\text{UE}} \log_2\left(1 + \kappa D_{\text{UE}}^{-1} \text{Tr}\left(\bar{\mathbf{\Sigma}}_k\right)\right) & \text{(P3)} \\ \left(1 - \omega(\mathcal{W})\right) D_{\text{UE}} \log_2\left(1 + \kappa D_{\text{UE}}^{-1} \text{Tr}\left(\bar{\mathbf{\Sigma}}_k\right) \delta_k\left(\bar{\mathbf{\Sigma}}_1, \dots, \bar{\mathbf{\Sigma}}_k\right)\right) & \text{(P4)} \end{cases} \tag{5.28}$$

The intuition behind the proposed scheme is to let the k-th UE select the $\mathbf{W}_k \in \mathcal{W}$ maximizing the k-th term of the sum in the respective objective function, in a *greedy* manner. The remaining constraint $(K-1)D_{\text{UE}} < D_{\text{BS}}$ can be enforced at the BS through

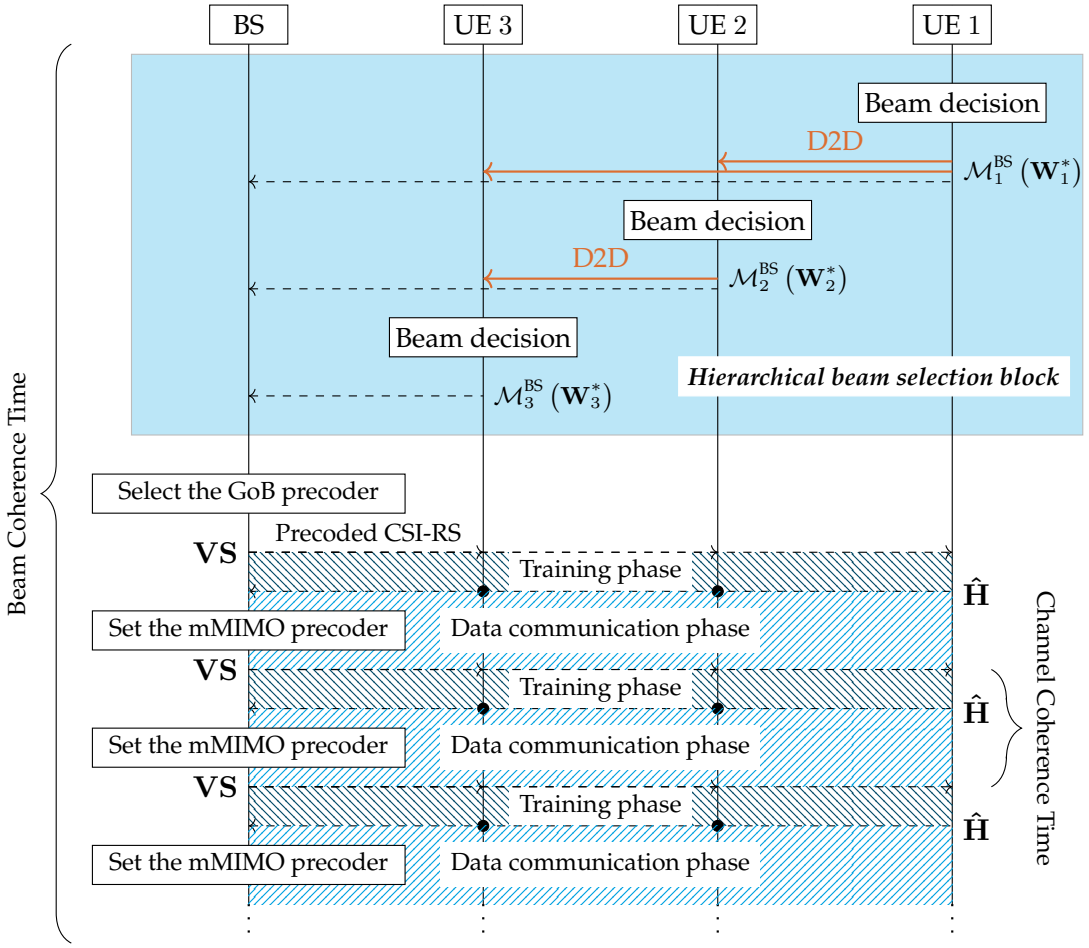

Figure 5.5 – Signaling sequence of the proposed coordinated beam selection (P3) for $K = 3$. The beam decision made at each UE leverages the D2D-enabled long-term statistical information coming from the lower-ranked UEs in a hierarchical fashion.

e.g. activating predefined beams until the constraint is respected. This decentralized problem can be addressed using linear (exhaustive) search in the codebook $\mathcal{W}$ at each UE. In particular, the linear search does not involve a large computational burden as the k-th UE has to evaluate the respective objective function in (5.28) in $\binom{M_{\mathrm{UE}}}{D_{\mathrm{UE}}}$ points. On the other hand, the direct solving of the optimization problems (P1)-(P4) requires combinatorial (exhaustive) search.

5.6 Simulation Results

We evaluate here the performance of the proposed decentralized beam selection algorithms. We assume $N_{\text{BS}} = 64$ and $N_{\text{UE}} = 4$. The beamforming vectors in $\mathcal{V}$ and $\mathcal{W}$ are Discrete Fourier Transform (DFT)-based orthogonal beams, according to the codebook-based transmission in 3GPP NR [34]. Furthermore, we assume that the UEs are allowed to indicate at most 4 relevant beam pairs each to the BS, i.e. the PMI $\mathcal{M}_k^{\text{BS}}(\mathbf{W}_k^*)$ is truncated to its 4 strongest elements $\forall k$. This is equivalent to the *Type II* CSI reporting in NR [34]. We assume that the UEs use the popular LMMSE method to estimate their instantaneous effective channels (refer to (5.5) and (5.6)), which are then fed back to the BS for BD-based precoder design (refer to Fig. 5.5). The *Zadoff-Chu* sequences are used for channel training [34]. According to 3GPP specifications, we consider a resource block consisting in 12 sub-carriers and 14 OFDM symbols [34]. All the metrics in the next plots are averaged over 10000 Monte-Carlo iterations with *varying network scenario*.

5.6.1 Winner II Channel Model

The channel model used for the simulations is the cluster-based Winner II model, which extends the 3GPP spatial channel model. The channel parameters are generated through statistical distributions extracted from channel measurements. Several measurement campaigns provide the background for the parametrization of the propagation scenarios. In particular, we consider the urban micro-cell scenario operating at 2.1 GHz. In urban micro-cell scenarios, both the BS and the UEs are assumed to be located outdoors in an area where the streets are laid out in a Manhattan-like grid. This scenario considers both line-of-sight and non-line-of-sight links. Like in all cluster-based models, the channel realizations are generated through summing the contributions of the multiple paths within each cluster. Those paths come with their own small scale parameters such as amplitude, angle-of-departure and angle-of-arrival. The superposition of several paths results in correlation between antenna elements and temporal fading with corresponding Doppler spectrum. Further information about the Winner II channel model can be found in [81].

5.6.2 Results and Discussion

In what follows, we show and discuss the performance achieved via the proposed algorithms. In particular, we will consider two different network scenarios: the *i)* with *randomly-located* UEs, and the *ii)* with *closely-located* UEs, i.e. *highly spatially-correlated* channels among the UEs.

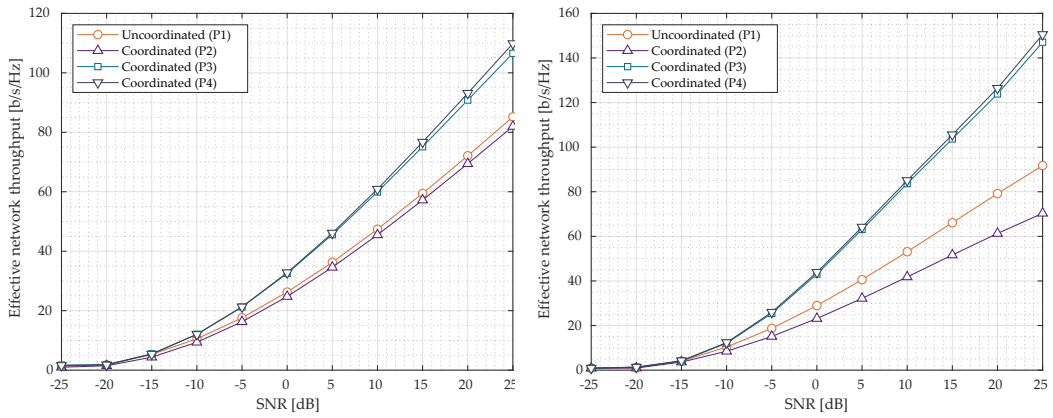

(a) $K = 7$ UEs (b) $K = 11$ UEs

Figure 5.6 – Average effective throughput vs SNR for (a) $K = 7$ and (b) $K = 11$ *randomly-located* UEs. $D_{\text{UE}} = 3$ beams activated at each UE. $T_{\text{coh}} = 15$ ms. The coordinated algorithms (P3) and (P4) outperform the uncoordinated (P1), as opposed to (P2).

We start with configuration *i)*. In Fig. 5.6a, we show the average effective network throughput as a function of the SNR for $K = 7$ UEs and a channel coherence time $T_{\text{coh}} = 15$ ms. Both the coordinated algorithms (P3) and (P4) outperform the uncoordinated benchmark (P1), with equal average effective throughput values obtained with up to 10 dBs less. Since T_{coh} is small, the pre-log factor dominates the log factor in (5.10). Therefore, just a small performance gap divides (P3) from (P4) and, as such, according to Table 5.2, the algorithm (P3) is preferable in this case (as much less information needs to be shared among the UEs). On the other hand, the coordinated algorithm (P2) performs even worse than the uncoordinated benchmark (P1). In particular, when the channel coherence time T_{coh} is small, shaping the covariances so as to maximize the *spatial separability* of the UEs is counter-effective. Some more insights on this are given in the next paragraph. Since the training overhead increases with K, the performance gain achieved via the coordinated algorithms (P3) and (P4) surges in Fig. 5.7b for $K = 11$. For the same reason, the gap between (P2) and the other solutions increases.

Fig. 5.7a shows the average throughput gain over the uncoordinated benchmark (P1) as a function of T_{coh} for $K = 7$ UEs. In particular, two areas can be identified. We describe them in the following.

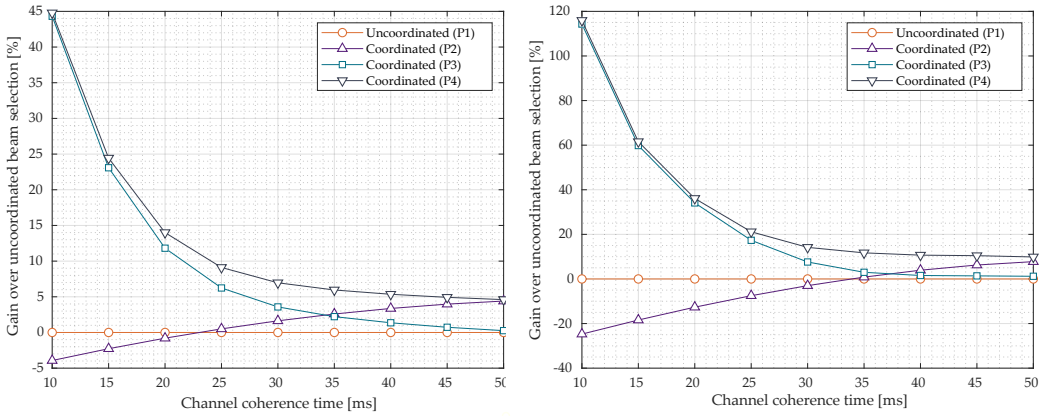

(a) $K = 7$ UEs (b) $K = 11$ UEs

Figure 5.7 – Average effective throughput gain over uncoordinated beam selection (P1) vs T_{coh} for $K = 7$ UEs. The SNR is 11 dB. Taking the pre-log factor into account is essential for an effective coordinated beam selection under *fast-varying* channels where $T_{\text{coh}} < 20$ ms.

$T_{\text{coh}} < 20$ ms, i.e. vehicular or fast pedestrian channels

where (P3) and (P4) have high gains compared to the other solutions (up to 45%) and where the coordinated algorithm (P2) performs even worse than the uncoordinated (P1). Indeed, as we can see in Fig. 5.8, in order to achieve greater spatial separation across the UEs, the algorithm based on (P2) activates a much greater number of beams at the BS side. Under *fast-varying* channels, and in particular for a greater number of UEs, this leads to unbearable training overhead.

$T_{\text{coh}} \geq 20$ ms, i.e. pedestrian channels

where the gap between (P3)-(P4) and (P1) reduces (up to 15%). In particular, (P3) converges to the uncoordinated benchmark (P1). This is because the training overhead becomes negligible for long channel coherence times, and it is more important to focus on the log factor in (5.10). For the same reason, (P2) experiences gains over the uncoordinated solution (P1) for $T_{\text{coh}} \geq 20$ ms. The coordinated algorithm (P4) converges to (P2). Therefore, for long channel coherence times, (P2) allows to avoid some additional coordination overhead, according to Table 5.2 and, as such, is preferable.

The same reasoning holds for Fig. 5.7b with $K = 11$ UEs, where the positive and negative behaviors described above are intensified. In particular, for $T_{\text{coh}} < 20$ ms, (P3) and (P4) achieve up to 120% gain over (P1), while 20% loss is achieved with (P2).

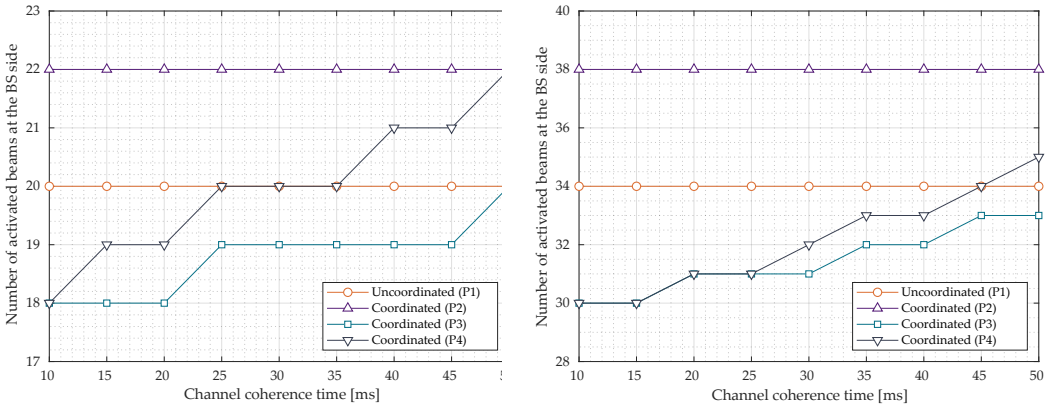

(a) $K = 7$ UEs (b) $K = 11$ UEs

Figure 5.8 – Average D_{BS} for the proposed algorithms vs T_{coh} for (a) $K = 7$ and (b) $K = 11$ UEs. The SNR is 11 dB. The coordinated algorithm (P2) activates more beams at the BS side in order to achieve greater spatial separation among the UEs.

Let us now focus on the configuration *ii)*, where neighboring UEs are considered and a higher spatial correlation is found among them. Fig. 5.9 shows the average throughput gain over the uncoordinated benchmark as a function of the channel coherence time T_{coh}. We can see that the coordinated algorithm (P2) outperforms the uncoordinated solution (P1) for all the considered values of T_{coh}. Indeed, due to the increasing spatial correlation among the UEs, the multi-user interference becomes non-negligible even for small channel coherence times below 20 ms. Moreover, in this case, the performance gain obtained through (P4) justifies more the need to exchange some additional long-term information compared to the other solutions (refer to Table 5.2).

5.7 Conclusions

In this chapter, we have proposed a decentralized multi-user beam selection algorithm exploiting long-term statistical information and its exchange through D2D side-links. The proposed scheme explores the interesting *trade-off* between *i)* harvesting large effective channel gain, *ii)* avoiding catastrophic multi-user interference (low spatial separation among the UEs), and *iii)* minimizing the training overhead, which arises in networks where the *scalability* of the RSs is a main concern. We have shown the effectiveness of the proposed algorithm through numerical results. In particular, under *fast-varying* channels where the channel coherence time is below 20 ms, the proposed algorithm allows for substantial performance gains compared to other solutions in the literature which aim at the maximum spatial separation of the UEs.

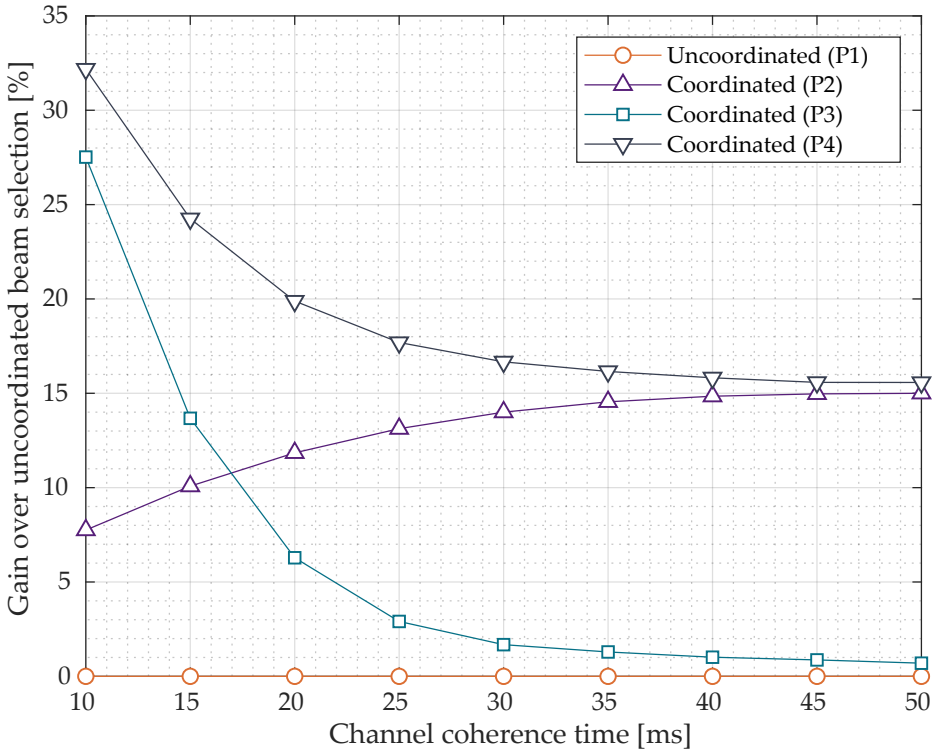

Figure 5.9 – Average effective throughput gain over uncoordinated beam selection (P1) vs T_{coh} for $K = 7$ *closely-located* UEs. The SNR is 11 dB. Owing to high spatial correlation among the UEs, the algorithm (P2) achieves high gains compared to the solutions which neglect the multi-user interference.

Chapter 6

Spectrum Sharing in mmWave: Coordination vs Privacy Trade-Off

6.1 Introduction

Millimeter Wave (mmWave) communications have given a renewed impetus to spectrum sharing, which allows multiple mobile operators to pool their spectral resources. Compared to conventional (sub-6 GHz) mobile communications, less interference is in general produced in mmWave networks due to the inherent propagation characteristics and *highly-directional* beamforming [41, 102]. In particular, even without coordination, sharing spectrum and Base Stations (BSs) among operators shows great potential in mmWave scenarios when massive antennas are used at both the BS and User Equipment (UE) sides [103]. In addition to such technical gains, sharing resources translates into substantial economic profit for the mobile operators. For example, dense infrastructure is an expected need for effective mmWave coverage in 5G networks and spectrum sharing among operators can help decrease equipment and operating costs [104]. In parallel, expenditure arising from spectrum licensing could be reduced as well.

Although uncoordinated mmWave shared spectrum access is beneficial under certain circumstances, further gains can be achieved through inter-operator coordination. Indeed, non-negligible interference is experienced when e.g. non-massive antennas are used at the UE side, or also when the densities of either the UEs or the BSs increase, i.e. for reduced spatial separation among the UEs [105] or increased multi-cell interference.

Nevertheless, the potential in coordinated spectrum sharing across operators implies several practical challenges. For example, as seen in Chapter 1, global Channel State Information (CSI) should be obtained for transmission optimization, leading to

substantial signaling overhead. Perhaps even more acute is the problem of *data privacy preservation* between otherwise competing operators. Since coordination entails some CSI flowing from one mobile operator to another, *information privacy* issues emerge. This problem is severe in mmWave networks where, owing to strong Line-of-Sight (LOS) propagation behavior [82, 102], the CSI data bears correlation with UE location information, which for obvious reasons is undesirable for an operator to reveal [106].

In this work, we look at the third and last case of Table 1.1, where K BSs coordinate to achieve greater performance in mmWave spectrum sharing. In this context, we investigate the *trade-off* between *coordination* and *privacy*. We propose a low-overhead Signal-to-Leakage-and-Noise Ratio (SLNR)-based scheduling algorithm exploiting statistical side-information. To tackle the aforementioned *privacy* problem, we consider an information exchange scheme including an obfuscation mechanism borrowed from the *security* literature [107–109]. In mmWave spectrum sharing, this mechanism allows to mitigate the one-to-one correspondence between beams and UEs' locations.

6.2 Models and Problem Formulation

We consider a multi-cell multi-operator downlink mmWave scenario in Fig. 6.1, where several mobile operators coexist and share the available mmWave spectrum. We consider B BSs, all equipped with $N_{\text{BS}} \gg 1$ antennas, and K associated UEs per BS, using single omni-directional antennas. To ease the exposition, we assume *analog-only* beamforming with a single RF chain [41, Fig. 2]. Therefore, each BS uses a single beam *only* per resource slot. In particular, in a given slot, the b-th BS precodes the signal to the k-th UE using the unit norm vector $\mathbf{w}_{b,k}$, extracted from a codebook with constant-magnitude elements, due to hardware constraints (phase shifters) [41].

6.2.1 3D Millimeter Wave Channel Model

In this chapter, we extend the two-dimensional geometric channel described in Chapter 2 to a three-dimensional geometric channel. The channel $\mathbf{h}_{b,k} \in \mathbb{C}^{N_{\text{BS}} \times 1}$ between the b-th BS and the k-th UE can be expressed as follows [51]:

$$\mathbf{h}_{b,k} \triangleq \sqrt{N_{\text{BS}}} \sum_{\ell=1}^{L} \alpha_{b,k,\ell} \mathbf{a}_{\text{BS}} \left(\theta_{b,k,\ell}, \phi_{b,k,\ell}\right), \tag{6.1}$$

where $\alpha_{b,k,\ell} \sim \mathcal{CN}(0, \sigma^2_{\alpha_{b,k,\ell}})$ denotes the complex gain of the ℓ-th path and where $\mathbf{a}_{\text{BS}}(\theta_{b,k,\ell}, \phi_{b,k,\ell}) \in \mathbb{C}^{N_{\text{BS}} \times 1}$ denotes the antenna steering vector at the b-th BS with the

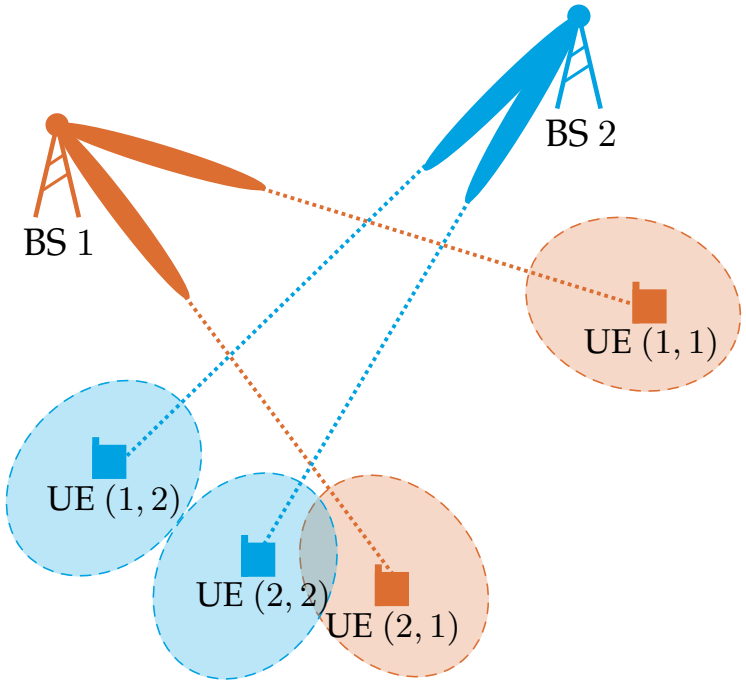

Figure 6.1 – Scenario example with $B = 2$ BSs. Each base station serves its UEs through forming *highly-directional* beams towards them. We consider 3D beamforming with UPAs, such that beam footprints result around the UEs and *possibly overlap*.

corresponding Angle-of-Departure (AoD) $(\theta_{b,k,\ell}, \phi_{b,k,\ell}) \in [0, 2\pi) \times (0, \frac{\pi}{2}]$ in its azimuth and elevation components. In order to enable 3D beamforming, we assume to use *Uniform Planar Arrays (UPAs)*, so that [41]

$$\mathbf{a}_{\mathrm{BS}}(\theta, \phi) \triangleq \mathbf{a}_{\mathrm{H}}(\theta, \phi) \otimes \mathbf{a}_{\mathrm{E}}(\phi), \tag{6.2}$$

where $\otimes$ denotes the Kronecker product, and with

$$\mathbf{a}_{\mathrm{H}}(\theta, \phi) \triangleq \sqrt{\frac{1}{N_{\mathrm{BS_H}}}} \left[1 \quad \dots \quad e^{-i\pi(N_{\mathrm{BS_H}}-1)\cos(\theta)\cos(\phi)}\right]^{\mathrm{T}}, \tag{6.3}$$

$$\mathbf{a}_{\mathrm{E}}(\phi) \triangleq \sqrt{\frac{1}{N_{\mathrm{BS_E}}}} \left[1 \quad \dots \quad e^{-i\pi(N_{\mathrm{BS_E}}-1)\sin(\phi)}\right]^{\mathrm{T}}, \tag{6.4}$$

where $N_{\mathrm{BS_H}}$ (resp. $N_{\mathrm{BS_E}}$) defines the number of horizontal (resp. vertical) UPA elements.

6.2.2 Beam Codebook

To design the beamforming vector $\mathbf{w}_{b,k}$, we assume that each BS selects the beam configuration within a predefined beam codebook [41]. To benefit from Full-Dimensional MIMO (FD-MIMO), a Discrete Fourier Transform (DFT)-based codebook has been proposed in [110]. Such a codebook results from the Kronecker product of two oversampled DFT codebooks. In particular, we have

$$\mathbf{w}_{\eta(w,v)} \triangleq \mathbf{w}_{\mathrm{H},w} \otimes \mathbf{w}_{\mathrm{E},v}, \quad w \in [\![1, N_{\mathrm{BS_H}}]\!], \quad v \in [\![1, N_{\mathrm{BS_E}}]\!], \tag{6.5}$$

where $\mathbf{w}_{\mathrm{H},w}$ and $\mathbf{w}_{\mathrm{E},v}$ are as in [110, eq. (5)], and $\eta(w,v) : [\![1, N_{\mathrm{BS_H}}]\!] \times [\![1, N_{\mathrm{BS_E}}]\!] \to [\![1, N_{\mathrm{BS}}]\!]$ is a bijection, e.g. $f(w,v) = N_{\mathrm{BS_E}}(w-1) + v$.

6.2.3 Coordinated Time Division Scheduling Problem

We first present the centralized coordination problem towards spectrum sharing, based on scheduling and beamforming. We assume a time division framework [111] in which each scheduling period, i.e. a time frame with length T, is divided into N_s slots with length $T_s = T/N_s$, as shown in Figure 6.2. The channel coherence time is assumed to be long enough so that all the UEs can be scheduled in one time frame. Based on their available information, and aiming to improve the spectrum sharing performance, the BSs assign one UE each per time slot.

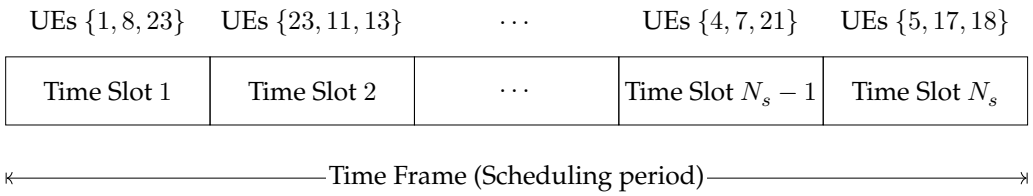

Figure 6.2 – Time division scheduling with $B = 3$ BSs and a sample assignment. In each time slot, each BS selects one UE to schedule. In this example, the BS 1 chose the UEs $\{1, 23, \ldots, 4, 5\}$ overall.

In the following, we assume that the association between BSs and UEs has been accomplished based on minimum UE-BS distance criterion. The association between one BS and one UE in a mmWave network involves a beam choosing stage for which a transmit beam is selected to communicate. We assume a Signal-to-Noise Ratio (SNR) maximization scheme such that the b-th BS serves its k-th UE using the following beam index $\eta_k \in [\![1, N_{\mathrm{BS}}]\!]$:

$$\eta_k = \underset{\eta \in [\![1, N_{\mathrm{BS}}]\!]}{\operatorname{argmax}} \left| \mathbf{h}_{b,k} \mathbf{w}_\eta \right|^2. \tag{6.6}$$

Let us denote with $\mathcal{S}(n)$ the set containing all the UEs scheduled in the time slot n. The instantaneous SINR for the k-th UE, where $k \in \mathcal{S}(n)$, can be expressed as follows:

$$\gamma_k\left(\mathcal{S}(n), \mathcal{P}\right) \triangleq \frac{\mathcal{P}_{k,k}}{\sum\limits_{j \in \mathcal{S}(n)} \mathcal{P}_{j,k} + \sigma_n^2}, \tag{6.7}$$

where we have defined the received power at the k-th UE being intended for the j-th one, as

$$\mathcal{P}_{j,k} \triangleq \left|\mathbf{h}_{q,k}\mathbf{w}_{\eta_j}\right|^2. \tag{6.8}$$

Remark 6.1. We have made here the abuse of notation $\mathbf{h}_{q,k}$ to denote the channel between the q-th BS (associated with the j-th UE)and the k-th UE (associated with the b-th BS). The BS indexes b and q are thus implicit in $\mathcal{P}_{j,k}$ from now on. □

The scheduling problem consists in selecting the subset of UEs to schedule in each time slot so as to maximize the average network sum-rate. Let $\mathcal{S} = \{\mathcal{S}(1), \ldots, \mathcal{S}(N_s)\}$ denote the overall scheduling assignments, then the optimal scheduling decision $\mathcal{S}^*$ can be found as follows:

$$\mathcal{S}^* = \underset{\mathcal{S}}{\operatorname{argmax}} \sum_{(k,n) \in \mathcal{S}(n) \times [\![1, N_s]\!]} \log_2\left(1 + \gamma_k(\mathcal{S}(n), \mathcal{P})\right). \tag{6.9}$$

The optimization problem in (6.9) is a challenging subset selection problem. In addition, to solve (6.9), the instantaneous CSI of all the UEs need to be shared across the BSs, or as an alternative be provided to a centralized coordinator. We are interested instead in distributed approaches to solve the scheduling problem. In what follows, we first present a version of such algorithm *without* privacy considerations, we then turn to the coordination-privacy trade-off in Section 6.4.

6.3 Successive Scheduling

In the decentralized case, opposite to (6.9), the operators need to enforce coordination while not being able to *accurately* predict each other scheduling actions. Since each scheduling decision impacts on the overall network performance (and on the other scheduling decisions), the problem becomes even more challenging and requires some iterations with guessing. To go around this issue, we follow the well-known successive scheduling approach, such as presented in [112].

6.3.1 SINR-Based Successive Coordinated Scheduling

In successive scheduling, a *ranking* is first defined among the BSs and allows for consecutive scheduling decisions, in a *greedy sub-optimal* manner. In particular, at the b-th step of the successive scheduling algorithm, the b-th BS knows the $b-1$ scheduling decisions made at the lower-ranked BSs $\{1,\dots,b-1\}$. In this work, we assume an *arbitrary* ranking. Fixing some scheduling decisions allows to evaluate the so-called *partial* Signal-to-Interference-and-Noise Ratio (SINR), in which the b-th BS solely considers the leakage coming from the UEs selected by the lower-ranked BSs in the considered time slot. Since the same operation is carried out for each time slot, we drop from now on the time slot index n to lighten the notation.

Let us denote with $\mathcal{S}^b_{\text{SINR}} = \{k^1_{\text{SINR}},\dots,k^b_{\text{SINR}}\} = \{\mathcal{S}^{b-1}_{\text{SINR}}, k^b_{\text{SINR}}\}$ the set consisting of all the scheduling decisions completed at the b-th step of the successive scheduling. Then the *partial* SINR $\hat{\gamma}_k$ for the k-th UE can be expressed as follows:

$$\hat{\gamma}_k\big(\mathcal{S}^{b-1}_{\text{SINR}}, \mathcal{P}\big) \triangleq \frac{\mathcal{P}_{k,k}}{\sum\limits_{j\in\mathcal{S}^{b-1}_{\text{SINR}}} \mathcal{P}_{j,k} + \sigma_n^2}, \tag{6.10}$$

where the denominator includes the received power at the k-th UE being intended for the j-th one, where $j \in \mathcal{S}^{b-1}_{\text{SINR}}$, i.e. the other UEs being scheduled in the considered time slot.

Assuming that the scheduling information $\mathcal{S}^{b-1}_{\text{SINR}}$, from lower-ranked BSs $\{1,\dots,b-1\}$ have been received[1] at the b-th BS, the optimal successive scheduling decision $\mathcal{S}^b_{\text{SINR}}$ at the b-th BS can be expressed as follows:

$$\mathcal{S}^b_{\text{SINR}} = \underset{k}{\text{argmax}}\ \log_2\big(1+\hat{\gamma}_k(\mathcal{S}^{b-1}_{\text{SINR}}, \mathcal{P})\big). \tag{6.11}$$

6.3.2 SLNR-Based Successive Coordinated Scheduling

Using the SLNR to optimize the scheduling decisions – rather than the SINR as in (6.11) – can prove advantageous as it does not require the knowledge of the channel between the considered k-th UE and other BSs, which might be unpractical to obtain or estimate.

[1] This information is assumed to be sent via dedicated channels and to be *perfectly* decoded at the intended BS.

Let us consider the k-th UE, then its *partial* SLNR $\underline{\gamma}_k$ can be expressed as follows:

$$\underline{\gamma}_k(\mathcal{S}_{\text{SLNR}}^{b-1}, \mathcal{P}) \triangleq \frac{\mathcal{P}_{k,k}}{\sum\limits_{j \in \mathcal{S}_{\text{SLNR}}^{b-1}} \mathcal{P}_{k,j} + \sigma_n^2}, \tag{6.12}$$

where, as opposite to (6.10), the denominator includes the leakage $\mathcal{P}_{k,j}$ produced by the k-th UE on the other UEs being scheduled in the considered time slot, denoted with $\mathcal{S}_{\text{SLNR}}^{b-1}$.

Assuming that the scheduling information $\mathcal{S}_{\text{SLNR}}^{b-1}$ from lower-ranked BSs $\{1, \ldots, b-1\}$ have been received, the optimal SLNR-based successive scheduling decision $\mathcal{S}_{\text{SLNR}}^{b}$ at the b-th BS is obtained through solving the following optimization problem:

$$\mathcal{S}_{\text{SLNR}}^{b} = \underset{k}{\text{argmax}} \ \underline{\gamma}_k(\mathcal{S}_{\text{SLNR}}^{b-1}, \mathcal{P}). \tag{6.13}$$

Note that the above requires instantaneous CSI in principle. However, the method can be modified to leverage statistical CSI instead as is shown in the following.

6.3.3 Average Leakage Power Through Beam Footprints

To reduce the severe overhead arising from global CSI exchange with massive antennas, we seek a coordination protocol which instead allows exchanging low-rate[2] *beam index* information between the operators. In the following, we show that such information allows the BSs to estimate the potential (average) SLNR, without resorting to instantaneous CSI. Towards this, we assume that when the b-th BS receives the scheduling information $\mathcal{S}^{b-1}$, a beam-related information $\eta_j, \ j \in \mathcal{S}^{b-1}$ is appended as well.

Let us consider the leakage $\mathcal{P}_{k,j}$ for a full-LOS case, i.e. $\alpha_{b,k,\ell}^2 = 0, \ \forall \ell$ relative to Non-Line-of-Sight (NLOS) paths. We are interested in its expected value (over small-scale fading), which is

$$\begin{aligned}
\mathbb{E}\left[\mathcal{P}_{k,j}\right] &= \mathbb{E}_{\alpha_{b,j}}\left[\left|\sqrt{N_{\text{BS}}}\alpha_{b,j}\mathbf{a}_{\text{BS}}(\theta_{b,j}, \phi_{b,j})\mathbf{w}_{\eta_k}\right|^2\right] \\
&= \mathbb{E}_{\alpha_{b,j}}\left[\left|\mathcal{G}_{\eta_k}(\theta_{b,j}, \phi_{b,j})\alpha_{b,j}\right|^2\right] \\
&= \mathcal{G}_{\eta_k}(\theta_{b,j}, \phi_{b,j})\sigma_{\alpha_{b,j}}^2,
\end{aligned} \tag{6.14}$$

where $\mathcal{G}_{\eta_k}(\theta_{b,j}, \phi_{b,j})$ denotes the beamforming gain received at the j-th UE with the beam η_k intended for the k-th one.

[2]The so-called *beam coherence time* has been reported to be in general much longer than the channel coherence time [97].

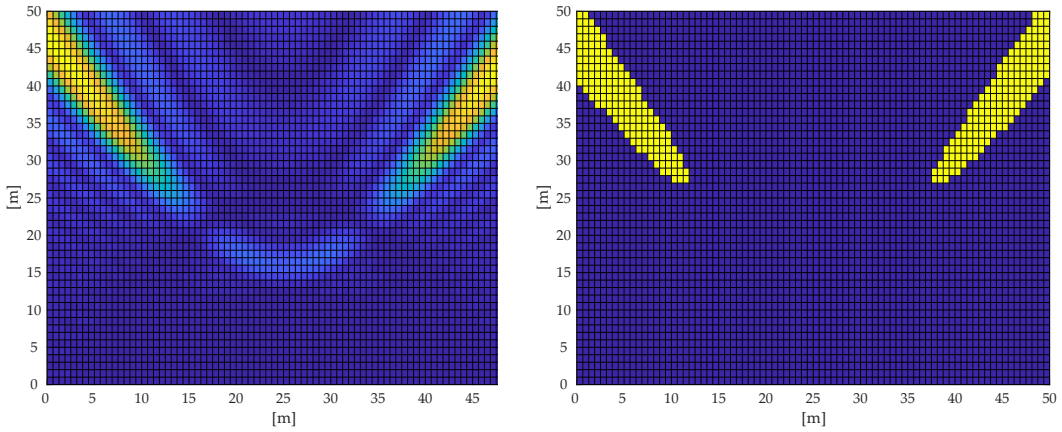

Figure 6.3 – Beamforming gain per location obtained with two beams in (6.5) and their associated footprints, considered as the spatial region where the normalized gain is higher than $1/2$.

To evaluate (6.14), the b-th BS needs to know the AoD $(\theta_{b,j}, \phi_{b,j})$ and the average path gain $\sigma^2_{\alpha_{b,j}}$. Note that, although the latter is a long-term *locally-available* statistical information (it is the average gain observed on a particular local direction), the former is hard to obtain in a scenario with multiple operators. Still, beam-related information exchanged with the q-th BS can assist in evaluating $\mathbb{E}\big[\mathcal{P}_{k,j}\big]$. In particular, the beams in (6.5) concentrate on different spatial regions [110]. Their main lobes illuminate non-overlapping regions, also known as *beam footprints* (refer to Fig. 6.3).

As a consequence, beam-related information might *implicitly* circumscribe the UEs' locations within the *beam footprints* – in particular in LOS-dominated environments as the mmWave one [82, 102]. Let us assume that the j-th UE is served through a LOS path, then we can bound its actual location $\boldsymbol{\ell}_j \in \mathbb{R}^2$ within the footprint of its serving beam η_j. It is possible then to compute the average leakage $\mathbb{E}\big[\mathcal{P}_{k,j}\big]$ with respect to all the plausible positions of the j-th UE within the footprint of η_j.

In particular, we can evaluate $\mathbb{E}\big[\mathcal{P}_{k,j}\big]$ as follows:

$$\begin{aligned}\mathbb{E}\left[\mathcal{P}_{k,j}\right] &= \mathbb{E}_{(\theta_{b,j},\phi_{b,j})|\eta_k}\left[\mathcal{G}_{\eta_k}(\theta_{b,j},\phi_{b,j})\sigma^2_{\alpha_{b,j}}\right] \\ &= \int_{(\theta_{b,j},\phi_{b,j})\in\mathcal{Q}_{\eta_j}} \mathcal{G}_{\eta_k}(\theta_{b,j},\phi_{b,j})\sigma^2_{\alpha_{b,j}} d(\theta_{b,j},\phi_{b,j}) \\ &\overset{(a)}{=} \int_{(\theta_{b,j},\phi_{b,j})\in\mathcal{Q}_{\eta_j}\cap\mathcal{Q}_{\eta_k}} G\sigma^2_{\alpha_{b,j}} d(\theta_{b,j},\phi_{b,j}) \\ &+ \int_{(\theta_{b,j},\phi_{b,j})\notin\mathcal{Q}_{\eta_j}\cap\mathcal{Q}_{\eta_k}} g\sigma^2_{\alpha_{b,j}} d(\theta_{b,j},\phi_{b,j}),\end{aligned} \tag{6.15}$$

where $\mathcal{Q}_\eta$ contains the AoD related to the footprint of the generic beam $\eta \in [\![1, N_{\text{BS}}]\!]$, and where (a) follows the well-known sectored antenna model [113], i.e.

$$\mathcal{G}_\eta(\theta,\phi) \triangleq \begin{cases} G, & (\theta,\phi)\in\mathcal{Q}_\eta \\ g, & \text{otherwise}\end{cases} \tag{6.16}$$

which results in considering $\mathcal{G}_{\eta_j}(\theta_{j,k},\phi_{j,k}) = G$ in the overlapping sector of the footprints relative to η_k and η_j, and $\mathcal{G}_{\eta_j}(\theta_{j,k},\phi_{j,k}) = g$ in the non-overlapping one.

6.3.4 Low-Overhead SLNR-Based Coordinated Scheduling

In this section, we introduce the proposed low-overhead SLNR-based scheduling algorithm exploiting the beam-related information (as described in Section 6.3.3) available at each operator. The intuition behind such an approach is that the UEs served with beams whose footprints are non-overlapping can be scheduled *simultaneously*, aiming to reduce the overall interference and maximize the network Spectral Efficiency (SE).

Let us denote with $\mathcal{S}^{b-1}_{\text{LOW}}$ the scheduling information – here including both scheduling and beam-related information – received from the lower-ranked BSs $\{1,\dots,b-1\}$. Then, the scheduling decision $\mathcal{S}^{b}_{\text{LOW}}$ at the b-th BS can be obtained as follows:

$$\mathcal{S}^{b}_{\text{LOW}} = \underset{k}{\text{argmax}}\ \bar{\gamma}_k(\mathcal{S}^{b-1}_{\text{LOW}}, \hat{\mathcal{P}}^{b}_{\text{LOW}}), \tag{6.17}$$

where $\bar{\gamma}_k$ is the approximated average *partial* SLNR defined as

$$\bar{\gamma}_k\big(\mathcal{S}^{b}_{\text{LOW}}, \mathcal{P}\big) \triangleq \frac{\mathbb{E}\big[\mathcal{P}_{k,k}\big]}{\sum\limits_{j\in\mathcal{S}^{b}_{\text{LOW}}} \mathbb{E}\big[\mathcal{P}_{k,j}\big] + \sigma^2_n}, \tag{6.18}$$

and where $\hat{\mathcal{P}}^{b}_{\text{LOW}}$ collects all the required $\mathbb{E}\big[\mathcal{P}_{k,j}\big],\ \forall j \in \mathcal{S}^{b-1}_{\text{LOW}}$ at the b-th BS.

Remark 6.2. The computation of the required $\hat{\mathcal{P}}^b_{\text{LOW}}$ can be done once for a given scenario as it depends *solely* on the beam footprints, which are static for some fixed cooperating BSs. □

We summarize the proposed low-overhead SLNR-based coordinated scheduling in Algorithm 4. The average leakage in (6.15) is evaluated through numerical integration.

Algorithm 4 Low-Overhead SLNR-based Coordinated Scheduling at the b-th BS

INPUT: $\mathcal{S}^{b-1}_{\text{LOW}}$, η_k, $\forall k \in [\![1, K]\!]$, $\hat{\mathcal{P}}^b_{\text{LOW}}$

if $b = 1$ **then** ▷ The b-th BS is the first to decide
  $\mathcal{S}^b_{\text{LOW}} \leftarrow \text{argmax}_k \, |\mathbf{h}_{b,k}\mathbf{w}_{\eta_k}|^2$ ▷ SNR-based scheduling
else ▷ The b-th BS is not the first to decide
  Retrieve $\mathbb{E}[\mathcal{P}_{k,j}]$, $\forall j \in \mathcal{S}^{b-1}_{\text{LOW}}$ from $\hat{\mathcal{P}}^b_{\text{LOW}}$
  $\mathcal{S}^b_{\text{LOW}} \leftarrow$ Solve (6.17) using the retrieved information
end if
return $\mathcal{S}^b_{\text{LOW}}$

6.4 Privacy-Preserving Coordinated Scheduling

In the previous section, we have introduced a low-overhead scheduling algorithm exploiting beam-related information. In particular, such approach relies on estimating the leakage through the beam footprints. In this section, aware of the *information privacy* issues outlined in Section 6.1, we propose a *privacy-preserving* exchange mechanism allowing coordination between the operators. Then, we introduce a robust scheduling algorithm exploiting the altered beam-related information.

6.4.1 Trade-Off Between Coordination and Privacy

As described in Section 6.3.3, beam-related information might *implicitly* offer an insight into the UEs' locations. If the j-th UE is served through a LOS path, then we can bound its actual location $\boldsymbol{\ell}_j \in \mathbb{R}^2$ within the footprint of its serving beam η_j. In particular, assuming *uniformly*-distributed UEs in the network area $\mathcal{A}$, we can write the Probability Density Function (PDF) $f(\boldsymbol{\ell}_j|\eta_j)$ as follows:

$$f(\boldsymbol{\ell}_j|\eta_j) \triangleq \begin{cases} 0, & \boldsymbol{\ell}_j \notin \mathcal{A}_{\eta_j} \subset \mathcal{A} \\ |\mathcal{A}_{\eta_j}|^{-1}, & \boldsymbol{\ell}_j \in \mathcal{A}_{\eta_j} \subset \mathcal{A} \end{cases} \tag{6.19}$$

where $\mathcal{A}_{\eta_j}$ is the footprint relative to η_j, and $|\mathcal{A}_{\eta_j}|$ is its area.

We are interested in evaluating how uncertain is the generic BS about $\boldsymbol{\ell}_j$ given η_j. This can be measured through the information-theoretical equivocation, which also indicates the *confidentiality* attributed to $\boldsymbol{\ell}_j$ [114]. The equivocation is defined as follows:

$$\begin{aligned} H(\boldsymbol{\ell}_j|\eta_j) &\triangleq -\int_{\boldsymbol{\ell}_j \in \mathcal{A}_{\eta_j}} f(\boldsymbol{\ell}_j|\eta_j) \log_2(f(\boldsymbol{\ell}_j|\eta_j)) d\boldsymbol{\ell}_j \\ &= \log_2\left(|\mathcal{A}_{\eta_j}|\right). \end{aligned} \tag{6.20}$$

Sending *obfuscated* beam-related information to other operators involves injecting on purpose some additional *uncertainty* about the actual location $\boldsymbol{\ell}_j \in \mathbb{R}^2$ of the j-th UE. In this respect, an operator can provide increased *privacy* to its customers. Spatial information is in general obfuscated through enhancing its *inaccuracy*, i.e. the incorrespondence between information and actual location, and *imprecision*, i.e. the inherent vagueness in location information [107–109]. For example, in [108], several false locations (dummies) are associated to each protected and real UE, thus making its location information harder to infer. We consider an equivalent obfuscation mechanism for which multiple possible beams (thus locations) are associated to the j-th UE. Let $\boldsymbol{\eta}_j^{(b)}$ denote the information about η_j available at the b-th BS. Considering for the sake of exposition that each BS belongs to a different operator, we have

$$\boldsymbol{\eta}_j^{(b)} = \left\{\eta_{\omega_j(1)}, \ldots, \eta_{\omega_j(X)}, \eta_j\right\}, \tag{6.21}$$

where $\omega_j : [\![1, X]\!] \to [\![1, N_{\text{BS}}]\!]$ is the deterministic obfuscating function relative to the j-th UE, with X being the number of obfuscating beams (or *dummy beams*).

Lemma 6.1. *Following the obfuscation mechanism, the equivocation on $\boldsymbol{\ell}_q$ becomes*

$$H\left(\boldsymbol{\ell}_j|\boldsymbol{\eta}_j^{(b)}\right) = \log_2\left((X+1)|\mathcal{A}_{\eta_j}|\right), \tag{6.22}$$

having assumed that the area illuminated with the beams in $\boldsymbol{\eta}_j^{(b)}$ is the same[3] as $|\mathcal{A}_{\eta_j}|$.

Proof. Refer to Appendix A.4. □

The obfuscation mechanism results in a $\log_2(X+1)$ factor added to the equivocation in (6.20) obtained with non-obfuscated information η_j.

[3] Although the beams in (6.5) illuminate bigger regions as the elevation angle increases, the UEs are expected to reside on average within regions ($30^\circ - 60^\circ$ in elevation) where the beam footprints can be assumed to be almost identical.

6.4.2 Privacy-Preserving SLNR-Based Coordinated Scheduling

In a robust scheduling decision, each operator should account for the alterations in the exchanged beam-related information. In practice, the expectation in (6.15) needs to be further averaged over all the possible footprints to which the j-th UE might belong to. In order to avoid dealing with the expectation – which could be approximated (with a discrete summation) through Monte-Carlo iterations – we consider the following conservative approach leading to a much less complex algorithm.

Let us consider the obfuscated and received beam-related information $\boldsymbol{\eta}_q^{(b)}$. Given such information, the b-th BS knows the set of the plausible beams used to serve the j-th UE. In order to derive a simple scheduling decision, the b-th BS can assume that all those beams are *actually* being used to serve some *phantom* UEs, and evaluate their average leakage through (6.15).

Let us denote with $\mathcal{S}_{\text{ROB}}^{b-1}$ the scheduling information – here enlarged with spurious obfuscating information – received from lower-ranked BSs $\{1,\dots,b-1\}$. Then, the robust *privacy-preserving* scheduling decision $\mathcal{S}_{\text{ROB}}^{b}$ at the b-th BS is obtained as follows:

$$\mathcal{S}_{\text{ROB}}^{b} = \underset{k}{\text{argmax}}\ \bar{\gamma}_k(\mathcal{S}_{\text{ROB}}^{b-1}, \hat{\mathcal{P}}_{\text{ROB}}^{b}), \tag{6.23}$$

where $\bar{\gamma}_k$ is the approximated *partial* SLNR defined in (6.18).

The robust scheduling algorithm can be solved via the proposed low-overhead Algorithm 4, substituting $\mathcal{S}_{\text{LOW}}^{b-1}$ and $\hat{\mathcal{P}}_{\text{LOW}}^{b}$ with the enlarged $\mathcal{S}_{\text{ROB}}^{b-1}$ and $\hat{\mathcal{P}}_{\text{ROB}}^{b}$.

Remark 6.3. Solving the optimization in (6.23) means considering the alterations in the exchanged information, but not the fact that the UEs in $\mathcal{S}_{\text{ROB}}^{b-1}$ might not be in LOSs with their associated BSs. In mmWave networks, the percentage of NLOS links is small [82, 102]. Still, a performance loss due to such mismatches is expected, and will be quantified in the following Section 6.5. □

6.5 Simulation Results

We evaluate here the performance of the proposed scheduling algorithms. We assume that the BSs are non-colocated (no infrastructure sharing between the operators) and equipped with $N_{\text{BS}} = 128$ antennas (16×8 UPA). We evaluate a simple non-dense scenario with two mobile operators and $B = 2$ BSs, one each operator. We assume a squared network area with side equal to 100 m. We further assume $K = 10$ UEs per BS/operator and $N_s = 10$ scheduling time slots in which the channel is assumed to be coherent. All the plotted results are averaged over 5000 Monte-Carlo runs.

6.5.1 Results and Discussion

We consider stronger (on average) LOS paths with respect to the NLOS ones [102]. In particular, we adopt the following large-scale pathloss model:

$$\mathrm{PL}(\delta) = \alpha + \beta \log_{10}(\delta) + \xi \qquad [\mathrm{dB}] \tag{6.24}$$

where δ is the path length and the parameters α, β, ξ are taken from Tables III and IV in [102] for both LOS and NLOS paths.

We introduce now the average UE *location detection probability* (LDP) so as to relate the information-theoretical equivocation to a more practical *privacy* metric. The LDP measures the likelihood to correctly infer the location of the UEs – up to a given area A – from the exchanged information. It is defined as

$$\mathrm{LDP} = \mathbb{E}_j \left[\frac{A}{(X+1)|\mathcal{A}_{\eta_j}|} \right]. \tag{6.25}$$

In Fig. 6.4, we show the performance of the proposed algorithm as a function of the UE *detection probability*, in a full-LOS scenario, i.e. $\alpha^2_{b,k,\ell} = 0,\ \forall \ell$ relative to NLOS paths. The UE LDP is controlled through the number X of obfuscating beams in the exchanged information. Note that the parameter X impacts our proposed *privacy-preserving* algorithm *only*. The idealized scheduling algorithms and the uncoordinated one have a fixed LDP level, which is $\mathbb{E}\big[X/|\mathcal{A}_{\eta_j}|\big]$.

In [108], two algorithms have been proposed so as to generate *realistic* false locations, which should exhibit some correlation with the actual location data. We generate instead the obfuscating beams according to a discrete uniform distribution over $[\![1, N_{\mathrm{BS}}]\!]$, and consider their obfuscating properties as in a one-shot exchange mechanism.

Note that even with $X = 0$ (no obfuscating beams), there is still a remaining *uncertainty* with respect to the UEs' location, as the UEs can reside anywhere within their beam footprints. The gap for $X = 0$ between the proposed coordinated algorithm and the idealized one – obtained with perfect knowledge of the matrix $\mathcal{P}$ – is due to both average SLNR and sectored antennas approximations. Our *privacy-preserving* scheduling algorithm converges to the uncoordinated solution (based on SNR, i.e. neglecting interference) as the average LDP decreases, i.e. for *higher privacy*.

In Fig. 6.5, we measure the performance loss due to the NLOS/LOS mismatch, for a given LDP, with $L = 5$ paths. In this plot, we assume $\sum_\ell \hat{\sigma}^2_{b,k,\ell} = 1,\ \forall b, k$, where $\hat{\sigma}^2_{b,k,\ell}$ is the normalized variance of the ℓ-path of $\mathbf{h}_{b,k}$. As expected, the proposed low-overhead coordinated algorithm loses up to a 7% over the uncoordinated solution as the variance

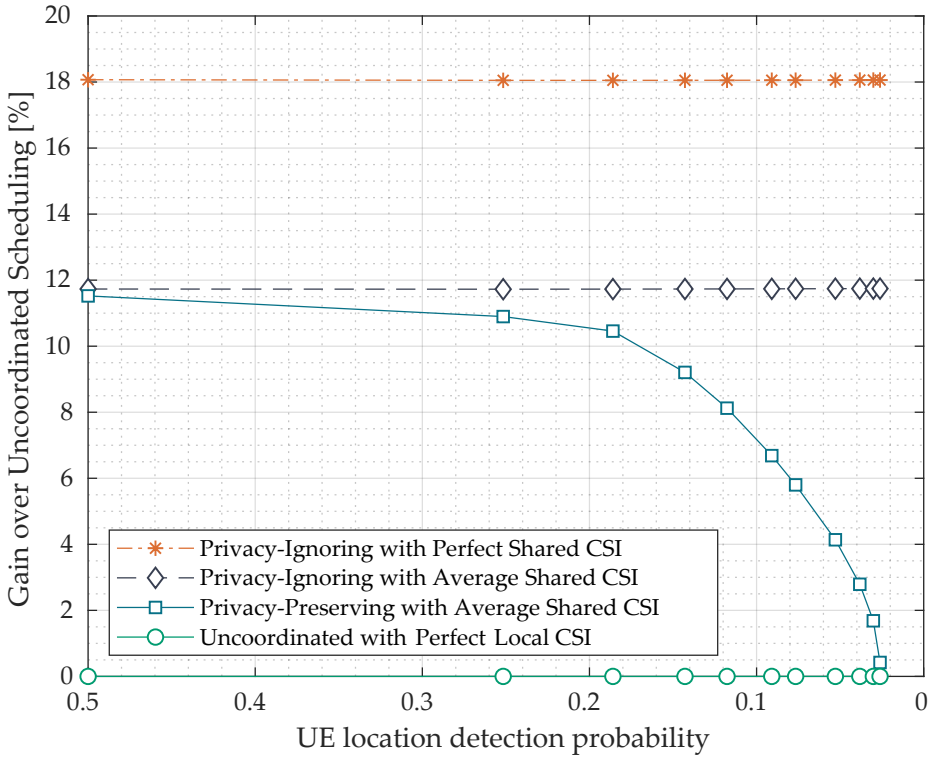

Figure 6.4 – Average SE per UE vs average LDP in a full-LOS scenario. The proposed *privacy-preserving* algorithm succeeds in striking a balance between privacy and average SE performance.

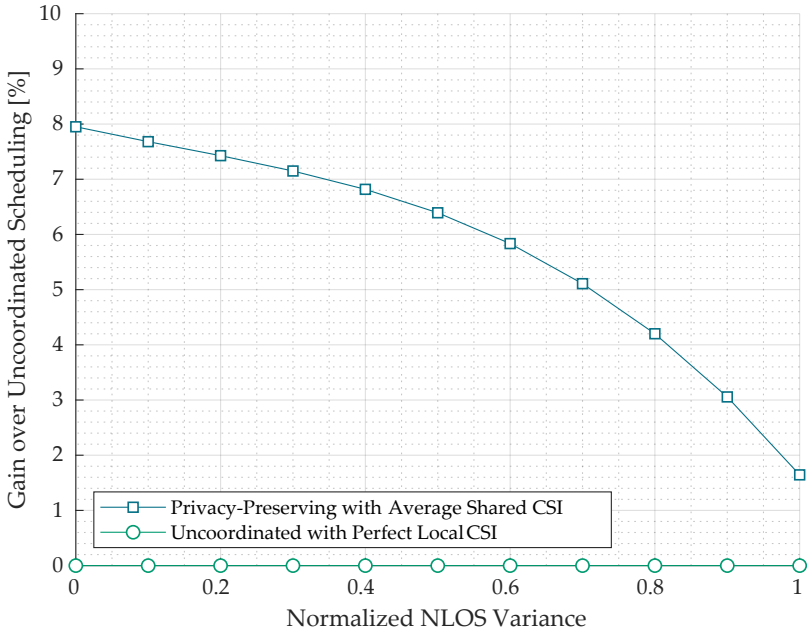

Figure 6.5 – Gain over uncoordinated scheduling vs normalized NLOS variance. Here, the UE LDP $\simeq 0.1$. The performance of the proposed *privacy-preserving* low-overhead scheduling algorithm decreases as more NLOS links are used to communicate.

of the NLOS links increases, which means that more NLOS paths are chosen as best path for communicating. There still exists a gap between the proposed algorithm and the uncoordinated one for a full-NLOS scenario. Indeed, the knowledge of the path-loss is exploited in the proposed algorithm, for which UEs which are quite far from each other are preferred for simultaneous scheduling.

6.6 Conclusion

Dealing with inter-operator interference in mmWave spectrum sharing is essential for improving performance. Since multiple mobile operators are involved in the operation, *privacy-preserving* mechanisms and distributed approaches to performance maximization are suitable. In this chapter, we have proposed a low-overhead distributed SLNR-based scheduling algorithm exploiting obfuscated beam-related side-information. Numerical results indicate that a substantial gain is achieved through inter-operator cooperation even in non-dense scenarios with few BSs/operators. Further performance gain is expected in richer scenarios.

Chapter 7

Conclusions

This thesis focused on several novel aspects related to decentralized beam-domain coordination in the context of modern multi-antenna techniques.

In the first part of the thesis, we have shown how the consideration of information discrepancies between the cooperating devices impacts *beam alignment and selection* in Millimeter Wave (mmWave) Massive MIMO (mMIMO) scenarios. The main message is that robust solutions are essential to achieve beam decisions leading to high transmission rates, both in single- and multi-user scenarios. To meet limited feedback requirements, we have considered heuristic beam selection schemes exploiting spatial side-information such as location information and Out-of-Band (OOB) measurements. Our proposed algorithms achieve higher performance compared to uncoordinated or so-called naive-coordinated schemes.

Then, we have emphasized the importance of considering the training overhead when taking beam strategies in network where the *scalability* of the Reference Signals (RSs) constitutes a main concern, as e.g. FDD mMIMO networks. We have proposed a beam selection algorithm exploiting long-term statistical information and its exchange through Device-to-Device (D2D) side-links. Under *fast-varying* channels where the channel coherence time is below 20 ms, the proposed algorithm allows for high performance gains compared to other solutions in the literature which aim at the maximum spatial separation of the User Equipments (UEs).

In the last part of the thesis, we have exposed the existence of an additional trade-off between *coordination* and *privacy*, arising in cooperative scenarios where the exchange of the required CSI-related information raises sensitive *privacy* issues, as e.g. in mmWave spectrum sharing. To explore this trade-off, we have introduced a low-overhead Signal-to-Leakage-and-Noise Ratio (SLNR)-based scheduling algorithm exploiting *obfuscated* beam-related side-information exchanged among the operators. Substantial performance gains are achieved through the proposed solution even in non-dense scenarios.

All the problems we have faced in this thesis are reduced versions of the Team Decision problem formulated in Chapter 1, a non-trivial problem which can be tackled under different approaches. We have studied some aspects of the problem using some reduction techniques as the hierarchical information structure, obtainable e.g. through the use of D2D side-links. Solving the general Team Decision problem remains a real challenge, for which modern tools such as Machine Learning techniques [115], including Federated Learning [116], could be groundbreaking.

Appendices

A.1 Proofs of Chapter 3

Derivation of Lemma 3.1. Starting from the obtained channel gain, for a given pair of beamforming vectors as defined in (2.5) and (2.6), we have:

$$\left|\mathbf{w}_w^{\mathrm{H}}\mathbf{H}\mathbf{v}_v\right|^2 = \left|\sqrt{N_{\mathrm{BS}}N_{\mathrm{UE}}}\sum_{\ell=1}^{L}\alpha_\ell\left(\mathbf{w}^{\mathrm{H}}(\bar{\theta}_w)\mathbf{a}_{\mathrm{BS}}(\theta_\ell)\right)\left(\mathbf{a}_{\mathrm{UE}}^{\mathrm{H}}(\phi_\ell)\mathbf{v}(\bar{\phi}_w)\right)\right|^2 \tag{A.1}$$

$$= \left|\sqrt{N_{TX}N_{RX}}\sum_{\ell=1}^{L}\alpha_\ell\left(\frac{1}{N_{\mathrm{BS}}}\sum_{m=0}^{N_{\mathrm{BS}}-1}e^{-i\pi m\Delta_{\ell,w}}\right)\left(\frac{1}{N_{\mathrm{UE}}}\sum_{n=0}^{N_{\mathrm{UE}}-1}e^{-i\pi n\Delta_{\ell,v}}\right)\right|^2, \tag{A.2}$$

with $\Delta_{\ell,w} = (\cos(\theta_\ell) - \cos(\bar{\theta}_w))$ and $\Delta_{\ell,v} = (\cos(\bar{\phi}_v) - \cos(\phi_\ell))$.

The angle ϕ between the line connecting the points $\mathbf{p} = [p_x \quad p_y]$ and $\mathbf{q} = [q_x \quad q_y]$, and the vertical line $x = q_x$ can be calculated as follows:

$$\phi = \frac{\pi}{2} - \arctan\left(\frac{p_x - q_x}{p_y - q_y}\right), \tag{A.3}$$

where $\phi \in [0, \pi]$.

Equation (A.3) can be used to derive the actual or estimated Angles-of-Departure (AoD) and Angles-of-Arrival (AoA), from $\mathbf{P}$, $\hat{\mathbf{P}}^{(\mathrm{BS})}$ and $\hat{\mathbf{P}}^{(\mathrm{UE})}$. In particular, we have:

$$\phi_\ell = \frac{\pi}{2} - \arctan\left(\frac{p_{n_x} - p_{\mathrm{UE}_x}}{p_{n_y} - p_{\mathrm{UE}_y}}\right), \quad n \in \{\mathrm{BS}, \mathrm{R}_i\}, i \in [\![1, L-1]\!]; \tag{A.4}$$

$$\theta_\ell = \frac{\pi}{2} - \arctan\left(\frac{p_{n_x} - p_{\mathrm{BS}_x}}{p_{n_y} - p_{\mathrm{BS}_y}}\right), \quad n \in \{\mathrm{UE}, \mathrm{R}_i\}, i \in [\![1, L-1]\!]. \tag{A.5}$$

The sums which appear in (A.1) are the sums of the first N_{UE} and N_{BS} terms of the geometric series with ratio $e^{-i\pi\Delta_{\ell,v}}$ and $e^{-i\pi\Delta_{\ell,w}}$. We can thus write:

$$\begin{aligned}\left|\mathbf{w}_w^{\text{H}}\mathbf{H}\mathbf{v}_v\right|^2 &= \left|\sum_{\ell=1}^{L}\alpha_\ell\left(\sqrt{\frac{1}{N_{\text{BS}}}}\frac{1-e^{-i\pi N_{\text{BS}}\Delta_{\ell,w}}}{1-e^{-i\pi\Delta_{\ell,w}}}\right)\left(\sqrt{\frac{1}{N_{\text{UE}}}}\frac{1-e^{-i\pi N_{\text{UE}}\Delta_{\ell,v}}}{1-e^{-i\pi\Delta_{\ell,v}}}\right)\right|^2 \\ &= \left|\sum_{\ell=1}^{L}\alpha_\ell\left(\sqrt{\frac{1}{N_{\text{BS}}}}\frac{1-\frac{e^{-i(\pi/2)N_{\text{BS}}\Delta_{\ell,w}}}{e^{i(\pi/2)N_{\text{BS}}\Delta_{\ell,q}}}}{1-\frac{e^{-i(\pi/2)\Delta_{\ell,w}}}{e^{i(\pi/2)\Delta_{\ell,w}}}}\right)\left(\sqrt{\frac{1}{N_{\text{UE}}}}\frac{1-\frac{e^{-i(\pi/2)N_{\text{UE}}\Delta_{\ell,v}}}{e^{i(\pi/2)N_{\text{UE}}\Delta_{\ell,v}}}}{1-\frac{e^{-i(\pi/2)\Delta_{\ell,v}}}{e^{i(\pi/2)\Delta_{\ell,v}}}}\right)\right|^2 \end{aligned} \tag{A.6}$$

From (A.6), we get:

$$\begin{aligned}\left|\mathbf{w}_w^{\text{H}}\mathbf{H}\mathbf{v}_v\right|^2 = \Bigg|\sum_{\ell=1}^{L}\alpha_\ell\left(\sqrt{\frac{1}{N_{\text{BS}}}}\frac{e^{i(\pi/2)\Delta_{\ell,w}}}{e^{i(\pi/2)N_{\text{BS}}\Delta_{\ell,w}}}\frac{e^{i(\pi/2)N_{\text{BS}}\Delta_{\ell,w}}-e^{-i(\pi/2)N_{\text{BS}}\Delta_{\ell,w}}}{e^{i(\pi/2)\Delta_{\ell,w}}-e^{-i(\pi/2)\Delta_{\ell,w}}}\right)\cdots \\ \cdots\left(\sqrt{\frac{1}{N_{\text{UE}}}}\frac{e^{i(\pi/2)\Delta_{\ell,v}}}{e^{i(\pi/2)N_{\text{UE}}\Delta_{\ell,v}}}\frac{e^{i(\pi/2)N_{\text{UE}}\Delta_{\ell,v}}-e^{-i(\pi/2)N_{\text{UE}}\Delta_{\ell,v}}}{e^{i(\pi/2)\Delta_{\ell,v}}-e^{-i(\pi/2)\Delta_{\ell,v}}}\right)\Bigg|^2.\end{aligned} \tag{A.7}$$

Since $\sin(x) = (e^{ix} - e^{-ix})/2i$, (A.7) results in:

$$\begin{aligned}\left|\mathbf{w}_w^{\text{H}}\mathbf{H}\mathbf{v}_v\right|^2 = \Bigg|\sum_{\ell=1}^{L}\alpha_\ell\left(\sqrt{\frac{1}{N_{\text{BS}}}}\frac{e^{i(\pi/2)\Delta_{\ell,w}}}{e^{i(\pi/2)N_{\text{BS}}\Delta_{\ell,w}}}\frac{\sin\left((\pi/2)N_{\text{BS}}\Delta_{\ell,w}\right)}{\sin\left((\pi/2)\Delta_{\ell,w}\right)}\right)\cdots \\ \cdots\left(\sqrt{\frac{1}{N_{\text{UE}}}}\frac{e^{i(\pi/2)\Delta_{\ell,v}}}{e^{i(\pi/2)N_{TX}\Delta_{\ell,v}}}\frac{\sin\left((\pi/2)N_{\text{UE}}\Delta_{\ell,v}\right)}{\sin\left((\pi/2)\Delta_{\ell,v}\right)}\right)\Bigg|^2.\end{aligned} \tag{A.8}$$

From (A.8), we can express the average beam gain matrix $\mathbf{G}$ in (3.1) as follows:

$$\begin{aligned}G_{v,w} &= \mathbb{E}_{\boldsymbol{\alpha}}\left[\left|\sum_{\ell=1}^{L}\alpha_\ell L_{\text{BS}}\left(\Delta_{\ell,w}\right)L_{\text{UE}}\left(\Delta_{\ell,v}\right)\right|^2\right] \\ &\overset{(a)}{=} \mathbb{E}_{\boldsymbol{\alpha}}\left[\left(\sum_{\ell=1}^{L}\left|\alpha_\ell\right|^2\left|L_{\text{BS}}(\Delta_{\ell,w})\right|^2\left|L_{\text{UE}}(\Delta_{\ell,v})\right|^2\right)\right] \\ &= \sum_{\ell=1}^{L}\sigma_\ell^2\left|L_{\text{BS}}(\Delta_{\ell,w})\right|^2\left|L_{\text{UE}}(\Delta_{\ell,v})\right|^2,\end{aligned} \tag{A.9}$$

where $L_{\text{UE}}\left(\Delta_{\ell,v}\right)$ and $L_{\text{BS}}\left(\Delta_{\ell,w}\right)$ are as in (3.5) and (3.4), and with (a) coming from the statistical independence of the path gains α_ℓ. □

A.2 Proofs of Chapter 4

Derivation of Proposition 4.1. The following lemma states an interesting consequence (constant inner product) of the inverse cosine spacing for the angles $\hat{\phi}_v, v \in [\![1, M_{\text{UE}}]\!]$ and $\hat{\theta}_w, w \in [\![1, M_{\text{BS}}]\!]$ [117], which will be useful in the derivation of Proposition 4.1.

Lemma A.1. *Let the angles $\hat{\phi}_v,\ v \in [\![1, M_{UE}]\!]$ and $\hat{\theta}_w,\ w \in [\![1, M_{BS}]\!]$ be spaced according to the inverse cosine function, as follows:*

$$\hat{\phi}_v = \arccos\Big(1 - \frac{2(v-1)}{M_{\text{UE}} - 1}\Big), \quad v \in [\![1, M_{UE}]\!] \tag{A.10}$$

$$\hat{\theta}_w = \arccos\Big(1 - \frac{2(w-1)}{M_{\text{BS}} - 1}\Big), \quad w \in [\![1, M_{BS}]\!], \tag{A.11}$$

then

$$\mathbf{a}_{\text{UE}}^{\text{H}}(\hat{\phi}_v)\mathbf{a}_{\text{UE}}(\hat{\phi}_{\tilde{v}}) = 1/N_{\text{UE}} \tag{A.12}$$

$$\mathbf{a}_{\text{BS}}^{\text{H}}(\hat{\theta}_w)\mathbf{a}_{\text{BS}}(\hat{\theta}_{\tilde{w}}) = 1/N_{\text{BS}} \tag{A.13}$$

for any $v \neq \tilde{v}$ and $w \neq \tilde{w}$.

Proof of Lemma A.1. In the following, we will consider w.l.o.g. the UE side.

Let $\Delta \triangleq \cos(\hat{\phi}_v) - \cos(\hat{\phi}_{\tilde{v}})$, then we have:

$$\mathbf{a}_{\text{UE}}^{\text{H}}(\hat{\phi}_v)\mathbf{a}_{\text{UE}}(\hat{\phi}_{\tilde{v}}) = \frac{1}{N_{\text{UE}}} \sum_{k=0}^{N_{\text{UE}}-1} e^{-i\pi k\Delta} \tag{A.14}$$

$$\overset{(a)}{=} \frac{1}{N_{\text{UE}}} \frac{1 - e^{-i\pi N_{\text{UE}}\Delta}}{1 - e^{-i\pi\Delta}} \tag{A.15}$$

where (a) is due to geometric series properties.

According to (A.10), we can write $\Delta = \frac{2(\tilde{v}-v)}{N_{\text{UE}}-1}$. Inserting this in (A.14) gives:

$$\mathbf{a}_{\text{UE}}^{\text{H}}(\hat{\phi}_v)\mathbf{a}_{\text{UE}}(\hat{\phi}_{\tilde{v}}) = \frac{1}{N_{\text{UE}}} \frac{e^{i\pi\Delta} - e^{-i\pi 2(\tilde{v}-v)}}{e^{i\pi\Delta} - 1} \tag{A.16}$$

$$\overset{(b)}{=} \frac{1}{N_{\text{UE}}} \tag{A.17}$$

where (b) follows from $2\pi(\tilde{v} - v) = 0 \pmod{2\pi}$ for $v \neq \tilde{v}$. □

According to Lemma A.1, in the limit of large N_{BS} and N_{UE}, we have $\mathbf{a}_{\text{UE}}(\hat{\phi}_v) \perp \text{span}(\mathbf{a}_{\text{UE}}(\hat{\phi}_{\tilde{v}}),\ \forall \tilde{v} \neq v)$. Likewise $\mathbf{a}_{\text{BS}}(\hat{\theta}_w) \perp \text{span}(\mathbf{a}_{\text{BS}}(\hat{\theta}_{\tilde{w}})\ \forall \tilde{w} \neq w)$. As a consequence, the matrices

$$\hat{\mathbf{A}}_{\text{BS}} = \left[\mathbf{a}_{\text{BS}}(\hat{\theta}_1) \quad \dots \quad \mathbf{a}_{\text{BS}}(\hat{\theta}_{M_{\text{BS}}})\right], \tag{A.18}$$

and

$$\hat{\mathbf{A}}_{\text{UE}} = \left[\mathbf{a}_{\text{UE}}(\hat{\phi}_1) \quad \dots \quad \mathbf{a}_{\text{UE}}(\hat{\phi}_{M_{\text{UE}}})\right], \tag{A.19}$$

are *asymptotically unitary*. To go further, we resort to the channel approximation in [77], which consists in approximating the channel given in (2.1) using the quantized angles, as follows:

$$\mathbf{H}_k \approx \sqrt{N_{\text{BS}} N_{\text{UE}}}\Big(\sum_{v=1}^{M_{\text{UE}}}\sum_{w=1}^{M_{\text{BS}}} \psi_{k,v,w}\mathbf{a}_{\text{BS}}(\hat{\theta}_w)\mathbf{a}_{\text{UE}}^{\text{H}}(\hat{\phi}_v)\Big) \tag{A.20}$$

where $\psi_{k,v,w}$ is equal to the sum of the gains of the paths whose angles lie in the *virtual spatial bin* centered on $(\hat{\phi}_v, \hat{\theta}_w)$.

We rewrite now (4.5) using the Schur complement as follows [118]:

$$\gamma_k\left(v_{1:K}, w_{1:K}\right) = \frac{1}{\sigma_{\tilde{n}}^2}\left[\bar{\mathbf{h}}_k^{\text{H}}\bar{\mathbf{h}}_k - \bar{\mathbf{h}}_k^{\text{H}}\mathbf{P}_{/k}\bar{\mathbf{h}}_k\right], \tag{A.21}$$

where $\mathbf{P}_{/k} \triangleq \bar{\mathbf{H}}_{/k}(\bar{\mathbf{H}}_{/k}^{\text{H}}\bar{\mathbf{H}}_{/k})^{-1}\bar{\mathbf{H}}_{/k}^{\text{H}}$ is the orthogonal projection onto the span$(\bar{\mathbf{H}}_{/k})$, with $\bar{\mathbf{H}}_{/k}$ being the submatrix obtained via removing the k-th column from $\bar{\mathbf{H}}$.

Since $\hat{\mathbf{A}}_{\text{UE}}$ and $\hat{\mathbf{A}}_{\text{BS}}$ are *asymptotically unitary*, it holds that

$$\mathbf{P}_{/k}\bar{\mathbf{h}}_k = \begin{cases} \mathbf{0} & \text{if } w_k \neq m_j\ \forall j \in \mathcal{K}\backslash\{k\} \\ \bar{\mathbf{h}}_k & \text{if } \exists\, j \in \mathcal{K}\backslash\{k\} : w_j = w_k \end{cases} \tag{A.22}$$

and, as a consequence, equation (A.21) becomes

$$\gamma_k\left(v_{1:K}, w_{1:K}\right) = \begin{cases} \dfrac{\|\bar{\mathbf{h}}_k\|^2}{\sigma_{\tilde{n}}^2}, & \text{if } w_k \neq w_j\ \forall j \in \mathcal{K}\backslash\{k\} \\ 0 & \text{if } \exists\, j \in \mathcal{K}\backslash\{k\} : w_j = w_k \end{cases} \tag{A.23}$$

whose expected value is as (4.13), which concludes the proof. □

A.3 Proofs of Chapter 5

Derivation of Lemma 5.2. From the definition of the error covariance $\mathbf{\Sigma}_{\mathbf{e}_k} \triangleq \mathbb{E}_{\mathbf{H}_k}\left[\mathbf{e}_k\mathbf{e}_k^{\mathrm{H}}\right]$, we have:

$$\begin{aligned}\mathbf{\Sigma}_{\mathbf{e}_k} &= \bar{\mathbf{\Sigma}}_k - \rho\bar{\mathbf{\Sigma}}_k\mathbf{A}^{\mathrm{H}}\left(\rho^2\mathbf{A}\bar{\mathbf{\Sigma}}_k\mathbf{A}^{\mathrm{H}} + \sigma_n^2\mathbf{\Gamma}\mathbf{\Gamma}^{\mathrm{H}}\right)^{-1}\rho\mathbf{A}\bar{\mathbf{\Sigma}}_k \\ &\overset{(a)}{=} \bar{\mathbf{\Sigma}}_k - \left(\bar{\mathbf{\Sigma}}_k^{-1} + \kappa\mathbf{A}^{\mathrm{H}}\left(\mathbf{\Gamma}\mathbf{\Gamma}^{\mathrm{H}}\right)^{-1}\mathbf{A}\right)^{-1}\kappa\mathbf{A}^{\mathrm{H}}\left(\mathbf{\Gamma}\mathbf{\Gamma}^{\mathrm{H}}\right)^{-1}\mathbf{A}\bar{\mathbf{\Sigma}}_k, \end{aligned} \tag{A.24}$$

where (a) is due to the *Woodbury identity* [119].

We can then rewrite the error covariance as

$$\begin{aligned}\mathbf{\Sigma}_{\mathbf{e}_k} &= \bar{\mathbf{\Sigma}}_k - \mathbf{D}^{-1}\kappa\mathbf{A}^{\mathrm{H}}\left(\mathbf{\Gamma}\mathbf{\Gamma}^{\mathrm{H}}\right)^{-1}\mathbf{A}\bar{\mathbf{\Sigma}}_k \\ &= \mathbf{D}^{-1}\left(\mathbf{D}\bar{\mathbf{\Sigma}}_k - \kappa\mathbf{A}^{\mathrm{H}}\left(\mathbf{\Gamma}\mathbf{\Gamma}^{\mathrm{H}}\right)^{-1}\mathbf{A}\bar{\mathbf{\Sigma}}_k\right) \\ &= \mathbf{D}^{-1}, \end{aligned} \tag{A.25}$$

where $\mathbf{D} = \left(\bar{\mathbf{\Sigma}}_k^{-1} + \kappa\mathbf{A}^{\mathrm{H}}\left(\mathbf{\Gamma}\mathbf{\Gamma}^{\mathrm{H}}\right)^{-1}\mathbf{A}\right)$, as given in (5.6). □

Derivation of Proposition 5.2. We first rewrite $\mathcal{R}_k^{\mathrm{SVD}}\left(\mathbf{V}, \mathbf{W}_k\right)$ as follows, using the properties of the $\det$ operator:

$$\mathcal{R}_k^{\mathrm{SVD}}\left(\mathbf{V}, \mathbf{W}_k\right) = \sum_{m=1}^{D_{\mathrm{UE}}} \log_2\left(1 + \kappa\lambda_m^2\right). \tag{A.26}$$

According to *Jensen's inequality*, we have:

$$\begin{aligned}\sum_{m=1}^{D_{\mathrm{UE}}} \log_2\left(1 + \kappa\lambda_m^2\right) &\leq D_{\mathrm{UE}}\log_2\left(1 + \kappa D_{\mathrm{UE}}^{-1}\sum_{m=1}^{D_{\mathrm{UE}}}\lambda_m^2\right) \\ &= D_{\mathrm{UE}}\log_2\left(1 + \kappa D_{\mathrm{UE}}^{-1}\mathrm{Tr}\left(\bar{\mathbf{H}}_k\bar{\mathbf{H}}_k^{\mathrm{H}}\right)\right). \end{aligned} \tag{A.27}$$

Now, considering the expectation and again exploiting *Jensen's inequality*, we can write:

$$\begin{aligned}\mathbb{E}_{\mathbf{H}_k}\left[D_{\mathrm{UE}}\log_2\left(1 + \kappa D_{\mathrm{UE}}^{-1}\mathrm{Tr}\left(\bar{\mathbf{H}}_k\bar{\mathbf{H}}_k^{\mathrm{H}}\right)\right)\right] &\leq D_{\mathrm{UE}}\log_2\left(1 + \kappa D_{\mathrm{UE}}^{-1}\mathbb{E}_{\mathbf{H}_k}\left[\mathrm{Tr}\left(\bar{\mathbf{H}}_k\bar{\mathbf{H}}_k^{\mathrm{H}}\right)\right]\right) \\ &= D_{\mathrm{UE}}\log_2\left(1 + \kappa D_{\mathrm{UE}}^{-1}\mathrm{Tr}\left(\bar{\mathbf{\Sigma}}_k\right)\right), \end{aligned} \tag{A.28}$$

as given in (5.23). □

Derivation of Lemma 5.4. From the properties of the vec $(\cdot)$ operator, we can write: $\text{vec}\left(\mathbf{w}^{\text{H}}\mathbf{H}\mathbf{v}\right) = \left(\mathbf{v}^{\text{T}} \otimes \mathbf{w}^{\text{H}}\right) \text{vec}\left(\mathbf{H}\right)$. Now, from the definition in (5.18), we have:

$$\begin{aligned}
\mathbb{E}_{\mathbf{H}_k}\left[\left|\mathbf{w}_w^{\text{H}}\mathbf{H}_k\mathbf{v}_v\right|^2\right] &= \mathbb{E}_{\mathbf{H}_k}\left[\text{vec}\left(\mathbf{H}\right)^{\text{H}}\mathbf{b}_{v,w}\mathbf{b}_{v,w}^{\text{H}}\text{vec}\left(\mathbf{H}\right)\right] \\
&= \mathbb{E}_{\mathbf{H}_k}\left[\text{Tr}\left(\mathbf{b}_{v,w}\mathbf{b}_{v,w}^{\text{H}}\text{vec}\left(\mathbf{H}\right)\text{vec}\left(\mathbf{H}\right)^{\text{H}}\right)\right] \\
&= \text{Tr}\left(\mathbf{b}_{v,w}^{\text{H}}\mathbb{E}_{\mathbf{H}_k}\left[\text{vec}\left(\mathbf{H}\right)\text{vec}\left(\mathbf{H}\right)^{\text{H}}\right]\mathbf{b}_{v,w}\right) \\
&= \mathbf{b}_{v,w}^{\text{H}}\boldsymbol{\Sigma}_k\mathbf{b}_{v,w}, \qquad \text{(A.29)}
\end{aligned}$$

as given in (5.19). □

Derivation of Lemma 5.5. Based on $\text{vec}\left(\mathbf{W}^{\text{H}}\mathbf{H}\mathbf{V}\right) = \left(\mathbf{V}^{\text{T}} \otimes \mathbf{W}^{\text{H}}\right) \text{vec}\left(\mathbf{H}\right)$, we have:

$$\begin{aligned}
\bar{\boldsymbol{\Sigma}}_k &\triangleq \mathbb{E}_{\mathbf{H}_k}\left[\text{vec}\left(\mathbf{W}_k^{\text{H}}\mathbf{H}_k\mathbf{V}\right)\text{vec}\left(\mathbf{W}_k^{\text{H}}\mathbf{H}_k\mathbf{V}\right)^{\text{H}}\right] \\
&= \mathbf{B}_k^{\text{H}}\mathbb{E}_{\mathbf{H}_k}\left[\text{vec}\left(\mathbf{H}_k\right)^{\text{H}}\text{vec}\left(\mathbf{H}_k\right)\right]\mathbf{B}_k \\
&= \mathbf{B}_k^{\text{H}}\boldsymbol{\Sigma}_k\mathbf{B}_k, \qquad \text{(A.30)}
\end{aligned}$$

as given in (5.21). □

Derivation of Corollary 5.1. From Lemma 5.5 we have:

$$\begin{aligned}
\text{Tr}\left(\bar{\boldsymbol{\Sigma}}_k\right) &= \text{Tr}\left(\mathbf{B}_k^{\text{H}}\boldsymbol{\Sigma}_k\mathbf{B}_k\right) \\
&= \sum_{m=1}^{D_{\text{BS}}D_{\text{UE}}} \mathbf{b}_m^{\text{H}}\boldsymbol{\Sigma}_k\mathbf{b}_m. \qquad \text{(A.31)}
\end{aligned}$$

The sum in (A.31) is maximized when the first $D_{\text{BS}}D_{\text{UE}}$ strongest channel components are selected for transmission, among the ones in $\mathcal{M}_k$. □

A.4 Proofs of Chapter 6

Derivation of Lemma 6.1. From the definition of the equivocation in (6.20), we have:

$$\begin{aligned} H\left(\boldsymbol{\ell}_j|\boldsymbol{\eta}_j^{(b)}\right) &= -\sum_{\eta\in\boldsymbol{\eta}_j^{(b)}}\int_{\boldsymbol{\ell}_j\in\mathcal{A}} f(\boldsymbol{\ell}_j,\eta)\log_2(f(\boldsymbol{\ell}_j|\eta))d\boldsymbol{\ell}_j \\ &= -\sum_{\eta\in\boldsymbol{\eta}_q^{(b)}}\frac{1}{(X+1)}\int_{\boldsymbol{\ell}_j\in\mathcal{A}_\eta} f(\boldsymbol{\ell}|\eta)\log_2(f(\boldsymbol{\ell}_j|\eta))d\boldsymbol{\ell}_j \\ &= -\sum_{\eta\in\boldsymbol{\eta}_j^{(b)}}\frac{1}{(X+1)}\int_{\boldsymbol{\ell}_j\in\mathcal{A}_\eta}\frac{-\log_2\left((X+1)|\mathcal{A}|\right)}{(X+1)|\mathcal{A}|}d\boldsymbol{\ell}_j \\ &= -\sum_{\eta\in\boldsymbol{\eta}_j^{(b)}}\frac{-\log_2\left((X+1)|\mathcal{A}|\right)}{X+1} \\ &= \log_2\left((X+1)|\mathcal{A}_{\eta_j}|\right), \end{aligned} \tag{A.32}$$

as in (6.22). □

Résumé [Français]

F.1 Introduction et Motivation

La réutilisation totale ou partielle des ressources radio (spectre, temps, puissance, pilotes, etc.) dans les réseaux mobiles entraînent de graves interférences, ce qui limite à son tour les performances offertes aux appareils connectés, en particulier ceux situés à la périphérie de la cellule [1]. Plusieurs approches visant à atténuer les brouillages sont apparues au cours de la dernière décennie. Une notion centrale dans toutes ces approches est la *coordination* : les émetteurs brouilleurs doivent s'entendre sur l'optimisation *conjointe* de leurs paramètres de transmission afin d'accroître les performances du réseau global. A cette fin, les stratégies d'optimisation devraient tenir compte de la contrainte d'overhead de feedback limité [2], qui autrement dégrade le débit du réseau. Dans la coopération multi-dispositifs, la notion de feedback est large et englobe plusieurs catégories d'informations a priori - telles que l'informations sur l'état du canal (CSI) - qui sont échangées entre les appareils. En général, les communications coopératives ou coordonnées avec feedback limité peuvent être divisées en *i)* méthodes de gestion des ressources radio (RRM), comme le contrôle de puissance ou le scheduling des utilisateur, et *ii)* méthodes basées sur le traitement du signal, telles que le traitement (coordonné) multi-antennes. Compte tenu de l'objet de cette thèse, une vue d'ensemble sur les techniques de coordination multi-antennes est présentée ci-après.

F.1.1 Coordination Multi-Antennes dans les Réseaux Mobiles

Le rôle joué par les antennes multiples sur les dispositifs dans l'atténuation des interférences et l'amélioration de l'efficacité spectrale du réseau est bien éprouvé [1]. La puissante combinaison des techniques multi-antennes et de la coopération entre les dispositifs a été étudiée en profondeur au cours de la dernière décennie. Pour donner quelques exemples, la coordination des émetteurs permet d'éviter l'interférence avant même qu'elle n'ait lieu, comme dans le Network MIMO [4]. Néanmoins, les avantages

de la coordination entre émetteurs multi-antennes dépendent d'une connaissance précise de la CSI [1, 4]. Afin de limiter les exigences en matière de partage de la CSI entre les dispositifs coopérants, un pas important a été franchi avec l'introduction du Massive MIMO (mMIMO) [7]. Dans le mMIMO, le nombre d'antennes à la station de base (BS) est beaucoup plus grand que le nombre de dispositifs. Par conséquent, le canal radio vers un dispositif cible tend à devenir orthogonal au canal d'un autre dispositif choisi au hasard, et de simples schémas de formation de faisceaux distribués tels que le *Maximum Ratio Combining* (MRC) peuvent éliminer *asymptotiquement* - pour un nombre infini d'antennes - les interférences et offrir des performances comparables aux solutions centralisées. Pour concevoir de tels schémas, la *CSI locale* est indispensable à l'émetteur. Dans le régime des antennes massives, l'acquisition de la CSI local n'est pas toujours facile. Plusieurs défis et facteurs limitatifs entravent l'application potentielle du mMIMO dans les futurs réseaux 5G/5G+. Nous décrirons ces défis et comment la coordination peut aider à les aborder dans la suite.

F.1.2 Coordination dans le Massive MIMO

L'implémentation classique du mMIMO est basée sur le duplexage par répartition temporelle (TDD), ce qui permet d'estimer le canal de liaison descendante (DL) par sondage orthogonal de la liaison montante (UL), en exploitant la *réciprocité de canal* [7]. La relative facilité avec laquelle la CSI locale peut être acquise en TDD dans le cas d'utilisateurs mono-antenne a conduit les groupes de recherche à se concentrer sur cette configuration mMIMO, où la *contamination des pilotes* représente la principale préoccupation. Pour éviter les transmissions pilotes conflictuelles, la coordination joue un rôle central et des efforts de recherche importants ont été entrepris [8–15].

Dans cette thèse, nous nous concentrons sur de différentes architectures mMIMO, qui devraient émerger dans la prochaine génération de réseaux mobiles : *i)* mMIMO en duplexage à répartition de fréquence (FDD) avec un nombre modéré d'antennes à l'équipement utilisateur (UE), et *ii)* mMIMO avec antennes massives à la BS et à l'UE en bande millimetrique (mmWave) [16]. Dans tous les cas ci-dessus, l'acquisition de la CSI locale à l'émetteur n'est pas simple, comme nous l'expliquons ci-après.

Défis dans l'acquisition de la CSI dans le FDD mMIMO

En mode de duplexage par répartition fréquentielle (FDD), les pilotes sur le DL et le subséquent feedback sur le UL sont nécessaires pour estimer le canal DL, puisque la réciprocité de canal ne tient pas. En général, il existe une correspondance biunivoque entre les pilotes et les éléments d'antenne. Par conséquent, l'overhead d'estimation du

canal ne permet pas d'appliquer le mMIMO en FDD, où il reste peu de ressources radio pour la transmission des données [17]. Plusieurs articles ont proposé des méthodes pour faire face à ce problème. On peut les diviser en trois catégories : *i)* les approches basées sur les statistiques de canal de second ordre, *ii)* les approches basées sur la détection compressive (CS), et *iii)* les approches basées sur la grille de faisceaux (GoB).

Parmi les approches basées sur les statistiques de second ordre, les travaux pionniers [11, 12] exploitent des covariances de canal strictement orthogonales pour discriminer entre les UEs brouilleurs même avec des séquences pilotes non orthogonales, réduisant ainsi l'overhead d'estimation du canal. Comme cette condition est rarement rencontrée dans la pratique [18], l'étude plus récente [19] a introduit une méthode de précodage pour forger artificiellement des canaux effectifs de faible dimension, indépendamment de la structure de covariance. Dans la littérature MIMO, de telles méthodes de précodage ont été connues sous le vocable *covariance shaping* [20–22].

Les techniques de CS pour l'estimation des canaux de haute dimension avec peu de mesures sont connus depuis des décennies [23] et ont également été appliquées au FDD mMIMO [24–27]. La réduction significative de l'overhead d'estimation de canal dans tous ces travaux repose sur l'existence d'une représentation *parcimonieuse* des canaux radio. Des méthodes alternatives basées sur la CS, telles que [28–32], capitalisent sur la *réciprocité angulaire* entre DL et UL. Dans de telles approches, le spectre spatiale est estimé par sondage UL et utilisé pour concevoir le précodeur mMIMO, dans l'assomption raisonnable que les angles de départs dominants soient presque invariants sur toute la gamme fréquentielle séparant les canaux DL et UL.

L'approche de la GoB a suscité beaucoup d'intérêt au sein du groupe 3GPP, en raison de sa facilité de mise en œuvre pratique [33]. Selon ce concept, des représentations de canal réduites sont obtenues par une transformation spatiale basée sur des faisceaux fixes [33,34]. Dans ce cas, il existe une correspondance biunivoque entre les pilotes et les faisceaux dans la grille [34], de sorte que l'estimation des canaux effectifs réduit l'overhead d'estimation du canal. Cependant, la réduction substantielle de l'overhead d'estimation de canal entraîne souvent une dégradation drastique des performances [35] car le précodeur mMIMO est optimisé pour des représentations de canal réduites qui pourraient ne pas saisir les caractéristiques proéminentes des canaux réels sous-jacents. D'un autre côté, il est possible d'obtenir des représentations de faible dimension rentables en activant un sous-ensemble approprié de faisceaux. En général, choisir ce sous-ensemble à la BS et à l'UE n'est pas simple, car plusieurs facteurs interviennent dans le problème d'optimisation global. Des approches coordonnées pour la sélection des faisceaux sont donc fondamentales, comme nous le verrons tout au long de cette thèse.

Défis dans l'acquisition de la CSI dans le mmWave mMIMO

Parmi les technologies habilitantes de futurs réseaux mobiles, la communication en ondes millimétriques (mmWave) offre la possibilité de faire face à la pénurie de spectre qui touche les opérateurs mobiles. Il existe en effet d'importantes portions de spectre inutilisé au-dessus de 30 GHz, qui peuvent être utilisées en complément des bandes de transmission actuelles, inférieures à 6 GHz. L'utilisation de fréquences plus élevées posent de nouveaux défis, par exemple en termes de contraintes hardware ou de caractéristiques architecturales. De plus, l'environnement de propagation est défavorable pour les signaux de longueur d'onde plus petite : par rapport aux caractéristiques des bandes inférieures, la diffraction tend à être plus faible alors que les pertes de pénétration ou de blocage peuvent être beaucoup plus importantes [36]. Par conséquent, les signaux mmWave subissent une importante perte de cheminement qui entrave l'établissement d'une liaison de communication fiable et nécessitent l'adoption d'antennes directionnelles à haut gain [37]. En revanche, les longueurs d'onde millimétriques permettent d'empiler un nombre élevé d'éléments d'antenne dans un espace réduit [38] permettant ainsi d'exploiter les performances supérieures résultant de la formation de faisceaux (ou *beamforming*) des antennes massives [39].

Acquérir l'information de canal essentielle dans le régime mMIMO n'est pas facile, en raison de l'overhead d'estimation élevé. En bande millimétrique, la configuration de ces antennes massives nécessite un effort supplémentaire [40]. Le coût et la consommation d'énergie élevés des composants radio ont une incidence négative sur les UEs et sur les petites BSs, ce qui limite la mise en œuvre pratique d'architectures de formation de faisceaux *entièrement* numériques [41]. Des architectures *hybrides* à faible coût sont donc suggérées, où un processeur numérique à faible dimension est concatené avec un *beamformer* analogique [43]. Dans ces solutions, on trouve un goulot d'étranglement dans le régime mMIMO en recherchant les combinaisons de faisceaux analogiques qui offrent le meilleur chemin de canal, un problème appelé *alignement des faisceaux* dans la littérature [45, 46]. Une approche pour réduire l'overhead d'alignement – sans compromettre les performances [47] – a été proposée dans [49]. Il consiste à exploiter l'information d'emplacement des dispositifs afin de réduire les zones effectives de recherche des faisceaux. On trouve des approches similaires dans [50–52], où l'information spatiale – obtenue par l'intermédiaire de radars, de capteurs automobiles, etc. – a été confirmée comme une source utile de *side-information*, capable d'aider l'établissement des liaisons dans les communications mmWave. La sélection des faisceaux est un problème complexe qui est exacerbé dans les scénarios multi-utilisateurs, où les meilleurs faisceaux dépendent de plusieurs facteurs, notamment le rapport signal-sur-interférence-et-bruit

(SINR), qui exigent une *coordination totale* entre les dispositifs. De plus, l'exploitation de la *side-information* pour répondre à la contrainte d'overhead de feedback limité impose la conception d'approches robustes pour la sélection coordonnée des faisceaux, car cette information pourrait ne donner qu'une vision partielle de l'état global du réseau. Comment traiter ces incertitudes supplémentaires est un *élément clé* de cette thèse.

Massive MIMO et D2D

Les progrès dans les communications entre dispositifs (D2D) permettent d'échanger des informations entre des UEs voisins avec peu d'overhead [53]. La normalisation des communications D2D au sein du groupe 3GPP [54] a suscité un intérêt pour l'exploration des possibilités découlant des techniques assistées par le D2D dans les réseaux mobiles modernes. Plusieurs travaux sur le D2D dans les réseaux mobiles ont donné des résultats prometteurs en matière de gestion des interférences et d'allocation des ressources radio [55–57]. Malgré une littérature abondante sur l'implémentation du D2D dans les réseaux mobiles [58], seuls quelques travaux étudient l'intégration potentielle du D2D et des techniques mMIMO. Dans [59,60], les auteurs introduisent une phase intermédiaire d'échange de la CSI dans la procédure classique d'estimation du canal. Une fois que le canal est acquis aux UEs, la CSI locale est échangé par le biais des liaisons D2D, de sorte que la CSI globale soit disponible pour tous les UEs. En conséquence, une réduction de l'overhead de feedback peut être atteinte. [61] envisage un système de multi-diffusion à deux phases dans lequel la BS mMIMO précode le message commun pour cibler un sous-ensemble approprié de dispositifs qui, à leur tour, coopèrent pour diffuser l'information dans le reste du réseau via D2D. Le gain de précodage à la BS et les liaisons D2D permettent d'atteindre le débit de multi-diffusion maximal. Dans cette thèse, nous nous concentrons sur des protocoles d'échange d'informations D2D qui permettent d'obtenir une coopération entre les dispositifs avec des informations limitées, beaucoup plus petites que la CSI local. Les méthodes que nous proposons sont basées en partie sur le partage d'informations relatives aux faisceaux à faible débit qui peuvent faciliter les stratégies de coordination dans le domaine spatiale.

La coordination peut être assurée par des approches centralisées ou décentralisées. Dans la section suivante, nous montrons les avantages et les inconvénients de ces approches opposées – mais possiblement complémentaires – et expliquons pourquoi les futurs réseaux mobiles devraient être partiellement décentralisés.

F.1.3 Coopération Décentralisée

L'approche conventionnelle pour permettre la coopération dans les réseaux mobiles est basée sur la concentration de toutes les données de mesure, ainsi que la puissance de calcul, dans un nœud central, comme par exemple la station de base (BS) ou le *cloud*. Par exemple, le Cloud-Radio Access Network (C-RAN) est un cadre centralisé populaire pour l'allocation efficace des ressources radio et la solution d'algorithmes avancés de coopération multi-cellulaire [62]. A cet égard, les dispositifs radio à la périphérie du réseau - tels que les UEs et les BSs - poussent leurs données mesurées dans un cloud supporté par un backhaul optique, où des serveurs dédiés exécutent les algorithmes d'optimisation de réseau requis. Les solutions de ces algorithmes, c'est-à-dire les décisions de transmission, sont ensuite retransmises aux dispositifs pour être appliquées. Bien que l'approche centralisée prédomine toujours dans la conception des réseaux mobiles, les architectures purement cloud-centrique sont plutôt coûteuses et comportent des limites techniques. Par exemple, le traitement centralisé augmente la *latence*, ce qui est fatal pour des applications 5G critiques telles que l'Internet tactile [63], et diminue l'actualité des informations sur la CSI, une information cruciale pour la transmission multi-antennes. L'augmentation exponentielle du nombre d'appareils connectés [64] exacerbe ces inconvénients, avec des répercussions potentielles sur les performances du réseau. Nous assistons donc à un intérêt croissant pour la conception d'un réseau plus adaptable de dispositifs qui peuvent coopérer de manière *autonome*, sans l'aide d'un nœud central. Les appareils devraient tirer parti de leurs capacités locales de calcul, détection et communication pour interagir les uns avec les autres afin d'augmenter les performances globales du réseau. Ainsi, les dispositifs coopérants exécutent des algorithmes décentralisés qui sont conçus pour maximiser une mesure de performance globale, comme par exemple le débit total du réseau, en ajustant les paramètres de transmission locaux tels que le niveau de puissance de transmission ou le précodeur, etc. Cependant, chaque décision relative aux paramètres locaux est prise en utilisant uniquement des informations locales, ce qui constitue souvent une estimation *bruyante* et partielle, différente pour chaque dispositif, de l'information globale sur l'état du réseau. A cet égard, l'approche décentralisée implique une perte de performance inévitable par rapport à l'approche centralisée avec des liaisons de backhaul idéales.

Nous désignons par "décentralisé" ou "distribué" tout mécanisme de coordination pour lequel les dispositifs coopérants n'ont qu'une vue partielle des informations globales sur l'état du réseau qui seraient autrement nécessaires pour une solution centralisée. Ici, "partiel" peut faire allusion à la disponibilité d'informations limitées, bruyantes ou à long terme.

F.1.4 Objet de la Thèse

Dans cette thèse, nous nous concentrons sur les méthodes de coordination décentralisée dans le contexte de la transmission massive multi-antennes. Dans le régime des antennes massives, les principales formes de coopération distribuée qui peuvent être envisagées sont *i)* la sélection et l'alignement des faisceaux entre plusieurs utilisateurs mobiles – en particulier aux fréquences d'ondes millimétriques [41] – et *ii)* la coopération entre stations de base pour le scheduling des utilisateurs. Les solutions centralisées de ces deux cadres de coordination exigent un overhead de coordination important. Dans cette thèse, nous exploitons la coordination dans le domaine spatial entre les dispositifs pour résoudre ces problèmes, qui peuvent le plus souvent être transformés en problèmes de *décision d'équipe* (TD). En général, les résultats présentés dans cette thèse ne s'appuient pas sur les résultats classiques de la théorie Team Decision, en raison de contraintes computationelles et pratiques. Nous exploitons plutôt les propriétés particulières de chaque problème d'optimisation considéré pour en déduire des solutions heuristiques. Cependant, garder à l'esprit la formulation TD s'avérera utile pour acquérir des connaissances intéressantes et comprendre les fondements des problèmes. Nous présentons le cadre théorique de décision d'équipe dans la section suivante.

F.1.5 Coordination avec l'Information Décentralisée

L'absence de données d'observation fiables à chaque dispositif exige des algorithmes robustes de coordination décentralisé, dont le but est de minimiser les pertes par rapport aux solutions centralisées. L'accent mis sur un objectif de performance *commun* et les contraintes de latence pour la communication entre les dispositifs nécessitent une approche différente des cadres classiques de coopération. Par exemple, dans les approches égoïstes de la théorie des jeux [65], les dispositifs radio sont en conflit les uns avec les autres et les équilibres potentiels ne se traduisent pas *automatiquement* par des gains de réseau globaux. Dans ce cas, les imperfections qui empêchent la maximisation de la mesure de performance globale proviennent de la nature distribuée des données observées, sur la base desquelles les décisions de transmission sont prises. Les racines théoriques de la coordination décentralisé *one-shot* peuvent être trouvées dans la théorie dite *Team Decision* [66], qui est connue depuis longtemps et souvent mène à affronter des problèmes complexes d'optimisation fonctionnelle distribuée. Toutefois, le fort développement des capacités de calcul au cours de la dernière décennie a ouvert de nouvelles voies pour résoudre ces problèmes aussi difficiles. Dans ce qui suit, nous formulons le problème de coordination dans le domaine spatial basé sur la théorie TD.

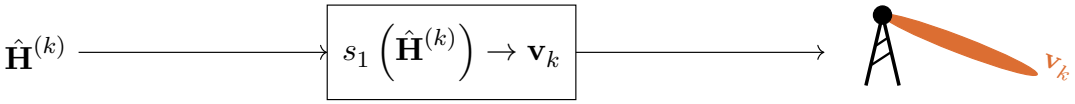

FIGURE F.1 – Sélection des faisceaux avec information distribuée. Le k-ème dispositif prend sa décision sur la base de sa propre estimation $\hat{\mathbf{H}}^{(k)}$ de l'état du réseau global.

Coordination Décentralisé dans le Domaine Spatial

Considérons un réseau avec K dispositifs coopérants, qui seront instanciés en tant que BS ou UE dans ce qui suit. Nous supposons que le k-ème dispositif adopte la stratégie $s_k : \mathbb{C}^m \to \mathcal{S}_k \subseteq \mathbb{C}^{d_k}$, basée sur des estimations locales, où $\mathcal{S}_k$ est son sous-espace de décision, c'est-à-dire son *codebook* de faisceaux dans le contexte consideré (voir Fig. F.1). Le problème général de décision d'équipe, dont l'objectif est de maximiser la mesure de performance globale $f : \mathbb{C}^m \times \prod_{k=1}^{K} \mathbb{C}^{d_k} \to \mathbb{R}$, peut être formulé comme suit :

$$\left(s_1^*, \ldots, s_K^*\right) = \underset{s_1,\ldots,s_K}{\operatorname{argmax}} \mathbb{E}_{\mathbf{H},\hat{\mathbf{H}}^{(1)},\ldots,\hat{\mathbf{H}}^{(K)}} \left[f\left(s_1\left(\hat{\mathbf{H}}^{(1)}\right), \ldots, s_K\left(\hat{\mathbf{H}}^{(K)}\right), \mathbf{H}\right)\right], \tag{F.1}$$

où

- $\mathbf{H} \in \mathbb{C}^m$ est l'état global du réseau[1] ;
- $\hat{\mathbf{H}}^{(k)} \in \mathbb{C}^m$ est l'estimation locale de $\mathbf{H}$ qui est disponible au k-ème dispositif.

La formulation en (F.1) fait référence à un cadre statique dans lequel chacun des dispositifs conçoit des stratégies de transmission en fonction de l'espérance de la fonction de densité de probabilité (PDF) conjointe de l'état réel du réseau et de toutes les estimations locales, définies comme

$$p_{\mathbf{H},\hat{\mathbf{H}}^{(1)},\ldots,\hat{\mathbf{H}}^{(K)}}. \tag{F.2}$$

Ainsi, la corrélation mutuelle entre les estimations locales $\hat{\mathbf{H}}^{(1)}, \ldots, \hat{\mathbf{H}}^{(K)}$ et la corrélation entre ces estimations et l'état réel $\mathbf{H}$ fixent une limite à la performance de coordination. En particulier, la solution à (F.1) dépend de la structure d'information associée, c'est-à-dire de la nature des observations faites à chaque dispositif et de la façon dont ces informations locales se rapportent à l'état global réel. Dans cette thèse nous definerons des structures d'information conduisant à des problèmes de décision d'équipe plus abordables et plus pratiques.

[1] Nous soulignons que $\mathbf{H}$ peut représenter la CSI ou bien des informations relatives à la CSI, comme par exemple les informations de localisation.

F.2 Coordination dans le Domaine Spatial pour le mMIMO

Nous nous attaquons d'abord au problème d'alignement et de sélection des faisceaux, dans lequel les dispositifs radio coordonnent leurs stratégies à l'aide d'informations spatiales à long terme telles que leurs emplacements, afin de réduire l'overhead de coordination.

F.2.1 Alignement des Faisceaux Robuste en Bande Millimetrique

Dans cette section, nous considérons d'importants facteurs de limitation pour l'alignement des faisceaux à l'aide de l'emplacement dans un contexte de transmission mono-utilisateur. Premièrement, il est peu probable que les terminaux d'utilisateur et les BSs puissent acquérir des informations de localisation avec le même degré de précision, pour les raisons suivantes. D'une part, la BS, étant statique, bénéficie d'informations précises sur sa propre position. En revanche, l'UE, étant mobile, est plus difficile à localiser par la BS. D'autre part, on peut s'attendre à ce que l'UE dispose d'informations plus actuelles sur sa propre localisation, bien qu'inévitablement *bruyantes*. En outre, les scénarios pratiques de propagation comprennent des trajets multiples supplémentaires créés par les réflecteurs dominants. On peut supposer que l'emplacement de ces réflecteurs est disponible (par le biais, par exemple, d'une estimation de l'angle d'arrivée), mais avec une certaine incertitude qui est généralement plus faible à la BS qu'à l'UE.

Nous transformons donc le problème d'alignement des faisceaux en problème de *décision d'équipe* (voir la formulation en (F.1)), où les membres de l'équipe, c'est-à-dire la station de base et l'utilisateur (UE), s'efforcent de coordonner leurs actions afin de maximiser leur taux de transmission, tout en n'étant pas en mesure de prédire avec précision leurs décisions respectives, en raison d'observations *bruyantes*.

Les stratégies de décision d'équipe optimales $(s^*_{\text{BS}}, s^*_{\text{UE}}) \in \mathcal{S}$ maximisant le taux de transmission $\mathcal{R}$ peuvent être trouvées en résolvant le problème d'optimisation suivant :

$$(s^*_{\text{BS}}, s^*_{\text{UE}}) = \underset{s_{\text{BS}}, s_{\text{UE}}}{\operatorname{argmax}} \mathbb{E}_{\mathbf{P}, \hat{\mathbf{P}}^{(\text{BS})}, \hat{\mathbf{P}}^{(\text{UE})}} \Big[\mathcal{R}\big(s_{\text{BS}}(\hat{\mathbf{P}}^{(\text{BS})}), s_{\text{UE}}(\hat{\mathbf{P}}^{(\text{UE})}), \mathbf{P}\big) \Big], \tag{F.3}$$

où $\mathbf{P}$ dénote la matrice des emplacements réels, et $\hat{\mathbf{P}}^{(\text{BS})}$, $\hat{\mathbf{P}}^{(\text{UE})}$ representent les matrices des emplacements estimés à la BS et à l'UE, respectivement.

L'optimisation en (F.3) est un problème d'optimisation fonctionnelle stochastique qui est notoirement difficile à résoudre directement [89]. Afin de contourner ce problème, nous examinons des stratégies qui offrent un éventail de compromis entre la robustesse optimale de (F.3) et la complexité de la mise en œuvre.

Alignement des Faisceaux Naïve

Une mise en œuvre simple, mais naïve, des mécanismes de coordination décentralisée consiste à ce que chaque déciseur prenne sa décision en traitant l'information locale (erronée) comme parfaite et globale. Ainsi, la BS suppose que $\hat{\mathbf{P}}^{(\mathrm{BS})} = \mathbf{P}$ et l'UE suppose que $\hat{\mathbf{P}}^{(\mathrm{UE})} = \mathbf{P}$. Nous désignons les mappages résultants par $(s_{\mathrm{BS}}^{\mathrm{naive}}, s_{\mathrm{UE}}^{\mathrm{naive}}) \in \mathcal{S}$, qui se présentent comme suit :

- Optimisation à la BS :

$$s_{\mathrm{BS}}^{\mathrm{naïve}}(\hat{\mathbf{P}}^{(\mathrm{TX})}) = \underset{\mathcal{D}_{\mathrm{BS}} \subset \mathcal{V}_{\mathrm{BS}}}{\operatorname{argmax}} \max_{\mathcal{D}_{\mathrm{UE}} \subset \mathcal{V}_{\mathrm{UE}}} \mathcal{R}\big(\mathcal{D}_{\mathrm{BS}}, \mathcal{D}_{\mathrm{UE}}, \hat{\mathbf{P}}^{(\mathrm{TX})}\big), \tag{F.4}$$

- Optimisation à l'UE :

$$s_{\mathrm{UE}}^{\mathrm{naïve}}(\hat{\mathbf{P}}^{(\mathrm{UE})}) = \underset{\mathcal{D}_{\mathrm{UE}} \subset \mathcal{V}_{\mathrm{UE}}}{\operatorname{argmax}} \max_{\mathcal{D}_{\mathrm{BS}} \subset \mathcal{V}_{\mathrm{BS}}} \mathcal{R}\big(\mathcal{D}_{\mathrm{BS}}, \mathcal{D}_{\mathrm{UE}}, \hat{\mathbf{P}}^{(\mathrm{RX})}\big). \tag{F.5}$$

La limite fondamentale de l'approche naïve en (F.4) et (F.5) découle du fait qu'il ne tient pas compte des éléments suivants : *i)* le bruit dans les emplacements chez les décideurs, et *ii)* les différences de qualité des informations d'emplacement entre la BS et l'UE.

Alignement des Faisceaux Deux-Etapes

Dans l'algorithme suivant, les statistiques du bruit local et les différences entre la qualité de l'information à la BS et à l'UE sont pris en compte. Nous désignons les mappages résultants par $(s_{\mathrm{BS}}^{\text{2-s}}, s_{\mathrm{UE}}^{\text{2-s}}) \in \mathcal{S}$, qui se lisent comme suit :

- Optimisation à la BS :

$$s_{\mathrm{BS}}^{\text{2-s}}(\hat{\mathbf{P}}^{\mathrm{BS}}) = \underset{\mathcal{D}_{\mathrm{BS}} \subset \mathcal{V}_{\mathrm{BS}}}{\operatorname{argmax}} \mathbb{E}_{\mathbf{P}, \hat{\mathbf{P}}^{\mathrm{UE}} | \hat{\mathbf{P}}^{\mathrm{BS}}} \Big[\mathcal{R}\big(\mathcal{D}_{\mathrm{BS}}, s_{\mathrm{UE}}^{\text{1-s}}(\hat{\mathbf{P}}^{(\mathrm{UE})}), \mathbf{P}\big) \Big], \tag{F.6}$$

- Optimisation à la BS :

$$s_{\mathrm{UE}}^{\text{2-s}}(\hat{\mathbf{P}}^{\mathrm{UE}}) = \underset{\mathcal{D}_{\mathrm{BS}} \subset \mathcal{V}_{\mathrm{BS}}}{\operatorname{argmax}} \mathbb{E}_{\mathbf{P}, \hat{\mathbf{P}}^{\mathrm{BS}} | \hat{\mathbf{P}}^{\mathrm{UE}}} \Big[\mathcal{R}\big(s_{\mathrm{UE}}^{\text{1-s}}(\hat{\mathbf{P}}^{(\mathrm{BS})}), \mathcal{D}_{\mathrm{UE}}, \mathbf{P}\big) \Big]. \tag{F.7}$$

Les stratégies $s_{\mathrm{BS}}^{\text{1-s}}(\hat{\mathbf{P}}^{(\mathrm{BS})})$ et $s_{\mathrm{UE}}^{\text{1-s}}(\hat{\mathbf{P}}^{(\mathrm{UE})})$ font référence à l'algorithme *Une-Etape*, qui prend en considération le bruit local dans l'information estimée sans se soucier des différences entre la qualité de cette information à la BS et à l'UE.

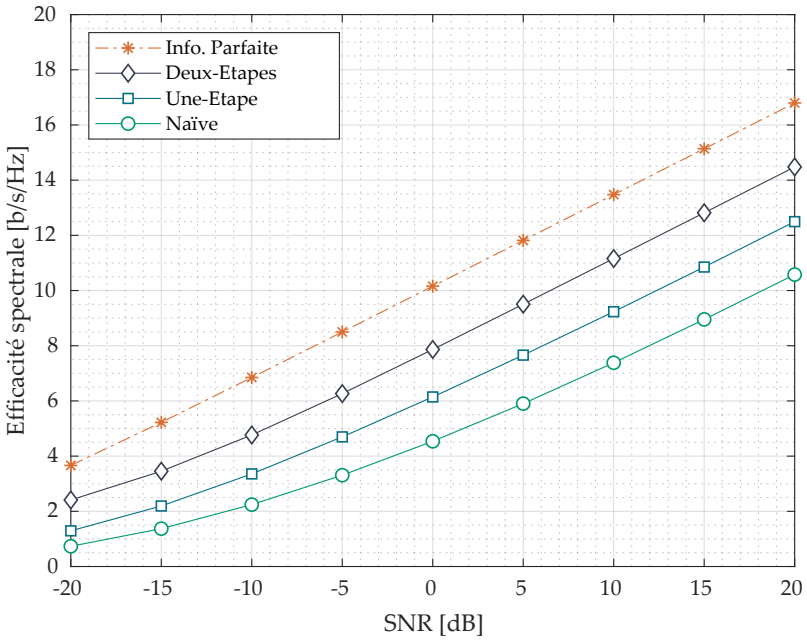

FIGURE F.2 – Efficacité spectrale contre rapport signal-à-bruit (SNR).

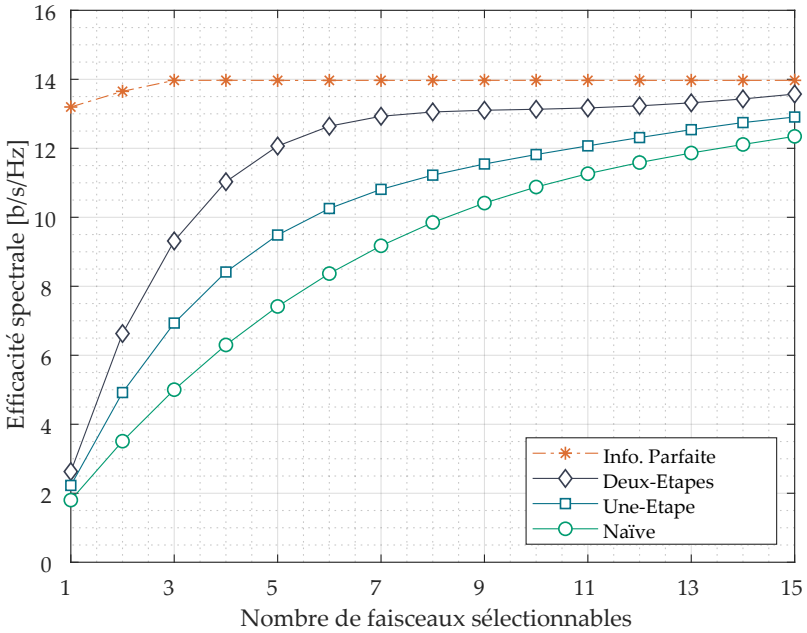

FIGURE F.3 – Efficacité spectrale contre nombre de faisceaux présélectionnés à la BS et à l'UE parmi un total de 64 faisceaux. SNR $= 10$ dB.

Comme prévu, un nombre plus élevé de faisceaux présélectionnables permet d'augmenter les performances. Les simulations montrent que l'algorithme *Deux-Etapes* atteint presque l'approche centralisée avec déjà 5 faisceaux présélectionnés. Cet algorithme est en effet capable de focaliser la recherche des faisceaux sur les directions angulaires liées à la trajectoire LOS la plus forte. De plus, la Fig. F.3 confirme que l'exploitation des informations d'emplacement permet de réduire l'overhead d'alignement tout en n'ayant qu'un faible impact sur l'efficacité spectrale du réseau.

F.2.2 Sélection des Faisceaux à l'aide d'Information Hors Bande

Pour résoudre le problème du brouillage irréductible à la BS dans la sélection des faisceaux multi-utilisateurs (voir la Fig. F.4), une approche possible consiste à s'attaquer au brouillage avant qu'il ne se produise, c'est-à-dire du côté de l'UE, comme c'est le cas par exemple dans [120]. Au lieu de supposer une CSI parfaite pour la formation des faisceaux analogiques, nous proposons une mécanisme de coordination entre les UEs qui exploit les informations statistiques hors bande (OOB). Le mécanisme de coordination repose sur l'idée que chaque UE sélectionne de manière autonome des faisceaux analogiques pour la transmission afin de trouver un compromis entre *i)* capturer un gain de canal suffisant et *ii)* s'assurer que les signaux des UEs empiètent sur des faisceaux distincts du côté de la BS. L'intuition derrière le point *ii)* est de s'assurer que la matrice de canal effective préserve les propriétés de rang complet, permettant ainsi d'atténuer les brouillages inter-UE dans le domaine numérique.

Le problème de sélection des faisceaux multi-utilisateurs en communication mmWave consiste à sélectionner les faisceaux d'émission et de réception analogiques dans les codebooks $\mathcal{V}$ et $\mathcal{W}$ afin de maximiser le débit global défini comme suit :

$$\mathcal{R}\left(v_{1:K}, w_{1:K}\right) \triangleq \sum_{k=1}^{K} \log_2\left(1+\gamma_k(v_{1:K}, w_{1:K})\right), \tag{F.8}$$

où $v_{1:K}$ (resp. $w_{1:K}$) sont les index des faisceaux sélectionnés à l'UE (resp. à la BS), tandis que γ_k est le SINR pour le k-ème UE, défini comme suit (après Zéro-Forçage à la BS) :

$$\gamma_k\left(v_{1:K}, w_{1:K}\right) = \frac{1}{\sigma_{\tilde{n}}^2 \left\{\left(\bar{\mathbf{H}}^{\mathrm{H}}\bar{\mathbf{H}}\right)^{-1}\right\}_{k,k}}, \tag{F.9}$$

avec $\{\cdot\}_{k,k}$ désignant le k-ème élément sur la diagonale de $(\bar{\mathbf{H}}^{\mathrm{H}}\bar{\mathbf{H}})^{-1}$.

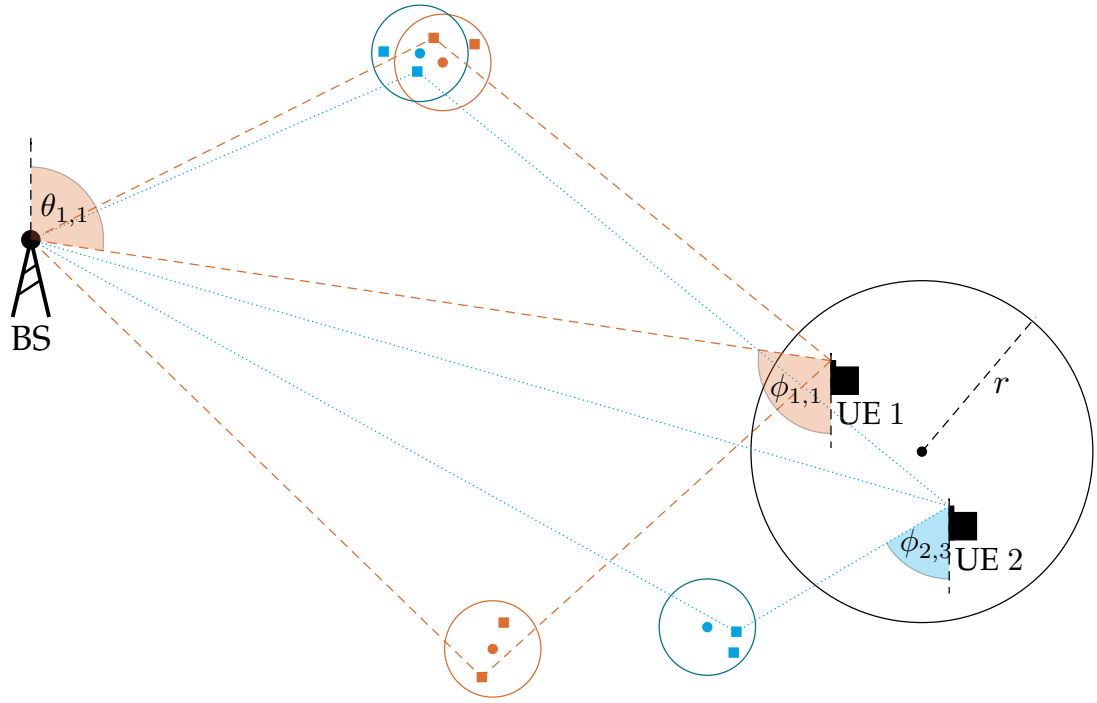

FIGURE F.4 – Exemple d'interférence de faisceau avec $K = 2$ UEs. Les UEs sont supposés résider dans un disque de rayon r. Dans cette illustration, deux UEs situés à proximité partagent certains réflecteurs et les ondes de signal réfléchissant sur les réflecteurs du haut arrivent quasi-alignées à la BS – bref, captées par le même faisceau à la BS - alors qu'elles proviennent de différentes UEs.

Exploitation d'Informations Hors Bande (Sub-6 GHz)

Les informations spatiales disponibles sur les fréquences inférieures à 6 GHz peuvent être exploitées pour obtenir une estimation approximative des caractéristiques angulaires du canal mmWave. En effet, en raison de la plus grande largeur des faisceaux sub-6 GHz, un faisceau utilisé pour la transmission inférieure à 6 GHz peut être associé à un *ensemble* de faisceaux mmWave, comme défini ci-dessous.

> **Definition F.1.** Pour une paire de faisceaux sub-6 GHz $(\underline{v}, \underline{w})$, nous introduisons l'ensemble $\mathcal{S}(\underline{v}, \underline{w}) \triangleq \mathcal{S}_{\text{UE}}(\underline{v}) \times \mathcal{S}_{\text{BS}}(\underline{w})$ où $\mathcal{S}_{\text{UE}}(\underline{v})$ (resp. $\mathcal{S}_{\text{BS}}(\underline{w})$) contient tous les faisceaux mmWave appartenant à la largeur de faisceau de 3 dB du faisceau sub-6 GHz $\underline{v}$-ème (respectivement $\underline{w}$-ème).

Sélection des Faisceaux Coordonnée Hiérarchiquement

Afin d'assurer la coordination entre les UEs, nous proposons d'utiliser une structure d'information hiérarchique distribuée. En supposant que les indices des faisceaux sub-6 Ghz $\underline{w}_{1:k-1}$ ont été reçus, la paire optimale de faisceaux sub-6 GHz $(\underline{v}_k^{\text{co}} \in \underline{\mathcal{V}}, \underline{w}_k^{\text{co}} \in \underline{\mathcal{W}})$ au k-ème UE est obtenue par :

$$(\underline{v}_k^{\text{co}}, \underline{w}_k^{\text{co}}) = \underset{\underline{v}_k, \underline{w}_k}{\text{argmax}} \ \log_2 \left(1 + \mathbb{E}_{v_{1:K}, w_{1:K} | \underline{v}_k, \underline{w}_{1:k+1}} \left[\gamma_k(v_{1:K}, w_{1:K})\right]\right). \tag{F.10}$$

Résoudre (F.10) n'est pas facile, étant un problème de sélection de sous-ensembles pour lequel une approche de Monte-Carlo pour approximer l'ésperance en (F.10) avec une somme discrète conduit à un temps de calcul peu pratique.

Fait intéressant, pour un grand nombre d'antennes, c'est-à-dire $N_{\text{BS}} \gg 1$ et $N_{\text{UE}} \gg 1$, nous pouvons dériver une approximation pour l'espérance dans (F.10) qui sera utile pour la dérivation d'algorithmes à faible complexité.

Proposition F.1. *Dans la limite d'un grand nombre d'antennes N_{BS} et N_{UE}, la valeur attendue de l'SINR du k-ème UE obtenu après Zero-Forçage à la BS est*

$$\mathbb{E}\left[\gamma_k(v_{1:K}, w_{1:K})\right] = \begin{cases} \dfrac{g_{k,v_k,w_k}}{\sigma_{\tilde{n}}^2} & \text{if } w_k \neq w_j \ \forall j \in [\![1, K]\!] \backslash \{k\} \\ 0 & \text{if } \exists\, j \in [\![1, K]\!] \backslash \{k\} : w_j = w_k \end{cases}. \tag{F.11}$$

En utilisant ce résultat, l'ésperance en (F.10) peut être approximée comme suit :

$$\mathbb{E}_{v_{1:K}, w_{1:K} | \underline{v}_k, \underline{w}_{1:k}} \left[\gamma_k(v_{1:K}, w_{1:K})\right] \approx \sum_{\substack{(v_k, w_k) \in \mathcal{S}(\underline{v}_k, \underline{w}_k) \\ w_k \notin \cup_{j=1}^{k-1} \mathcal{S}_{\text{BS}}(\underline{w}_j)}} \frac{g_{v_k, w_k}}{S_k \sigma_{\tilde{n}}^2}. \tag{F.12}$$

Utiliser (F.12) dans (F.10) pour choisir les faisceaux sub-6 GHz au k-ème UE permet de prendre en compte l'interférence *potentielle* des faisceaux transférés aux utilisateurs de rang inférieur avec une complexité faible.

Dans la Fig. F.5, nous montrons l'efficacité spectrale globale de l'algorithme proposé en fonction de l'SNR, où la distance moyenne entre les UEs est de 13 mètres. Pour référence, nous traçons également la limite supérieure obtenue sans interférence multi-utilisateurs. L'algorithme coordonné assisté par l'information hors bande (OOB) surpasse l'algorithme non coordonné, qui vise à sélectionner les faisceaux de manière à maximiser le SNR pour chaque UE.

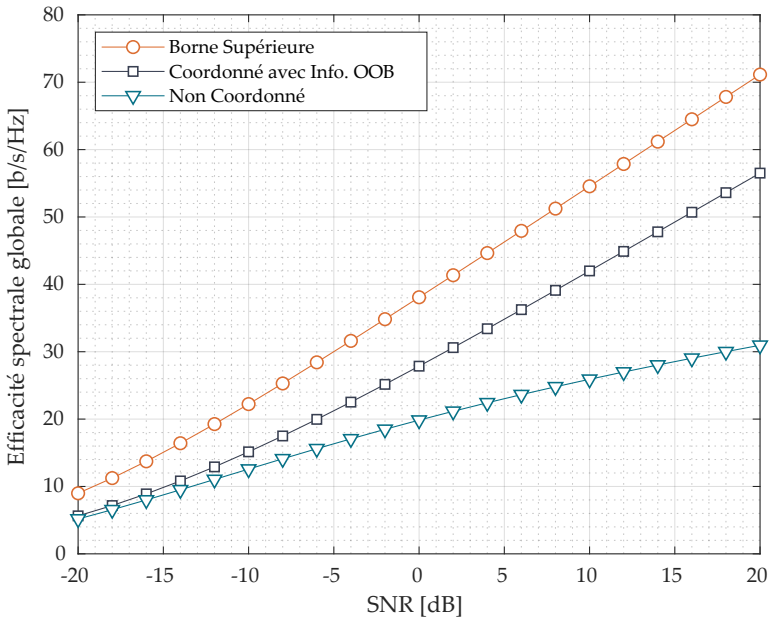

FIGURE F.5 – Efficacité spectrale globale contre SNR. L'algorithme coordonné surpasse l'algorithme non-coordonné. Le gain de coordination augmente avec le SNR.

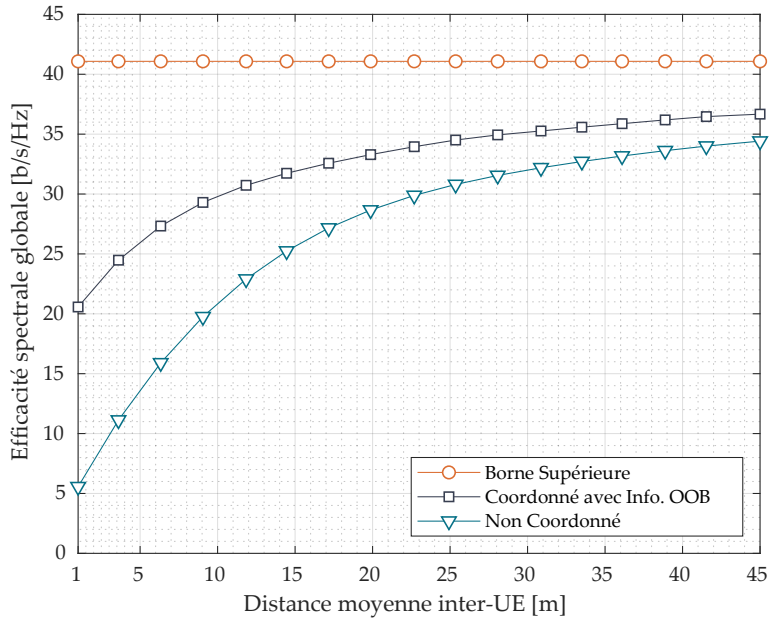

FIGURE F.6 – Efficacité spectrale globale contre distance moyenne entre les UEs. Le gain de performance atteint avec la coordination diminue avec la distance inter-UE.

Dans la Fig. F.6, nous montrons le débit total de l'algorithme proposé contre la distance inter-UE moyenne, pour un SNR en bande mmWave de 1 dB. La coordination entre les UE permet d'énormes gains de performance pour des distances inter-UE inférieures à 15 mètres. Au fur et à mesure que la distance moyenne entre les UEs s'accroît, l'écart de performance entre l'algorithme coordonné et celui non coordonné se rétrécit.

F.3 Partage du Spectre en Bande Millimetrique : Selection des Faisceaux et Conservation de la Vie Privée

Les communications mmWave ont donné un nouvel élan au partage du spectre, qui permet à plusieurs opérateurs mobiles de mettre en commun leurs ressources spectrales. Comparé aux communications mobiles conventionnelles, moins de brouillage est produit dans les réseaux mmWave. En particulier, même sans coordination, le partage du spectre et des BSs entre opérateurs présente un grand potentiel dans les scénarios mmWave lorsque des antennes massives sont utilisées du côté des stations de base et des utilisateurs. Outre ces gains techniques, le partage des ressources se traduit par un profit économique substantiel pour les opérateurs mobiles [104].

Néanmoins, le potentiel du partage coordonné du spectre entre les opérateurs pose plusieurs défis pratiques. Par exemple, l'information globale sur l'état du canal (CSI) devrait être obtenue pour optimiser la transmission, ce qui entraîne une surcharge de signalisation importante. Le problème de la préservation de la confidentialité des données entre opérateurs concurrents est peut-être encore plus aigu. Etant donné que la coordination implique une certaine circulation de l'information d'un opérateur mobile à l'autre, des problèmes de protection des données personnelles se posent. Ce problème est grave dans les réseaux mmWave où les données CSI sont fortement corrélées avec les emplacements des utilisateurs [106].

Dans cette section, nous examinons le compromis entre la coordination et la protection de la vie privée dans le partage du spectre en bande millimetrique. Nous considérons des informations statistiques secondaires (*side information*) pour optimiser la transmission. En particulier, les informations relatives aux faisceaux sont supposées être échangées entre les opérateurs. Pour s'attaquer au problème de protection de la vie privée susmentionné, nous considérons un protocole d'échange d'informations comprenant un mécanisme d'occultation des données [107–109]. Dans le partage du spectre en mmWave, ce mécanisme permet d'atténuer la correspondance biunivoque entre les faisceaux et les emplacements des utilisateurs.

F.3.1 Formulation du Problème de Scheduling

Dans le *successive scheduling*, un classement est d'abord défini parmi les stations de base et permet de prendre des décisions de scheduling consécutives, d'une maniére sous-optimale. En particulier, à la b-ème étape de l'algorithme de scheduling, la b-ème BS connaît les $b-1$ décisions de scheduling prises par les BSs de rang inférieur. La fixation de certaines décisions de scheduling permet d'évaluer ce qu'on appelle le *SLNR partiel* attendu, dans lequel la b-ème BS ne prend en compte que l'interférences potentielles causée aux utilisateurs sélectionnés par les stations de base $\{1,\ldots,b-1\}$. Dénotons $\mathcal{S}^b_{\text{SLNR}} = \{k^1_{\text{SLNR}},\ldots,k^b_{\text{SLNR}}\} = \{\mathcal{S}^{b-1}_{\text{SLNR}}, k^b_{\text{SLNR}}\}$ l'ensemble composé de toutes les décisions de scheduling prises à la b-ème étape du scheduling successif. Alors le SLNR partiel $\bar{\gamma}_k$ relatif au k-ème UE peut être exprimé comme suit :

$$\bar{\gamma}_k\big(\mathcal{S}^b_{\text{LOW}}, \mathcal{P}\big) \triangleq \frac{\mathbb{E}\big[\mathcal{P}_{k,k}\big]}{\sum\limits_{j\in\mathcal{S}^b_{\text{LOW}}} \mathbb{E}\big[\mathcal{P}_{k,j}\big] + \sigma_n^2}, \tag{F.13}$$

où $\mathcal{P}_{j,k} \triangleq |\mathbf{h}_{q,k}\mathbf{w}_{\eta_j}|^2$ est l'énergie des signaux reçus au j-ème UE mais étant destinés au k-ème UE.

En supposant que les informations de scheduling $\mathcal{S}^{b-1}_{\text{SLNR}}$ des BSs de rang inférieur $\{1,\ldots,b-1\}$ ont été reçues, nous obtenons la décision de scheduling successif optimale à la b-ème BS en résolvant le problème d'optimisation suivant :

$$\mathcal{S}^b_{\text{LOW}} = \underset{k}{\text{argmax}}\ \bar{\gamma}_k(\mathcal{S}^{b-1}_{\text{LOW}}, \hat{\mathcal{P}}^b_{\text{LOW}}). \tag{F.14}$$

F.3.2 Compromis entre la Coordination et la Protection de la Vie Privée

Les informations relatives aux faisceaux qui sont utilisées pour résoudre (F.14) pourraient donner un indice sur l'emplacement des UEs. Si le j-ème UE est servi par un chemin LOS, alors nous pouvons lier son emplacement réel $\boldsymbol{\ell}_j \in \mathbb{R}^2$ à l'empreinte de son faisceau η_j. En particulier, en supposant que les UE sont distribués uniformément dans la zone de réseau $\mathcal{A}$, nous pouvons écrire la PDF $f(\boldsymbol{\ell}_j|\eta_j)$ comme suit :

$$f(\boldsymbol{\ell}_j|\eta_j) \triangleq \begin{cases} 0, & \boldsymbol{\ell}_j \notin \mathcal{A}_{\eta_j} \subset \mathcal{A} \\ |\mathcal{A}_{\eta_j}|^{-1}, & \boldsymbol{\ell}_j \in \mathcal{A}_{\eta_j} \subset \mathcal{A} \end{cases} \tag{F.15}$$

où $\mathcal{A}_{\eta_j}$ est l'empreinte relative à η_j, et $|\mathcal{A}_{\eta_j}|$ est son aire.

Nous sommes intéressés à évaluer le degré d'incertitude de la BS générique par rapport à $\boldsymbol{\ell}_j$ étant donné η_j. Ceci peut être mesuré par l'équivocation de l'information, qui indique également la *confidentialité* attribuée à $\boldsymbol{\ell}_j$ [114]. L'équivoquation est définie conventionnellement comme suit :

$$\begin{aligned} H(\boldsymbol{\ell}_j|\eta_j) &\triangleq -\int_{\boldsymbol{\ell}_j\in\mathcal{A}_{\eta_j}} f(\boldsymbol{\ell}_j|\eta_j)\log_2(f(\boldsymbol{\ell}_j|\eta_j))d\boldsymbol{\ell}_j \\ &= \log_2\left(|\mathcal{A}_{\eta_j}|\right). \end{aligned} \tag{F.16}$$

L'envoi d'informations obscurcies à d'autres opérateurs implique l'injection intentionnelle d'une incertitude supplémentaire sur l'emplacement réel $\boldsymbol{\ell}_j \in \mathbb{R}^2$ du j-ème UE. L'information spatiale est généralement obscurcie par l'augmentation de son *inexactitude* et son *imprecision* [107–109]. Par exemple, dans [108], plusieurs faux emplacements sont associés à chaque UE protégé et réel, rendant ainsi son emplacement plus difficile à déduire. Nous considérons un mécanisme d'obscurcissement équivalent pour lequel plusieurs faisceaux possibles (donc emplacements) sont associé au j-ème UE.

Soit $\boldsymbol{\eta}_j^{(b)}$ l'information sur η_j disponible à la b-ème BS. Considérant par souci de clarté que chaque BS appartient à un opérateur différent, nous avons

$$\boldsymbol{\eta}_j^{(b)} = \left\{\eta_{\omega_j(1)},\ldots,\eta_{\omega_j(X)},\eta_j\right\}, \tag{F.17}$$

où $\omega_j : [\![1,X]\!] \to [\![1,N_{\text{BS}}]\!]$ est la fonction d'obscurcissement relative au j-ème UE et X est le nombre de faisceaux d'obscurcissement ou *dummy beams*.

Lemma F.1. *Suite au mécanisme d'obscurcissement, l'équivoquation sur $\boldsymbol{\ell}_j$ est*

$$\begin{aligned} H\left(\boldsymbol{\ell}_j|\boldsymbol{\eta}_j^{(b)}\right) &= -\sum_{\eta\in\boldsymbol{\eta}_j^{(b)}}\int_{\boldsymbol{\ell}_j\in\mathcal{A}} f(\boldsymbol{\ell}_j,\eta)\log_2\left(f(\boldsymbol{\ell}_j|\eta)\right)d\boldsymbol{\ell}_j \\ &= -\sum_{\eta\in\boldsymbol{\eta}_j^{(b)}}\frac{1}{(X+1)}\int_{\boldsymbol{\ell}_j\in\mathcal{A}_\eta}\frac{-\log_2\left((X+1)|\mathcal{A}|\right)}{(X+1)|\mathcal{A}|}d\boldsymbol{\ell}_j \\ &= -\sum_{\eta\in\boldsymbol{\eta}_j^{(b)}}\frac{-\log_2\left((X+1)|\mathcal{A}|\right)}{X+1} \\ &= \log_2\left((X+1)|\mathcal{A}_{\eta_j}|\right). \end{aligned} \tag{F.18}$$

Le mécanisme d'obscurcissement résulte en un facteur $\log_2(X+1)$ ajouté à l'équivoquation en (F.16) obtenue avec des informations non obscurcies η_j.

F.3.3 Scheduling Coordonné visé à la Protection de la Vie Privée

Dans le cadre d'une décision de scheduling robuste, chaque opérateur doit tenir compte des modifications apportées aux informations sur les faisceaux échangés. En pratique, la valeur attendue en (F.13) doit être calculée sur toutes les empreintes de faisceau possibles auxquelles le j-ème UE pourrait appartenir. Afin d'éviter d'approximer cette valeur attendue avec une somme discrète – par le biais d'itérations Monte-Carlo – nous considérons l'approche conservatrice suivante conduisant à un algorithme beaucoup moins complexe. Considérons les informations obscurcies $\boldsymbol{\eta}_j^{(b)}$. Compte tenu de ces informations, la b-ème BS connaît l'ensemble des faisceaux plausibles utilisés pour desservir le j-ème UE. Afin de dériver une simple décision de scheduling, la b-ème BS peut supposer que tous ces faisceaux sont utilisés pour servir des UEs *fantômes*.

Ensuite, la décision de scheduling robuste et *privacy-preserving* $\mathcal{S}_{\text{ROB}}^b$ à la b-ème BS est obtenue comme suit :

$$\mathcal{S}_{\text{ROB}}^b = \underset{k}{\text{argmax}}\ \bar{\gamma}_k(\mathcal{S}_{\text{ROB}}^{b-1}, \hat{\mathcal{P}}_{\text{ROB}}^b), \tag{F.19}$$

Dans la Fig. F.7, nous montrons le gain en termes d'efficacité spectrale de l'algorithme proposé par rapport au scheduling non coordonné en fonction de la *probabilité de détection* des UEs. L'algorithme de scheduling robuste proposé en (F.19) parvient à trouver un équilibre entre la protection de la vie privée et l'efficacité spectrale. L'algorithme proposé converge vers la solution non coordonnée basée sur le SNR et négligeant l'interférence, tout en gardant un niveau de confidentialité élevé.

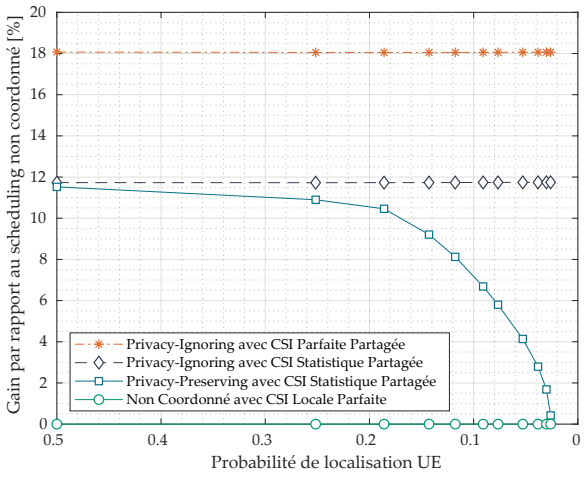

FIGURE F.7 – Gain en termes d'efficacité spectrale par rapport au scheduling non coordonné contre probabilité de localisation des UEs (avec une précision de 10 mètres).

References

[1] D. Gesbert, S. G. Kiani, A. Gjendemsjo, and G. E. Oien, "Adaptation, coordination, and distributed resource allocation in interference-limited wireless networks," *Proc. IEEE*, Dec. 2007.

[2] D. J. Love, R. W. Heath, V. K. N. Lau, D. Gesbert, B. D. Rao, and M. Andrews, "An overview of limited feedback in wireless communication systems," *IEEE J. Sel. Areas Commun.*, Oct. 2008.

[3] D. Gesbert, M. Kountouris, R. W. Heath, C. Chae, and T. Salzer, "Shifting the MIMO paradigm," *IEEE Signal Process. Mag.*, Sep. 2007.

[4] D. Gesbert, S. Hanly, H. Huang, S. S. Shitz, O. Simeone, and W. Yu, "Multi-cell MIMO cooperative networks: A new look at interference," *IEEE J. Sel. Areas Commun.*, Dec. 2010.

[5] M. A. Maddah-Ali, A. S. Motahari, and A. K. Khandani, "Communication over MIMO X channels: Interference alignment, decomposition, and performance analysis," *IEEE Trans. Inf. Theory*, Aug. 2008.

[6] B. Clerckx, H. Lee, Y. Hong, and G. Kim, "A practical cooperative multicell MIMO-OFDMA network based on rank coordination," *IEEE Trans. Wireless Commun.*, Apr. 2013.

[7] T. L. Marzetta, "Noncooperative cellular wireless with unlimited numbers of base station antennas," *IEEE Trans. Wireless Commun.*, Nov. 2010.

[8] F. Fernandes, A. Ashikhmin, and T. L. Marzetta, "Inter-cell interference in noncooperative TDD large scale antenna systems," *IEEE J. Sel. Areas Commun.*, Feb. 2013.

[9] J. H. Sørensen and E. de Carvalho, "Pilot decontamination through pilot sequence hopping in massive MIMO systems," in *Proc. IEEE GLOBECOM*, Dec. 2014.

[10] I. Atzeni, J. Arnau, and M. Debbah, "Fractional pilot reuse in massive MIMO systems," in *Proc. IEEE ICCW*, June 2015.

[11] H. Yin, D. Gesbert, M. Filippou, and Y. Liu, "A coordinated approach to channel estimation in large-scale multiple-antenna systems," *IEEE J. Sel. Areas Commun.*, Feb. 2013.

[12] A. Adhikary, J. Nam, J. Ahn, and G. Caire, "Joint spatial division and multiplexing — The large-scale array regime," *IEEE Trans. Inf. Theory*, Oct. 2013.

[13] M. Li, S. Jin, and X. Gao, "Spatial orthogonality-based pilot reuse for multi-cell massive MIMO transmission," in *Proc. IEEE WCSP*, Oct. 2013.

[14] L. You, X. Gao, X. Xia, N. Ma, and Y. Peng, "Pilot reuse for massive MIMO transmission over spatially correlated rayleigh fading channels," *IEEE Trans. Wireless Commun.*, June 2015.

[15] E. Björnson, J. Hoydis, and L. Sanguinetti, "Massive MIMO has unlimited capacity," *IEEE Trans. Wireless Commun.*, Jan. 2018.

[16] S. Buzzi and C. D'Andrea, "Doubly massive mmwave MIMO systems: Using very large antenna arrays at both transmitter and receiver," in *Proc. IEEE GLOBECOM*, Dec. 2016.

[17] J. Choi, D. J. Love, and P. Bidigare, "Downlink training techniques for FDD massive MIMO systems: Open-loop and closed-loop training with memory," *IEEE J. Sel. Topics Signal Process.*, Oct. 2014.

[18] X. Gao, O. Edfors, F. Rusek, and F. Tufvesson, "Massive MIMO performance evaluation based on measured propagation data," *IEEE Trans. Wireless Commun.*, July 2015.

[19] M. B. Khalilsarai, S. Haghighatshoar, X. Yi, and G. Caire, "FDD massive MIMO via UL/DL channel covariance extrapolation and active channel sparsification," *IEEE Trans. Wireless Commun.*, Jan. 2019.

[20] M. Newinger and W. Utschick, "Covariance shaping for interference coordination in cellular wireless communication systems," in *Proc. IEEE ASILOMAR*, Nov. 2015.

[21] N. N. Moghadam, H. Shokri-Ghadikolaei, G. Fodor, M. Bengtsson, and C. Fischione, "Pilot precoding and combining in multiuser MIMO networks," *IEEE J. Sel. Areas Commun.*, July 2017.

[22] P. Mursia, I. Atzeni, D. Gesbert, and L. Cottatellucci, "Covariance shaping for massive MIMO systems," in *Proc. IEEE GLOBECOM*, Dec. 2018.

[23] W. U. Bajwa, J. Haupt, A. M. Sayeed, and R. Nowak, "Compressed channel sensing: A new approach to estimating sparse multipath channels," *Proc. IEEE*, June 2010.

[24] X. Rao and V. K. N. Lau, "Distributed compressive CSIT estimation and feedback for FDD multi-user massive MIMO systems," *IEEE Trans. Signal Process.*, June 2014.

[25] Z. Gao, L. Dai, W. Dai, B. Shim, and Z. Wang, "Structured compressive sensing-based spatio-temporal joint channel estimation for FDD massive MIMO," *IEEE Trans. Commun.*, Feb. 2016.

[26] J. Shen, J. Zhang, E. Alsusa, and K. B. Letaief, "Compressed CSI acquisition in FDD massive MIMO: How much training is needed?" *IEEE Trans. Wireless Commun.*, June 2016.

[27] J. Dai, A. Liu, and V. K. N. Lau, "FDD massive MIMO channel estimation with arbitrary 2D-array geometry," *IEEE Trans. Signal Process.*, May 2018.

[28] Y. Ding and B. D. Rao, "Dictionary learning-based sparse channel representation and estimation for FDD massive MIMO systems," *IEEE Trans. Wireless Commun.*, Aug. 2018.

[29] A. A. Esswie, M. El-Absi, O. A. Dobre, S. Ikki, and T. Kaiser, "A novel FDD massive MIMO system based on downlink spatial channel estimation without CSIT," in *Proc. IEEE ICC*, May 2017.

[30] X. Luo, P. Cai, X. Zhang, D. Hu, and C. Shen, "A scalable framework for CSI feedback in FDD massive MIMO via DL path aligning," *IEEE Trans. Signal Process.*, Sep. 2017.

[31] X. Zhang, L. Zhong, and A. Sabharwal, "Directional training for FDD massive MIMO," *IEEE Trans. Wireless Commun.*, Aug. 2018.

[32] W. Shen, L. Dai, B. Shim, Z. Wang, and R. W. Heath, "Channel feedback based on AoD-adaptive subspace codebook in FDD massive MIMO systems," *IEEE Trans. Commun.*, Nov. 2018.

[33] 3GPP, "NR; physical layer procedures for data - Rel. 15," TS 38.214. Dec. 2018.

[34] E. Dahlman, S. Parkvall, and J. Sköld, *5G NR: the Next Generation Wireless Access Technology*. Academic Press, 2018.

[35] J. Flordelis, F. Rusek, F. Tufvesson, E. G. Larsson, and O. Edfors, "Massive MIMO performance — TDD versus FDD: What do measurements say?" *IEEE Trans. Wireless Commun.*, Apr. 2018.

[36] T. S. Rappaport, G. R. MacCartney, M. K. Samimi, and S. Sun, "Wideband millimeter-wave propagation measurements and channel models for future wireless communication system design," *IEEE Trans. Commun.*, Sept. 2015.

[37] S. Wyne, K. Haneda, S. Ranvier, F. Tufvesson, and A. F. Molisch, "Beamforming effects on measured mm-wave channel characteristics," *IEEE Trans. Wireless Commun.*, Nov. 2011.

[38] B. Biglarbegian, M. Fakharzadeh, D. Busuioc, M. R. Nezhad-Ahmadi, and S. Safavi-Naeini, "Optimized microstrip antenna arrays for emerging millimeter-wave wireless applications," *IEEE Trans. Antennas Propag.*, May 2011.

[39] F. Rusek, D. Persson, B. K. Lau, E. G. Larsson, T. L. Marzetta, O. Edfors, and F. Tufvesson, "Scaling up MIMO: Opportunities and challenges with very large arrays," *IEEE Signal Process. Mag.*, Jan. 2013.

[40] E. Bjornson, L. Van der Perre, S. Buzzi, and E. G. Larsson, "Massive MIMO in sub-6 ghz and mmwave: Physical, practical, and use-case differences," *IEEE Wireless Commun.*, Apr. 2019.

[41] R. W. Heath, N. González-Prelcic, S. Rangan, W. Roh, and A. M. Sayeed, "An overview of signal processing techniques for mmwave MIMO systems," *IEEE J. Sel. Topics Signal Process.*, Apr. 2016.

[42] J. Wang, Z. Lan, C. Pyo, T. Baykas, C. Sum, M. A. Rahman, J. Gao, R. Funada, F. Kojima, H. Harada, and S. Kato, "Beam codebook based beamforming protocol for multi-gbps millimeter-wave WPAN systems," *IEEE J. Sel. Areas Commun.*, Oct. 2009.

[43] A. Alkhateeb, O. E. Ayach, G. Leus, and R. W. Heath, "Channel estimation and hybrid precoding for mmwave cellular systems," *IEEE J. Sel. Top. Signal Process.*, Oct. 2014.

[44] F. Sohrabi and W. Yu, "Hybrid digital and analog beamforming design for large-scale antenna arrays," *IEEE J. Sel. Topics Signal Process.*, Apr. 2016.

[45] S. Haghighatshoar and G. Caire, "The beam alignment problem in mmWave wireless networks," in *Proc. IEEE ASILOMAR*, Nov. 2016.

[46] A. Alkhateeb, Y. H. Nam, M. S. Rahman, C. Zhang, and R. W. Heath, "Initial beam association in millimeter wave cellular systems: Analysis and design insights," *IEEE Trans. Wireless Commun.*, Feb. 2017.

[47] M. Giordani, M. Mezzavilla, C. N. Barati, S. Rangan, and M. Zorzi, "Comparative analysis of initial access techniques in 5G mmWave cellular networks," in *Proc. IEEE CISS*, Mar. 2016.

[48] H. Shokri-Ghadikolaei, L. Gkatzikis, and C. Fischione, "Beam-searching and transmission scheduling in millimeter wave communications," in *Proc. IEEE ICC*, June 2015.

[49] N. Garcia, H. Wymeersch, E. G. Ström, and D. Slock, "Location-aided mm-wave channel estimation for vehicular communication," in *Proc. IEEE SPAWC*, July 2016.

[50] J. Choi, V. Va, N. González-Prelcic, R. Daniels, C. R. Bhat, and R. W. Heath, "Millimeter-wave vehicular communication to support massive automotive sensing," *IEEE Commun. Mag.*, Dec. 2016.

[51] A. Ali, N. González-Prelcic, and R. W. Heath, "Millimeter wave beam-selection using out-of-band spatial information," *IEEE Trans. Wireless Commun.*, Feb. 2018.

[52] M. Dias, A. Klautau, N. González-Prelcic, and R. W. Heath, "Position and LIDAR-aided mmwave beam selection using deep learning," in *Proc. IEEE SPAWC*, July 2019.

[53] G. Fodor, S. Roger, N. Rajatheva, S. B. Slimane, T. Svensson, P. Popovski, J. M. B. D. Silva, and S. Ali, "An overview of device-to-device communications technology components in METIS," *IEEE Access*, June 2016.

[54] 3GPP, "NR; study on NR V2X," Work item RP-181429. June 2018.

[55] K. Doppler, M. Rinne, C. Wijting, C. B. Ribeiro, and K. Hugl, "Device-to-device communication as an underlay to LTE-advanced networks," *IEEE Commun. Mag.*, Dec. 2009.

[56] G. Fodor, E. Dahlman, G. Mildh, S. Parkvall, N. Reider, G. Miklós, and Z. Turányi, "Design aspects of network assisted device-to-device communications," *IEEE Commun. Mag.*, Mar. 2012.

[57] D. Feng, L. Lu, Y. Yuan-Wu, G. Y. Li, G. Feng, and S. Li, "Device-to-device communications underlaying cellular networks," *IEEE Trans. Commun.*, Aug. 2013.

[58] A. Asadi, Q. Wang, and V. Mancuso, "A survey on device-to-device communication in cellular networks," *IEEE Commun. Surveys Tuts.*, Oct. 2014.

[59] H. Yin, L. Cottatellucci, and D. Gesbert, "Enabling massive MIMO systems in the FDD mode thanks to D2D communications," in *Proc. IEEE ASILOMAR*, Nov. 2014.

[60] J. Chen, H. Yin, L. Cottatellucci, and D. Gesbert, "Feedback mechanisms for FDD massive MIMO with D2D-based limited CSI sharing," *IEEE Trans. Wireless Commun.*, Aug. 2017.

[61] P. Mursia, I. Atzeni, D. Gesbert, and M. Kobayashi, "D2D-aided multi-antenna multicasting," in *Proc. IEEE ICC*, May 2019.

[62] D. Wubben, P. Rost, J. S. Bartelt, M. Lalam, V. Savin, M. Gorgoglione, A. Dekorsy, and G. Fettweis, "Benefits and impact of cloud computing on 5G signal processing: Flexible centralization through cloud-RAN," *IEEE Signal Process. Mag.*, Nov. 2014.

[63] J. Sachs, L. A. A. Andersson, J. Araújo, C. Curescu, J. Lundsjö, G. Rune, E. Steinbach, and G. Wikström, "Adaptive 5G low-latency communication for tactile internet services," *Proc. IEEE*, Feb. 2019.

[64] Ericsson, "Ericsson mobility report," June 2019.

[65] W. Saad, Z. Han, M. Debbah, A. Hjorungnes, and T. Basar, "Coalitional game theory for communication networks," *IEEE Signal Process. Mag.*, Sep. 2009.

[66] R. Radner, "Team decision problems," *The Annals of Mathematical Statistics*, Sept. 1962.

[67] M. C. Filippou, P. de Kerret, D. Gesbert, T. Ratnarajah, A. Pastore, and G. A. Ropokis, "Coordinated shared spectrum precoding with distributed CSIT," *IEEE Trans. Wireless Commun.*, Aug. 2016.

[68] P. de Kerret and D. Gesbert, "Robust decentralized joint precoding using team deep neural network," in *Proc. IEEE ISWCS*, Aug. 2018.

[69] A. Bazco-Nogueras, L. Miretti, P. de Kerret, D. Gesbert, and N. Gresset, "Achieving vanishing rate loss in decentralized network MIMO," in *Proc. IEEE ISIT*, July 2019.

[70] C. T. K. Ng, D. Gündüz, A. J. Goldsmith, and E. Erkip, "Distortion minimization in gaussian layered broadcast coding with successive refinement," *IEEE Trans. Inf. Theory*, Nov. 2009.

[71] P. de Kerret, R. Fritzsche, D. Gesbert, and U. Salim, "Robust precoding for network MIMO with hierarchical CSIT," in *Proc. IEEE ISWCS*, Aug. 2014.

[72] F. Maschietti, D. Gesbert, P. de Kerret, and H. Wymeersch, "Robust location-aided beam alignment in millimeter wave massive MIMO," *Proc. IEEE GLOBECOM*, Dec. 2017.

[73] F. Maschietti, D. Gesbert, and P. de Kerret, "Coordinated beam selection in millimeter wave multi-user MIMO using out-of-band information," *Proc. IEEE ICC*, May 2019.

[74] F. Maschietti, G. Fodor, D. Gesbert, and P. de Kerret, "Coordinated beam selection for training overhead reduction in FDD massive MIMO," *Proc. IEEE ISWCS*, Aug. 2019.

[75] ——, "User coordination for fast beam training in FDD multi-user massive MIMO," *submitted to IEEE Trans. Wireless Commun.*, Dec. 2019.

[76] F. Maschietti, P. de Kerret, and D. Gesbert, "Exploring the trade-off between privacy and coordination in millimeter wave spectrum sharing," *Proc. IEEE ICC*, May 2019.

[77] A. M. Sayeed, "Deconstructing multiantenna fading channels," *IEEE Trans. Signal Process.*, Oct. 2002.

[78] D. Tse and P. Viswanath, *Fundamentals of Wireless Communication*. Cambridge University Press, 2005.

[79] C. Wang, J. Bian, J. Sun, W. Zhang, and M. Zhang, "A survey of 5G channel measurements and models," *IEEE Commun. Surveys Tuts.*, Nov. 2018.

[80] L. Liu, C. Oestges, J. Poutanen, K. Haneda, P. Vainikainen, F. Quitin, F. Tufvesson, and P. D. Doncker, "The COST 2100 MIMO channel model," *IEEE Wireless Commun.*, Dec. 2012.

[81] P. Kyösti, "Winner II channel models," IST-4-027756 Winner II Deliverable D1.1.2, Feb. 2008.

[82] M. R. Akdeniz, Y. Liu, M. K. Samimi, S. Sun, S. Rangan, T. S. Rappaport, and E. Erkip, "Millimeter wave channel modeling and cellular capacity evaluation," *IEEE J. Sel. Areas Commun.*, June 2014.

[83] S. Buzzi and C. D'Andrea, "A clustered statistical MIMO millimeter wave channel model," *CoRR*, vol. abs/1604.00648, 2016. [Online]. Available: http://arxiv.org/abs/1604.00648

[84] C. K. Anjinappa and I. Guvenc, "Angular and temporal correlation of v2x channels across sub-6 ghz and mmwave bands," in *Proc. IEEE ICC Workshops*, May 2018.

[85] V. Raghavan, A. Partyka, A. Sampath, S. Subramanian, O. H. Koymen, K. Ravid, J. Cezanne, K. Mukkavilli, and J. Li, "Millimeter-wave MIMO prototype: measurements and experimental results," *IEEE Commun. Mag.*, Jan. 2018.

[86] A. Ali, N. González-Prelcic, and R. W. Heath, "Estimating millimeter wave channels using out-of-band measurements," in *Proc. IEEE ITA*, Jan. 2016.

[87] A. Alkhateeb, G. Leus, and R. W. Heath, "Limited feedback hybrid precoding for multi-user millimeter wave systems," *IEEE Trans. Wireless Commun.*, Nov. 2015.

[88] R. Di Taranto, S. Muppirisetty, R. Raulefs, D. Slock, T. Svensson, and H. Wymeersch, "Location-aware communications for 5G networks: How location information can improve scalability, latency, and robustness of 5G," *IEEE Signal Process. Mag.*, Nov. 2014.

[89] P. de Kerret, S. Lasaulce, D. Gesbert, and U. Salim, "Best-response team power control for the interference channel with local CSI," in *Proc. IEEE ICC*, June 2015.

[90] A. Shapiro, D. Dentcheva, and A. Ruszczyński, *Lectures on stochastic programming*. Philadelphia, PA, USA: Soc. for Industrial and Applied Mathematics, 2014.

[91] S. Hur, T. Kim, D. J. Love, J. V. Krogmeier, T. A. Thomas, and A. Ghosh, "Millimeter wave beamforming for wireless backhaul and access in small cell networks," *IEEE Trans. Commun.*, Oct. 2013.

[92] T. S. Rappaport, S. Sun, R. Mayzus, H. Zhao, Y. Azar, K. Wang, G. N. Wong, J. K. Schulz, M. Samimi, and F. Gutierrez, "Millimeter wave mobile communications for 5G cellular: It will work!" *IEEE Access*, May 2013.

[93] J. Kim and A. F. Molisch, "Fast millimeter-wave beam training with receive beamforming," *IEEE J. Commun. Netw.*, Oct. 2014.

[94] S. S. Mahmoud, Z. M. Hussain, and P. O'Shea, "A space-time model for mobile radio channel with hyperbolically distributed scatterers," *IEEE Antennas and Wireless Propagation Letters*, Dec. 2002.

[95] S. M. Kay, *Fundamentals Of Statistical Signal Processing: Estimation Theory*. Prentice Hall, 1993.

[96] O. E. Ayach, S. Rajagopal, S. Abu-Surra, Z. Pi, and R. W. Heath, "Spatially sparse precoding in millimeter wave MIMO systems," *IEEE Trans. Wireless Commun.*, Mar. 2014.

[97] V. Va, J. Choi, and R. W. Heath, "The impact of beamwidth on temporal channel variation in vehicular channels and its implications," *IEEE Trans. Veh. Technol.*, June 2017.

[98] Q. H. Spencer, A. L. Swindlehurst, and M. Haardt, "Zero-forcing methods for downlink spatial multiplexing in multiuser MIMO channels," *IEEE Trans. Signal Process.*, Feb. 2004.

[99] W. Zirwas, M. B. Amin, and M. Sternad, "Coded CSI reference signals for 5G — Exploiting sparsity of FDD massive MIMO radio channels," in *Proc. IEEE WSA*, Mar. 2016.

[100] M. Herdin, N. Czink, H. Ozcelik, and E. Bonek, "Correlation matrix distance, a meaningful measure for evaluation of non-stationary MIMO channels," in *Proc. IEEE VTC*, May 2005.

[101] X. Xiong, X. Wang, X. Gao, and X. You, "Beam-domain channel estimation for FDD massive MIMO systems with optimal thresholds," *IEEE Trans. Wireless Commun.*, July 2017.

[102] M. K. Samimi and T. S. Rappaport, "3-D millimeter-wave statistical channel model for 5G wireless system design," *IEEE Trans. Microw. Theory Tech.*, July 2016.

[103] A. K. Gupta, J. G. Andrews, and R. W. Heath, "On the feasibility of sharing spectrum licenses in mmwave cellular systems," *IEEE Trans. Commun.*, Sept. 2016.

[104] M. Rebato, M. Mezzavilla, S. Rangan, and M. Zorzi, "Resource sharing in 5G mmwave cellular networks," in *Proc. IEEE INFOCOM WS*, Apr. 2016.

[105] H. Shokri-Ghadikolaei, F. Boccardi, C. Fischione, G. Fodor, and M. Zorzi, "Spectrum sharing in mmwave cellular networks via cell association, coordination, and beamforming," *IEEE J. Sel. Areas Commun.*, Nov. 2016.

[106] B. Liu, W. Zhou, T. Zhu, L. Gao, and Y. Xiang, "Location privacy and its applications: A systematic study," *IEEE Access*, Apr. 2018.

[107] M. Duckham and L. Kulik, "A formal model of obfuscation and negotiation for location privacy," in *Proc. PERVASIVE*, May 2005.

[108] H. Kido, Y. Yanagisawa, and T. Satoh, "An anonymous communication technique using dummies for location-based services," in *Proc. IEEE ICPS*, July 2005.

[109] C. Ardagna, M. Cremonini, E. Damiani, S. De Capitani di Vimercati, and P. Samarati, "Location privacy protection through obfuscation-based techniques," in *Proc. IFIP WG*, July 2007.

[110] Y. Xie, S. Jin, J. Wang, Y. Zhu, X. Gao, and Y. Huang, "A limited feedback scheme for 3D multiuser MIMO based on kronecker product codebook," in *Proc. IEEE PIMRC*, Sept. 2013.

[111] A. Alizadeh and M. Vu, "Time-fractional user association in millimeter wave MIMO networks," in *Proc. IEEE ICC*, May 2018.

[112] M. Trivellato, F. Boccardi, and F. Tosato, "User selection schemes for MIMO broadcast channels with limited feedback," in *Proc. IEEE VTC*, Apr. 2007.

[113] J. G. Andrews, T. Bai, M. N. Kulkarni, A. Alkhateeb, A. K. Gupta, and R. W. Heath, "Modeling and analyzing millimeter wave cellular systems," *IEEE Trans. Commun.*, Jan. 2017.

[114] I. Wagner and D. Eckhoff, "Technical privacy metrics: A systematic survey," *ACM Comput. Surv.*, June 2018.

[115] D. Gündüz, P. de Kerret, N. D. Sidiropoulos, D. Gesbert, C. R. Murthy, and M. Van der Schaar, "Machine learning in the air," *CoRR*, vol. abs/1904.12385, 2019. [Online]. Available: http://arxiv.org/abs/1904.12385

[116] J. Konecný, H. B. McMahan, D. Ramage, and P. Richtárik, "Federated optimization: Distributed machine learning for on-device intelligence," *CoRR*, vol. abs/1610.02527, 2016. [Online]. Available: http://arxiv.org/abs/1610.02527

[117] H. Q. Ngo, E. G. Larsson, and T. L. Marzetta, "Aspects of favorable propagation in massive MIMO," in *Proc. IEEE EUSIPCO*, Sept. 2014.

[118] C. Siriteanu, A. Takemura, S. Kuriki, D. S. P. Richards, and H. Shin, "Schur complement based analysis of MIMO zero-forcing for rician fading," *IEEE Trans. Wireless Commun.*, Apr. 2015.

[119] K. B. Petersen and M. S. Pedersen, *The Matrix Cookbook*. Technical University of Denmark, 2012.

[120] Y. Zhu and T. Yang, "Low complexity hybrid beamforming for uplink multiuser mmwave MIMO systems," in *Proc. IEEE WCNC*, Mar. 2017.